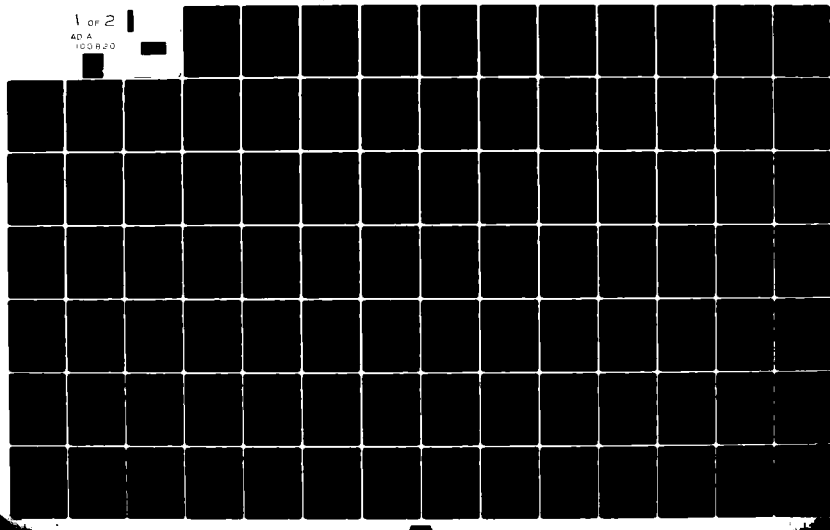


AD-A100 820 AIR FORCE INST OF TECH WRIGHT-PATTERSON AFB OH SCHO0--ETC F/B 12/1
A COMPARISON OF VARIOUS TECHNIQUES FOR THE PREDICTION OF MASS-L--ETC(U)
MAR 81 F B ATKINSON
UNCLASSIFIED AFIT/GAE/AA/80D-1 NL

1 of 2
40 A
ICOR 20



AFIT/GAE/AA/80D-1

Accession For	
NTIS GSA&I	X
DTIC TAB	
Unannounced	
Justification	
For	
Defense Agency	
Other	
Dist	
A	

A COMPARISON OF VARIOUS TECHNIQUES FOR
THE PREDICTION OF MASS-LOADED MODE
SHAPES AND NATURAL FREQUENCIES

THESIS,

AFIT/GAE/AA/80D-1 Frank B. Atkinson
Captain USAF

DTIC

UNCLASSIFIED

SECURITY CLASSIFICATION OF THIS PAGE (When Data Entered)

REPORT DOCUMENTATION PAGE		READ INSTRUCTIONS BEFORE COMPLETING FORM
1. REPORT NUMBER	2 GOVT ACCESSION NUMBER	
AFIT/GAE/AA/80D-1	AD-A100 820	
4. TITLE (and Subtitle)	5. TYPE OF REPORT & PERIOD COVERED	
A COMPARISON OF VARIOUS TECHNIQUES FOR THE PREDICTION OF MASS-LOADED MODE SHAPES AND NATURAL FREQUENCIES	6. PERFORMING ORG. REPORT NUMBER	
7. AUTHOR(s)	8. CONTRACT OR GRANT NUMBER(s)	
Frank B. Atkinson		
9. PERFORMING ORGANIZATION NAME AND ADDRESS	10. PROGRAM ELEMENT, PROJECT, TASK AREA & WORK UNIT NUMBERS	
Air Force Institute of Technology (AFIT-EN) Wright-Patterson AFB, Ohio 45433		
11. CONTROLLING OFFICE NAME AND ADDRESS	12. REPORT DATE	
	March 1981	
14. MONITORING AGENCY NAME & ADDRESS (if different from Controlling Office)	13. NUMBER OF PAGES	
	133	
16. DISTRIBUTION STATEMENT (of this Report)	15. SECURITY CLASS. (of this report)	
Approved for public release; distribution unlimited	Unclassified	
17. DISTRIBUTION STATEMENT (of the abstract entered in Block 20, if different from Report)	15a. DECLASSIFICATION DOWNGRADING SCHEDULE	
18. SUPPLEMENTARY NOTES	Approved for public release; IAW AFR 190-17	
16 JUN 1981	Frederick C. Lynch FREDERICK C. LYNCH, Major, USAF Director of Information	
19. KEY WORDS (Continue on reverse side if necessary and identify by block number)	Modal Prediction Techniques Whaley Algorithm Finite elements Mass-loaded mode shape prediction techniques	
20. ABSTRACT (Continue on reverse side if necessary and identify by block number)	The purpose of this investigation was to compare the results obtained from three modal prediction techniques. The first technique was an algorithm developed by Whaley for lightly damped structures (Method 1). Results using this algorithm were extracted from a thesis by Glenesk. The second method was the finite element method using NASTRAN (Method 2). The final method was the recovery of unloaded mass and stiffness matrices from the general matrix-vector differential equation of modal analysis using modal data obtained	

UNCLASSIFIED

SECURITY CLASSIFICATION OF THIS PAGE(When Data Entered)

from an unloaded test item (Method 3). Once these matrices had been recovered, a quantity of mass was added to the mass matrix to simulate a mass-loaded case. The generalized eigenvalue problem was solved for mass-loaded frequencies and mode shapes which were compared to experimental results for the same test item. Both square and rectangular modal matrices were considered in Method 3. The same test item and three discrete mass-loaded configurations which Glenesk used were tested. Percentage frequency deviations from the unloaded test item to the mass-loaded predictions ranged from -7.2-% to +7.4-% in Method 1, from -20.3-% to 17.84-% in Method 2, and from -20.6-% to +8.4-% in Method 3. Several discrepancies in each technique prevent a direct comparison of these results. The most noteworthy discrepancy was the fact that the modal measurement procedure generated nonorthogonal modes whereas the first method assumed the mode shapes to be unaltered between the unloaded and mass-loaded cases while the second method generated mutually orthogonal modes. The unloaded nonorthogonal mode vectors were used in Method 3 to generated mass-loaded modal quantities. Detailed procedures, results, and conclusions are obtained in the body and appendices of the report.

UNCLASSIFIED

SECURITY CLASSIFICATION OF THIS PAGE(When Data Entered)

AFIT/GAE/AA/80D-1

A COMPARISON OF VARIOUS TECHNIQUES FOR
THE PREDICTION OF MASS-LOADED MODE
SHAPES AND NATURAL FREQUENCIES

THESIS

Presented to the Faculty of the School of Engineering
of the Air Force Institute of Technology
Air University
in Partial Fulfillment of the
Requirements for the Degree of
Master of Science

by

Frank B. Atkinson, B.S.A.E.

Captain USAF

Graduate Aeronautical Engineering

March 1981

Approved for public release; distribution unlimited.

Preface

The purpose of this study was to compare several techniques for the prediction of mass-loaded natural frequencies and mode shapes. Of special interest in this study was the recovery of the unloaded mass, stiffness, and damping matrices from measured modal data using a non-square modal matrix and subsequent solution for mass-loaded modal data.

This study was somewhat limited in scope in that only one panel with three discrete mass loadings was experimentally tested and analysed. It is hoped the technique using pseudoinverses will be explored further to determine the general validity of this method. Appendices A, B, and C should be helpful in this endeavour.

I would like to thank my advisor, Capt. H. C. Briggs of the Air Force Institute of Technology, Mr. R. D. Talmadge of the Air Force Flight Dynamics Laboratory, and Dr. P. W. Whaley of the University of Nebraska for their support and guidance in this effort. Additionally, I would like to thank my wife, Janice, for her constant encouragement and inspiration. Finally, and most of all, I would like to thank my Savior, Jesus Christ, for that "Peace which passeth all understanding (Phillipians 4:7)." In keeping with Proverbs 3, versus 5 and 6,

"Trust in the Lord with all thine heart,
And lean not unto thine own understanding;
In all thy ways acknowledge Him,
And He will direct thy paths",

I dedicate this thesis to Him.

Frank B. Atkinson

Contents

	<u>Page</u>
Preface	ii
List of Figures	vi
List of Tables	viii
List of Symbols	ix
Abstract	xi
I. Introduction	1
Background	1
Purpose	5
Objectives	6
II. Modal Analysis and Test Procedures	7
Test Item	7
Mass-Loading Configurations	7
Structural Models	10
Modal Analysis Test Procedures	14
Modal Analysis Data Reduction	16
Results	23
III. The Whaley Algorithm Method	26
Overview	26
Results	27
IV. The Finite Element Method	31
Overview	31
Finite Element Models	31
Results	33
V. The Use of Pseudoinverses in the Recovery of the Discrete Mass, Stiffness, and Damp- ing Matrices and Solution of the Mass- Loaded Problem	41
Overview	41
Data Reduction	41
Results	42

Contents

	<u>Page</u>
VI. Discussion of the Methods	49
General	49
The Whaley Algorithm	50
The Finite Element Method	52
The Use of Pseudoinverses in the Recovery of the Discrete Mass, Stiffness, and Damping Matrices and Solution of the Eigenvalue Problem	58
VII. Recommendations	60
Bibliography	62
Appendix A: Mathematical Considerations and Example Problems in the Calculation and Use of the Pseudoinverse	64
Appendix B: Detailed Modal Analysis and Test Procedures	72
Appendix C: Computer Program, Sample NASTRAN Deck, and HP5451B Fourier Analyser Programs	83

List of Figures

Figure	Page
1 Acoustic Test Panel, USAF Drawing X704933	8
2 Mass-Loading Locations	9
3 Mode Shape Plots from HP5451B Fourier Analyser, Frequency=208 Hz. A.) Unloaded Panel, B.) Mass-Loaded Panel, Configuration 6	11
4 Smeared Stiffener Uniform Model	12
5 Discrete Stiffener Model	13
6 Bay Modes Model	15
7 Sample Modal Assurance Criteria (MAC) Plot	18
8 Sample Modal Assurance Criteria (MAC) Data	19
9 Sample Transfer Function Plot	20
10 Sample Transfer Function Data	21
11 Sample Mode Shape Plots for A.) Smeared Stiff- ener Uniform Model (Discrete Stiffener Mode shapes similar) and B.) Bay Modes Model	22
12 Mode Shapes, Bay Modes Finite Element Model, for A.) Clean Panel (206.55 Hz), B.) Con- figuration 2 (208.14 Hz), C.) Configuration 6 (206.42 Hz), and D.) Configuration 7 (213.84 Hz)	38
13 Nine Point Coarse Grid (unloaded) for A.) Configuration 6, B.) Configuration 2, and C.) Configuration 7 with D.) Cylindrical Coordinate System	43
14 Nine Point Coarse Grid Mode Shapes, Configur- ation 7, Mode 1, for A.) Unloaded Panel (169.437 Hz), B.) Loaded Panel (139.975 Hz), C.) Square Modal Matrix Prediction (168.847 Hz), and D.) Pseudoinverse Prediction (169. 437 Hz). (Deformed Panel denoted by dotted lines)	44
A-1 Three Degree-of-Freedom System	70
B-1 Force Window	76

List of Figures

Figures	Page
B-2 Exponential Decay Window	76
C-1 Program Matrix Listing	83
C-2 Edited Output From Program Matrix	102
C-3 Sample NASTRAN Deck	106
C-4 Data Acquisition Program for HP5451B Fourier Analyser	111
C-5 Sample Y-9 Modal Analysis Set up with A.) General Information, B.) Test Identifica- tion, and C.) Grid Points	112
C-6 Sample Y-9 Connectivity Vector	113

List of Tables

Table	Page
1 Mass-Loading Configuration Data	9
2 Experimental Natural Frequencies Obtained Using Modal Assurance Criteria (MAC) Function	17
3 Experimental Natural Frequencies Obtained Using Modal Analysis Software	24
4 Data Results - Configuration 2	28
5 Data Results - Configuration 6	28
6 Data Results - Configuration 7	29
7 Percentage of Frequency Shift Using Whaley's Algorithm versus Unloaded Measured Data . .	30
8 NASTRAN Modal Data - Unloaded Panel	34
9 NASTRAN Modal Data - Configuration 2	35
10 NASTRAN Modal Data - Configuration 6	36
11 NASTRAN Modal Data - Configuration 7	37
12 Natural Frequency Pairing Obtained Using NASTRAN	39
13 Frequency Predictions - Square and Rectangular Modal Matrix, Configuration 2	46
14 Frequency Predictions - Square and Rectangular Modal Matrix, Configuration 6	46
15 Frequency Predictions - Square and Rectangular Modal Matrix, Configuration 7	46
16 Computer Resources Used to Obtain Modal Results	58
A-1 Analytical Data From Three Degree-of-Freedom Spring-Mass-Damper System	69

List of Symbols

Symbol	Definition
A	Any Matrix, A
A^+	Pseudoinverse of Matrix A
[A]	Matrix Consisting of Generalized Mass and Generalized Force Quantities
\bar{b}	Vector b
[C]	The Damping Matrix
E	An Elementary Matrix
[I]	The Identity Matrix
[K]	The Stiffness Matrix
L	Lower Triangular Matrix
\bar{L}	Reduced Form of Matrix L
M_O	The Added Lumped Mass
[M]	The Mass Matrix
n	The Number of Measurement Points
P	Permutation Matrix
Q_i	Generalized Force
q_i	Generalized Coordinate
R_x	Radius of Gyration of Added Lumped Mass About Its x-Axis
R_y	Radius of Gyration of Added Lumped Mass About Its y-Axis
\bar{S}_{rr}	Autocorrelation of Stationary Accelerometer Response
\bar{S}_{yr}	Cross-correlation Between Stationary Accelerometer Response and Moveable Accelerometer Response

Symbol	Definition
\bar{S}_{YY}	Autocorrelation of Moveable Accelerometer Response
U	Upper Trapezoidal Matrix
\bar{U}	Reduced Form of U
[U]	The Modal Matrix
$[U]^T$	Transpose of the Modal Matrix
x_o	X-Coordinate of the Added Lumped Mass
\bar{x}	Displacement Vector
\dot{x}	Velocity Vector
\ddot{x}	Acceleration Vector
y_o	y-Coordinate of the Added Lumped Mass
ω_n	Natural Frequency
ξ_n	Damping Ratio
ϕ_i	Mode Shape
$\partial/\partial x$	Partial Derivative With Respect to X
$\partial/\partial y$	Partial Derivative With Respect to y
$\delta/\delta q$	First Variation With Respect to q
$[]^{-1}$	Inverse of the Given Matrix
$[]^+$	Pseudoinverse of the Given Matrix
$[]^T$	Transpose of the Given Matrix
$()^*$	Conjugate

Abstract

The purpose of this investigation was to compare the results obtained from three modal prediction techniques. The first technique was an algorithm developed by Whaley for lightly damped structures (Method 1). Results using this algorithm were extracted from a thesis by Glenesk. The second method was the finite element method using NASTRAN (Method 2). The final method was the recovery of unloaded mass and stiffness matrices from the general matrix-vector differential equation of modal analysis using modal data obtained from an unloaded test item (Method 3). Once these matrices had been recovered, a quantity of mass was added to the mass matrix to simulate a mass-loaded case. The generalized eigenvalue problem was solved for mass-loaded frequencies and mode shapes which were compared to experimental results for the same test item. Both square and rectangular modal matrices were considered in Method 3. The same test item and three discrete mass-loaded configurations which Glenesk used were tested. Percentage frequency deviations from the unloaded test item to the mass-loaded predictions ranged from -7.2-% to +7.4-% in Method 1, from -20.3-% to +17.84-% in Method 2, and from -20.6-% to +8.4-% in Method 3. Several discrepancies in each technique prevent a direct comparison of these results. The most noteworthy discrepancy was

the fact that the modal measurement procedure generated nonorthogonal modes. The first method assumed the mode shapes to be unaltered between the unloaded and mass-loaded cases while the second method generated mutually orthogonal modes. The unloaded nonorthogonal mode vectors were used in Method 3 to generate mass-loaded modal quantities. Detailed procedures, results, and conclusions are obtained in the body and appendices of the report.

A COMPARISON OF VARIOUS TECHNIQUES FOR
THE PREDICTION OF MASS-LOADED MODE
SHAPES AND NATURAL FREQUENCIES

I Introduction

Background

The ever-expanding performance envelopes of today's highly complex fighter aircraft subjects them to increasingly severe vibration environments. Coupled with these severe vibration environments is a desire to rapidly incorporate newly-developed weapons system technologies into the existing fleet of fighter aircraft. One such example is the application of laser physics technology to vibration-sensitive electro-optical equipment which would subsequently be installed in high-performance fighter aircraft.

The installation of electro-optical equipment in an aircraft presents a complex design problem in that it is necessary to know the post-installation modes of vibration and natural frequencies of the aircraft prior to the actual installation of this hardware. Frequently, the only modal data available to the designer are the pre-installation modal data. Thus, due to the vibration sensitivity of the electro-optical hardware, the designer must consider how to properly utilize the pre-installation vibration

data to correctly predict the post-inflation modes of vibration, damping, and natural frequencies. Whaley (Ref 12) summarized three analytical techniques to accomplish this task. Additionally, Glenesk (Ref 3) utilized an algorithm developed by Whaley for lightly damped structures (Ref 13) to predict the influence of added lumped masses on the vibration characteristics of unloaded structures.

According to the research conducted by Glenesk (Ref 3), as the size of the added mass increased relative to the mass of the unloaded structure, the accuracy of Whaley's algorithm was significantly affected. This degradation in algorithm performance might be attributed to the assumption that the unloaded mode shapes are unaffected by the addition of the lumped mass. Another possibility involves the fact that the effect of damping was ignored in this algorithm. Thus, an added mass might have significantly contributed to the overall structural characteristics in such a way as to modify the mode shapes and natural frequencies.

In addition to the various analytical techniques, a numerical technique, finite element analysis, has been widely used to predict mass-loaded natural frequencies, damping ratios, and mode shapes. This technique requires the construction of a computer model in which the continuous

structure is idealized as a combination of a finite number of various structural components (i.e., beams, rods, plates, etc.). Although accurate results can be obtained using the finite element method, one problem with this technique is the significant expenditure of human and computer resources necessary to build, debug, and run the finite element code.

The rapid development of portable modal analysis equipment has made it possible to eliminate the construction of a finite element model entirely. With this equipment one can lay out a suitable grid on the portion of structure to be modified, conduct standard modal analysis tests, and reduce the data so obtained to determine the desired unloaded modal data. The question then becomes how to properly use this data to determine the mass-loaded modal quantities for the modified structure. One approach to this dilemma has been suggested by Briggs and Whaley (Ref 1) whereby one uses the general matrix-vector differential equation of structural analysis, its solution using a generalized coordinates approach, and the resulting definitions

$$[U]^T [M] [U] = [I] \quad (1)$$

$$[U]^T [K] [U] = \begin{bmatrix} \ddots & & 0 \\ & \omega_n^2 & \\ 0 & & \ddots \end{bmatrix} \quad (2)$$

$$[U]^T [C] [U] = \begin{bmatrix} \ddots & & 0 \\ & 2\xi_n\omega_n & \\ 0 & & \ddots \end{bmatrix} \quad (3)$$

to analytically determine the mass-loaded modal data when only the experimentally determined unloaded modal data are known.

At the present time, the usual solution to equations 1 through 3 requires that the modal matrices, $[U]$ and $[U]^T$, be square matrices. If the mass, damping, and stiffness matrices, $[M]$, $[C]$, and $[K]$, are $n \times n$ matrices, $[U]$ and $[U]^T$ must also be $n \times n$ matrices (where "n" is the number of measurement points). If one measures fewer than "n" modes in the frequency range of interest, he must either extend this frequency range to accomodate "n" modes, or reduce the grid size to "n" grid points. As either of these approaches may be undesirable, a third approach using the method of pseudoinverses introduced by Penrose (Ref 10) may be used to isolate the mass, stiffness, and damping matrices on the left hand side of equations 1 through 3, respectively. Appendix A contains a sample problem for the reader who is unfamiliar with this technique. The resulting solution will be an approximate solution to the mass, damping, and stiffness matrices for the unloaded structure. Then, to find the corresponding matrices for the mass-loaded structure one would add appropriate mass, damping, and stiffness quantities at the proper locations in their respective matrices to

simulate the structural modification, and resolve equations 1 through 3 for the mass-loaded modal information. If damping is not a factor one wishes to consider in this analysis, one need only consider the solution to the standard eigenvalue problem

$$[K] - \omega^2 [M] = [0] \quad (4)$$

to determine the mass-loaded natural frequencies and mode shapes.

Purpose

The purpose of this investigation is to obtain data, and compare the modal data obtained, using several modal prediction techniques. The techniques chosen for this comparison are those discussed previously, namely: (1) Glenesk's use of Whaley's algorithm (Ref 3); (2) the finite element method; and (3) the method suggested by Briggs and Whaley (Ref 1). Since a basis for comparison is needed, the results obtained from modal prediction software developed by Brown (Ref 2) will be used as a datum in error percentage calculations for methods 2 and 3 presented later in this report. However, it is felt by the author that to recalculate error values for Method 1 which would be based on a different datum would be unfair to both Glenesk and Whaley's algorithm. Thus, all values presented in reference to the use of Whaley's

algorithm will be directly extracted from Reference 3. The same complex, rib-stiffened panel and several of the discrete mass-loading configurations investigated by Glenesk (Ref 3) will be used in this comparison.

Objectives

The objectives of this investigation are:

- (1) Experimentally measure the natural frequencies and mode shapes of a complex test panel in the frequency range from 0-500 hz.
- (2) Construct finite element models of this panel and conduct a modal analysis on both unloaded and mass-loaded configurations.
- (3) Use equations 1, 2, and 4 along with unloaded experimental data to obtain mass-loaded natural frequencies and mode shapes for the test panel.
- (4) Present a comparison of the results of Objectives 1 through 3.

II Modal Analysis and Test Procedures

Test Item

The test item was a panel fabricated using drawings of an upper fuselage panel of a C-140 aircraft (Figure 1). The curved panel consisted of the following components:

1. An outer skin
2. Five longerons of two different cross sections
3. Two curved main frame ring segments
4. Four edge doublers, and
5. Various attachment hardware and bonding to maintain structural integrity.

Mass-Loading Configurations

Based on the worst case errors presented by Glenesk (Ref 3) for the mass-loaded panel, four test configurations were chosen for comparison of the three methods. These were the unloaded panel and Glenesk's mass-loaded configurations 2, 6, and 7 (Table 1 and Figure 2). The unloaded panel was included as a means of comparing the change in mode shape with natural frequency which occurred between the unloaded case and each mass-loaded configuration. Plots of unloaded versus mass-loaded mode shapes allowed visualization of this

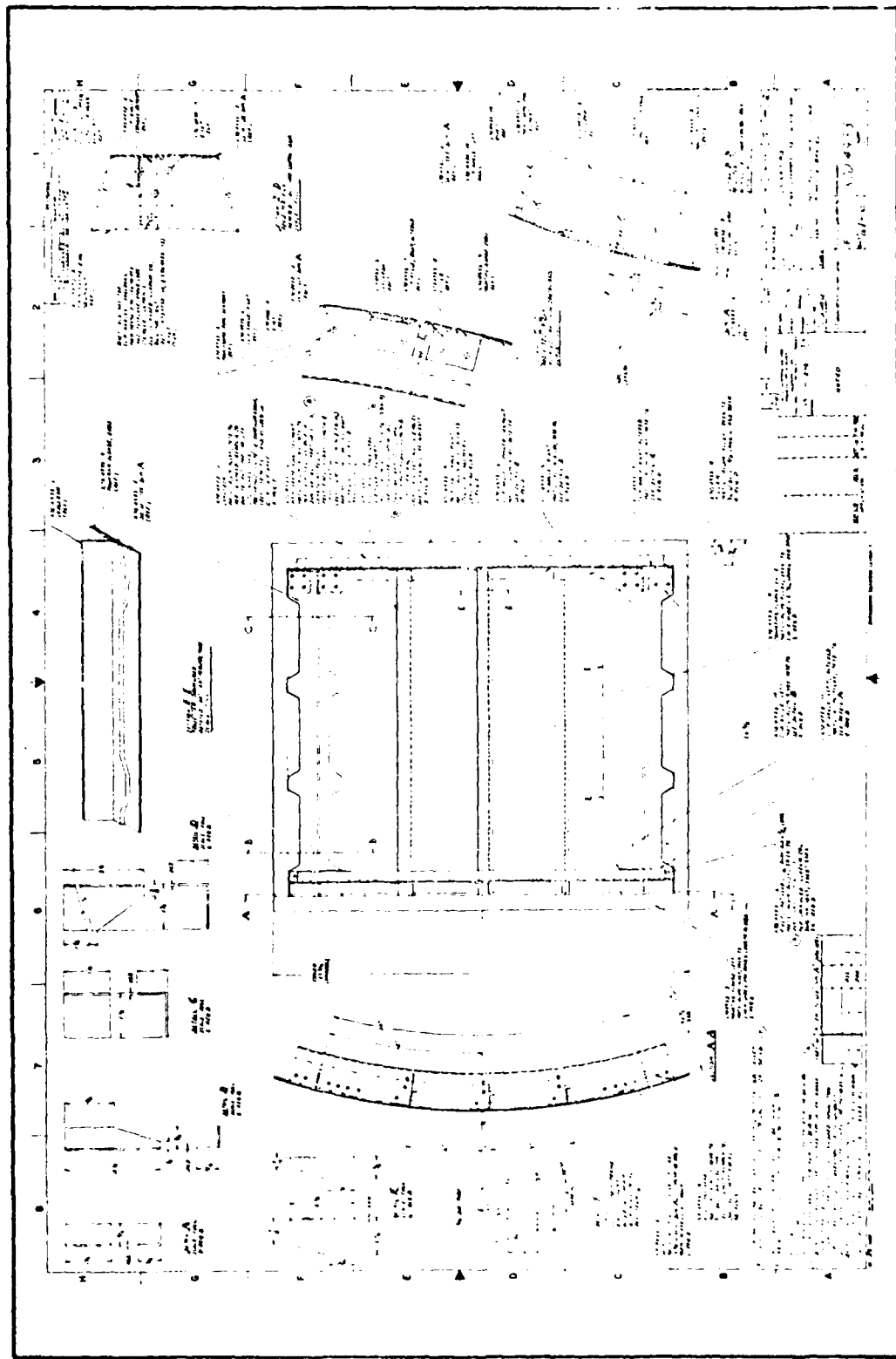
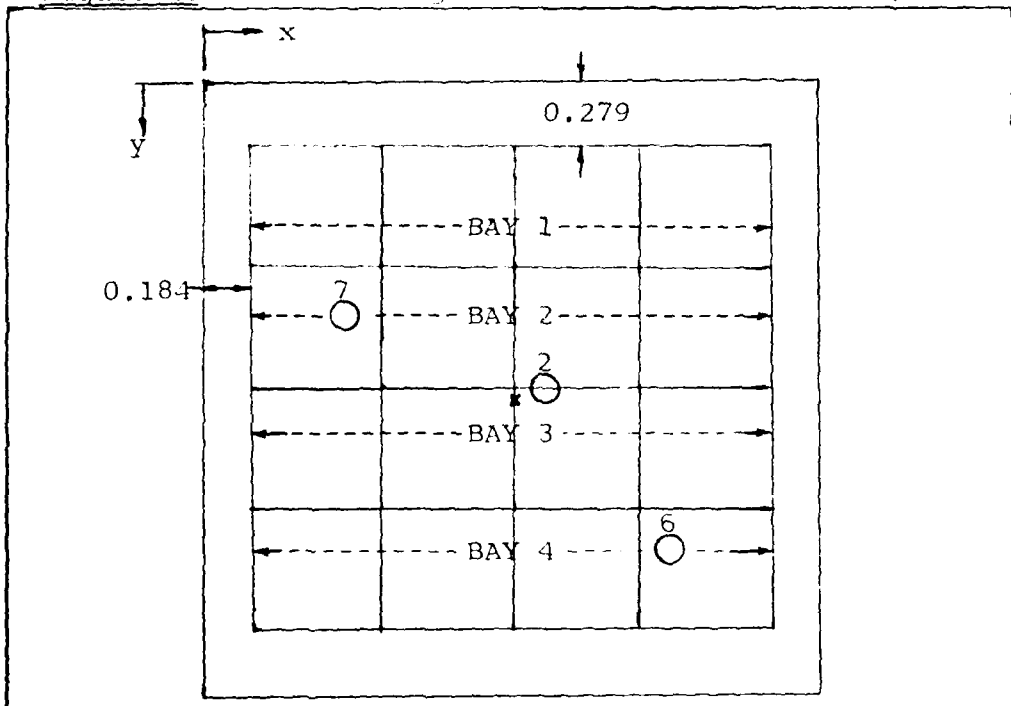


Figure 1. Test Panel, USAF Drawing X704933.

Table 1. Mass-loading configuration (after Glenesk, Ref 2)

Configuration	Mass (lb)	x_o (ft)	y_o (ft)
2	0.2420	1.168	1.168
6	0.4158	1.667	1.749
7	0.1144	0.499	0.915

Figure 2. Mass-loading locations (after Glenesk, Ref 2)



Notes:

1. Dimensions in feet.
2. Configuration 7 specifies mass-loading location.
3. BAY 1 specifies internal unsupported bay.

change in mode shape (Figure 3).

Structural Models

Three grid sets were chosen to model this panel. The first grid set was utilized in an effort to verify Glenesk's results by using Glenesk's grid set and modal analysis procedure. Glenesk's model did not consider the discrete components as separate members. Instead, it accounted for the total panel mass and smeared this mass over the grid which was inset somewhat from the panel edges. The result was a homogeneous, constant thickness flat plate with 25 grid points. This model will be referred to as the Smeared Stiffener Uniform Model (Figure 4).

The second grid was chosen to coincide with a finite element model which accurately modelled the discrete structural components by allowing for panel curvature, discrete member cross-sectional geometry, and offsets of component neutral axes. This model also consisted of 25 grid points. It will be referred to as the Discrete Stiffener Model (Figure 5).

The final model was chosen to investigate the modes of vibration of each of the internal bays (Figure 2). This grid was necessary because the previous two models basically ignored the motion of the unsupported

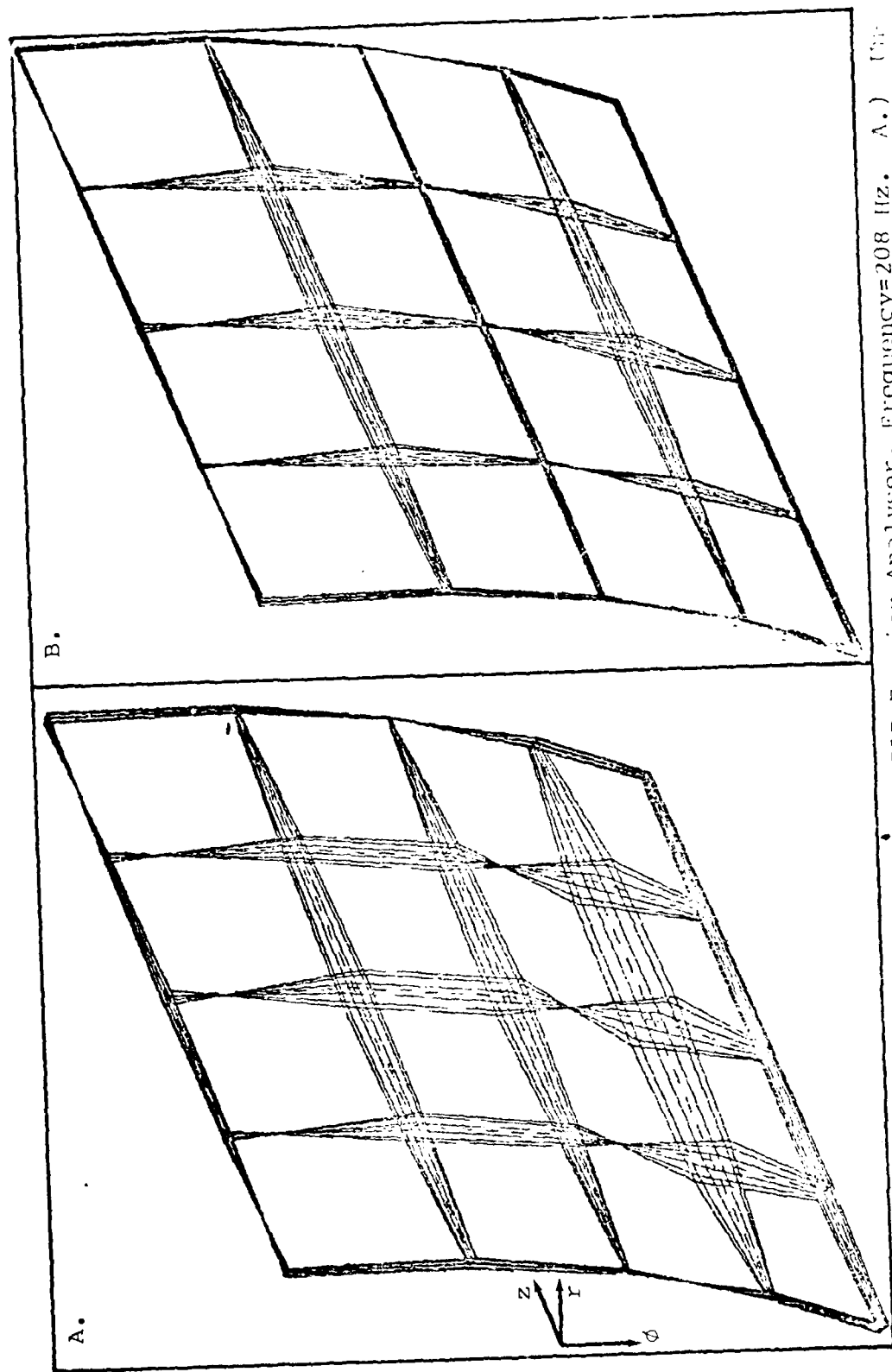


Figure 3. Mode Shape Plots from HP5451B Fourier Analyser, Frequency=208 Hz. A.) Mass-Loaded Panel, B.) Mass-Loaded Panel, Configuration 6.

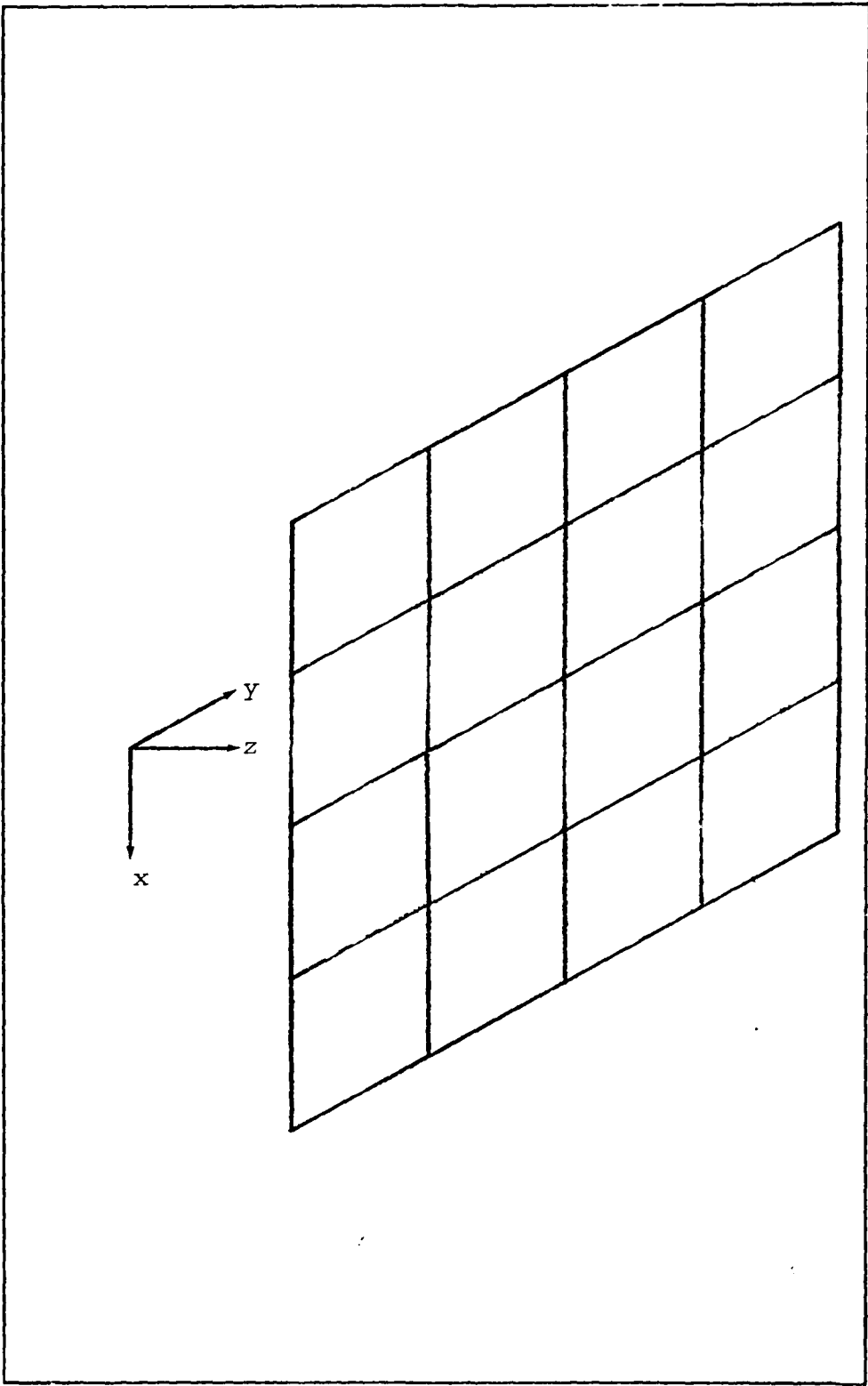


Figure 4. Smeared Stiffener Uniform Model.

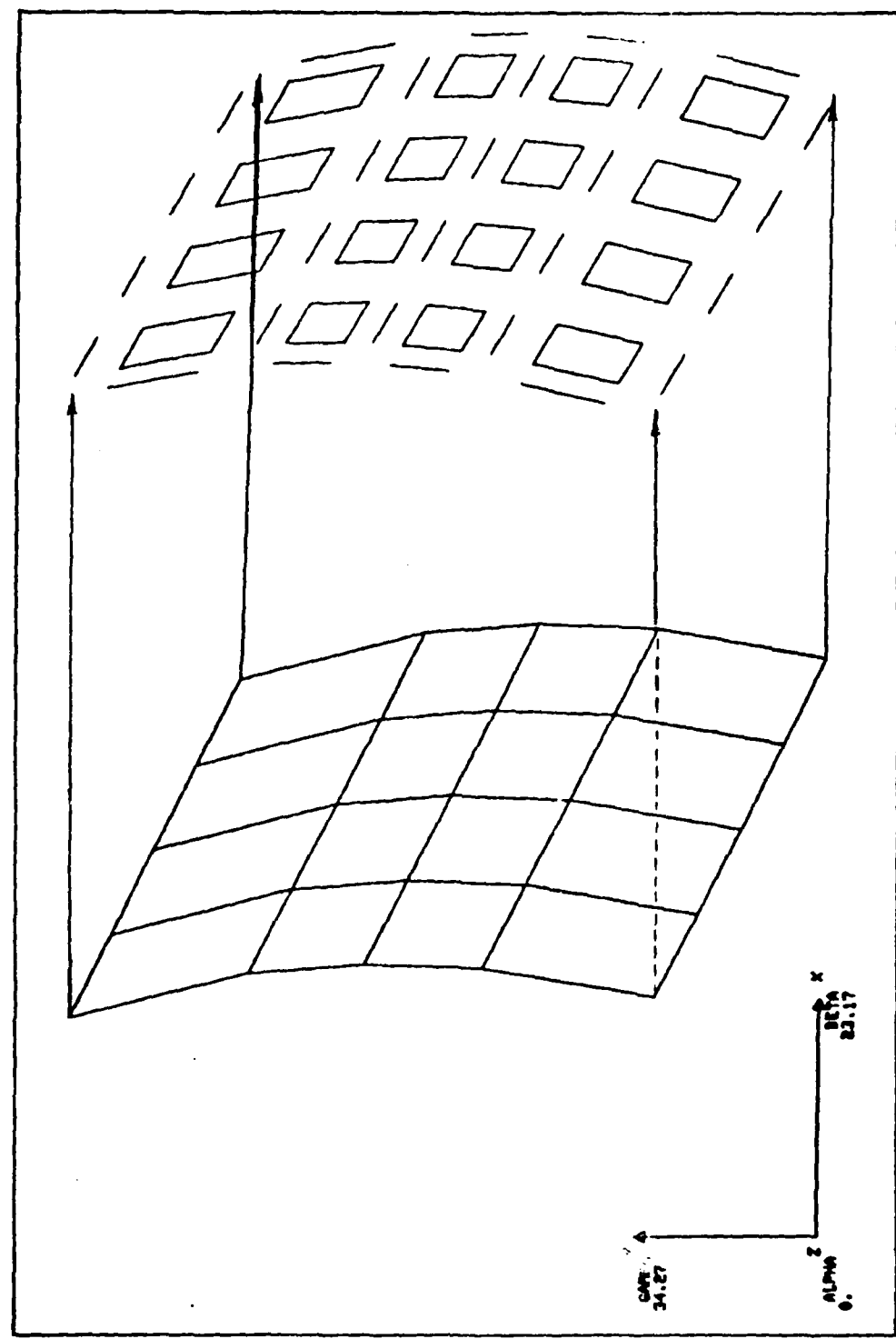


Figure 5. Discrete Stiffener Model.

internal bays. This model, which consisted of 65 grid points, will be referred to as the Bay Modes Model (Figure 6). This model contained the previous two models as subsets.

Modal Analysis Test Procedures

The Smeared Stiffener Uniform Model was tested first. The Modal Assurance Criterion (MAC) developed by Brown (Ref 3) along with discrete Transfer Function data were used as the basis for identifying candidate frequency ranges from which the natural frequencies for each configuration were determined. The MAC function is defined as (Ref 3)

$$\text{MAC} = \frac{|\bar{S}_{yr}(\omega)|^2}{\bar{S}_{rr}(\omega)\bar{S}_{yy}(\omega)}$$

where \bar{S}_{yr} = the stable average of the cross power spectrum between two response measurement points

\bar{S}_{rr} = the stable average of the auto power spectrum of the stationary accelerometer response

\bar{S}_{yy} = the stable average of the auto power spectrum of the moveable accelerometer response.

Note that the MAC Function differs from the more commonly used Coherence Function in that the two measurements in question in the former are two responses to an impulse excitation whereas like quantities for the latter

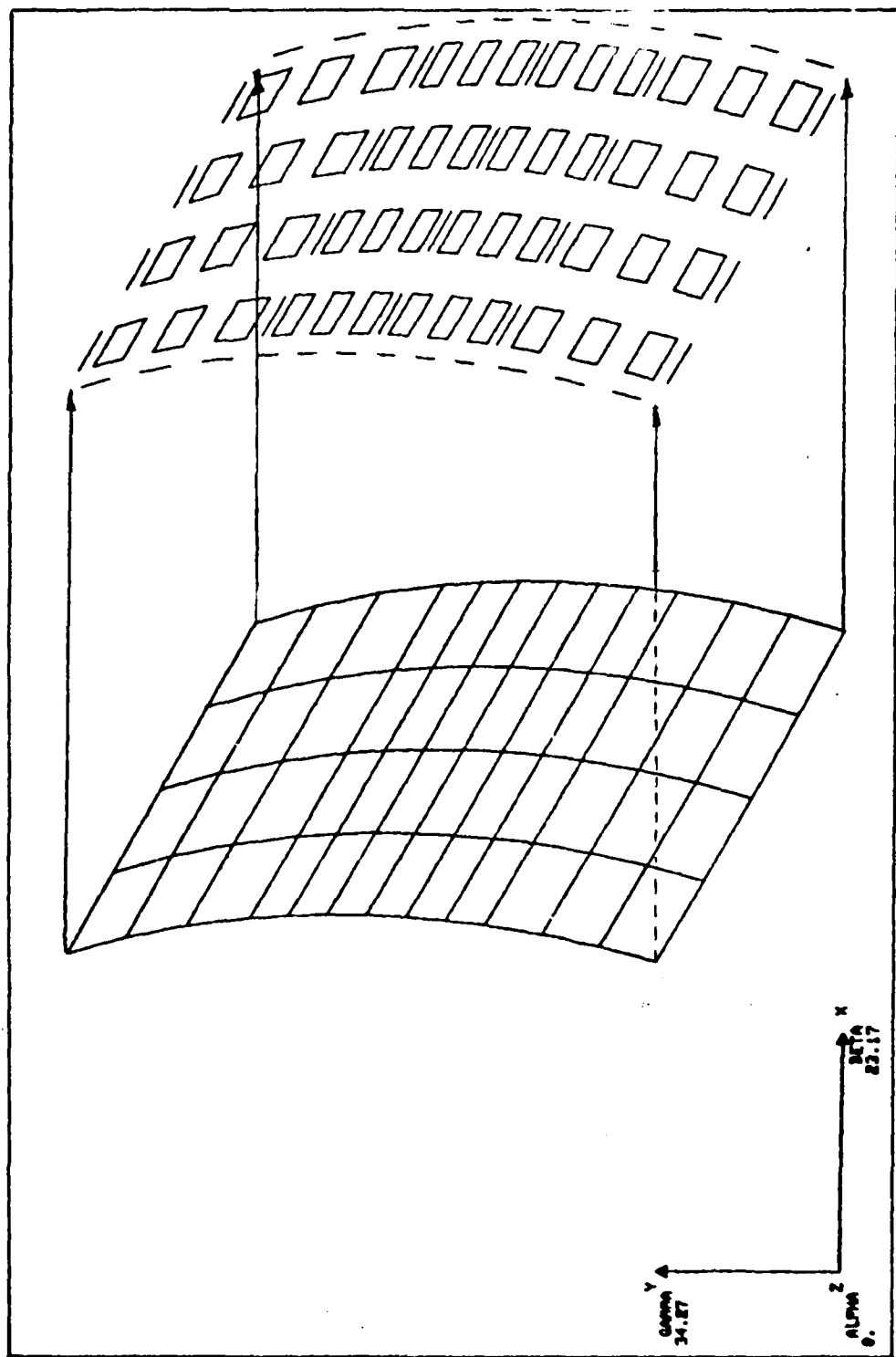


Figure 6. Bay Nodes Model

would be an impulse excitation input and the forced response. In both cases, the existence of a mode is indicated by a region of closely spaced frequencies where the MAC or Coherence Function is essentially equal to one.

Since the MAC and Transfer Function data were essentially identical with Glenesk's results, these data were not reduced to obtain natural frequencies and mode shapes. Instead, Glenesk's results (Ref 3) will be used in the techniques comparison. Table 2 contains a summary of the pertinent data. Sample MAC and Transfer Function plots and data are contained in Figures 7, 8, 9, and 10.

The Bay Modes Model was tested next using modal analysis software developed by Brown (Ref 2). This software allowed the user to select any subset of the model being tested and consider only the data relative to that subset. Thus, it was not necessary to repeat this test for either the Smeared Stiffener Uniform Model or the Discrete Stiffener Model. Representative mode shape data obtained for these models are contained in Figure 11.

Modal Analysis Data Reduction

To determine the natural frequencies of a given model and configuration, one grid point was selected which was believed to contain all of the modes in the frequency range from 0-500 hz. That is, it was believed

Table 2. Experimental Natural Frequencies Obtained Using Modal Assurance Criterion (MAC) Function (Extracted from Ref 3).

Mode Number	Configuration						% Chg
	Unloaded	2	% Chg	6	% Chg	7	
1	167.93	----	----	169.71	+ 1.06	143.10	- 14.79
2	180.50	174.08	- 3.56	180.72	.12	175.09	- 3.00
3	191.22	187.62	- 1.88	199.30	+ 4.23	184.83	- 3.34
4	207.31	204.00	- 1.60	208.27	+ .46	204.30	- 1.45
5	237.74	225.31	- 5.23	238.22	+ .20	238.22	+ .20
6	252.12	243.32	- 3.49	252.20	.46	257.50	+ 2.13
7	280.02	263.80	- 5.79	279.95	.20	279.88	.20
8	292.83	282.45	- 3.54	292.20	- .22	292.76	- .02
9	365.00	363.08	- .53	360.20	- 1.32	361.71	- .90

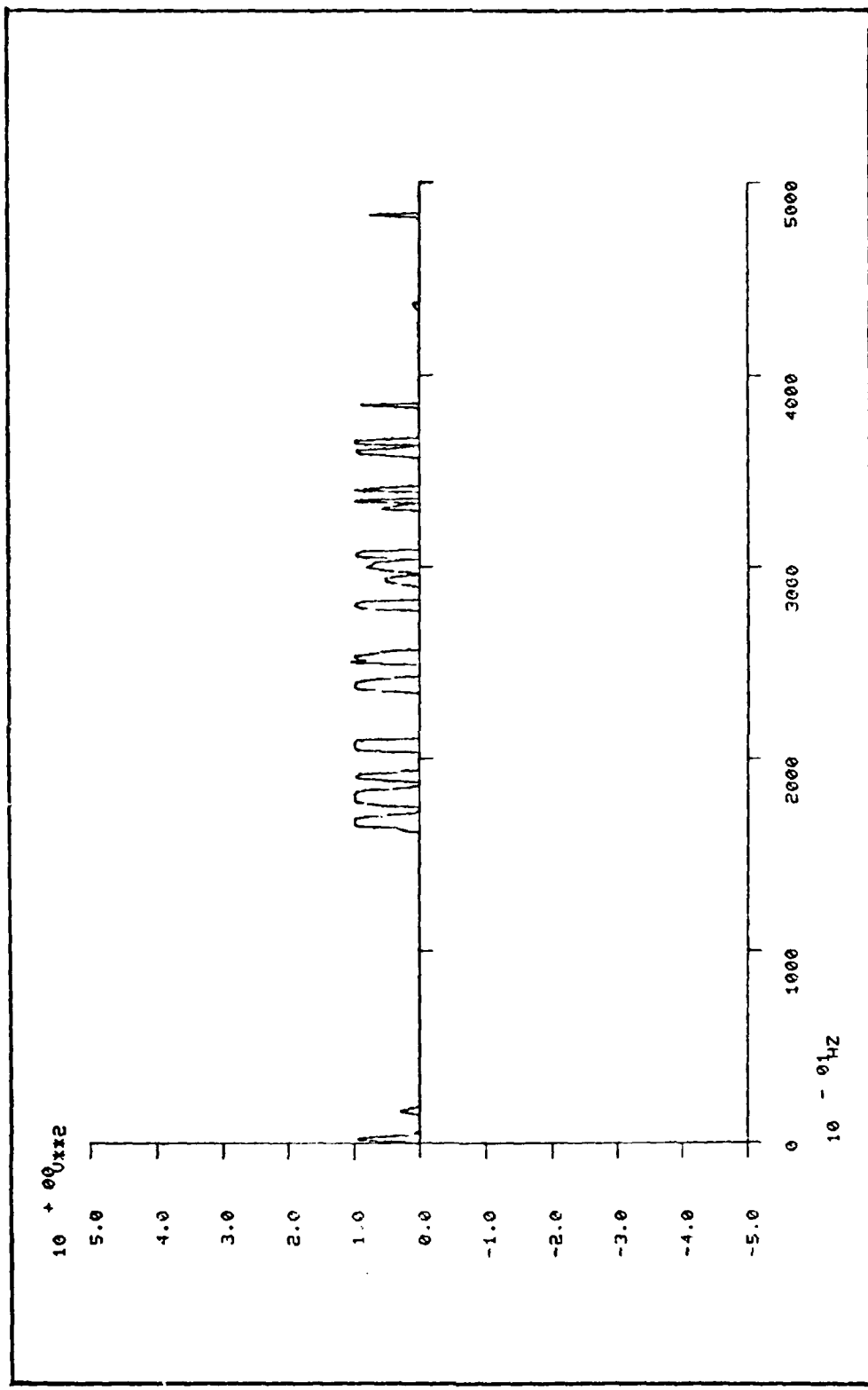


Figure 7. Sample Modal Assurance Criteria (MAC) Plot.

Figure 8. Sample Modal Assurance Criteria (MAC) Data.

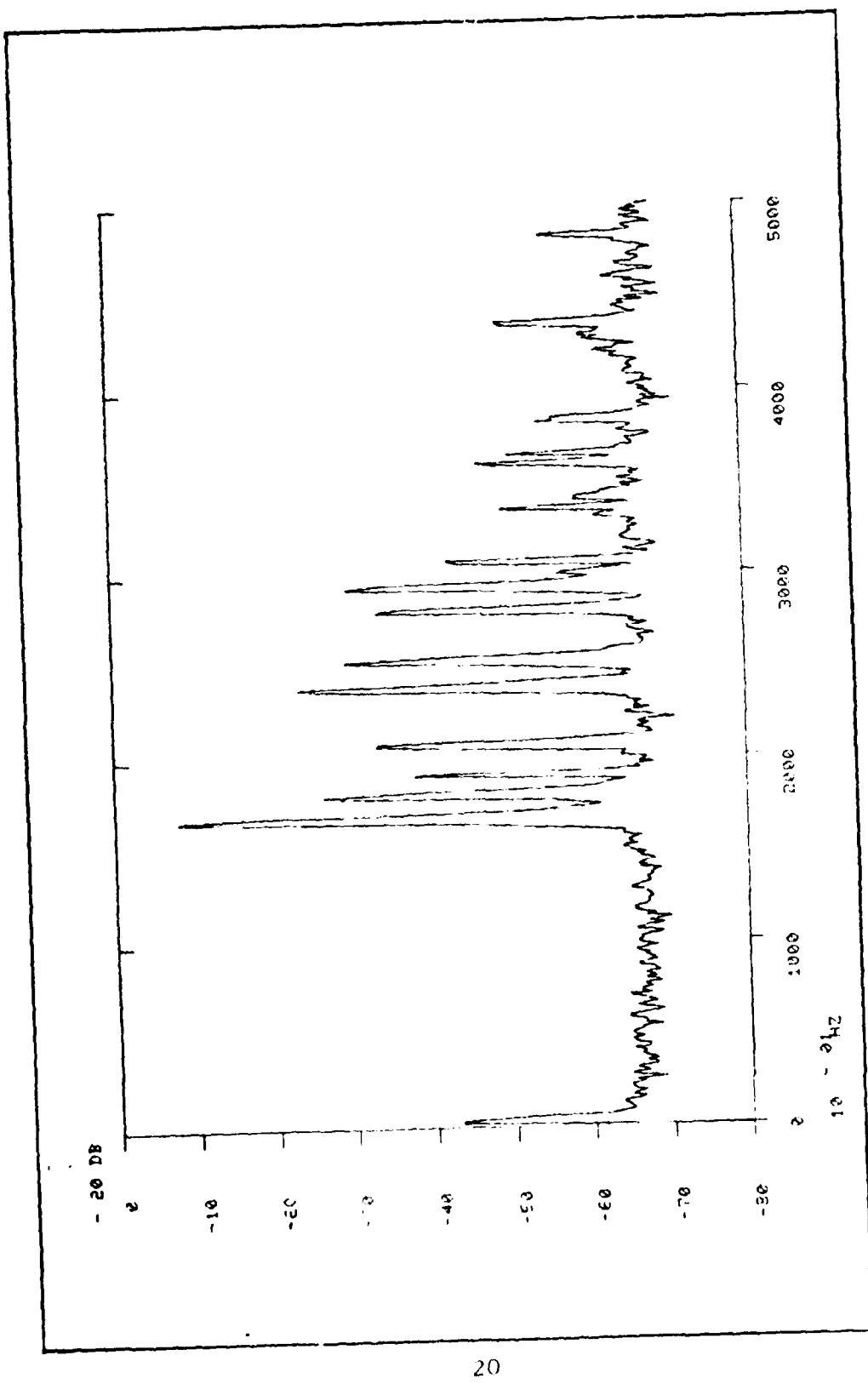


Figure 9. Sample Transfer Function Plot.

1	2	3	4	5	6	7	8	9	10	11	12	13	14	15	16	17	18	19	20	21	22	23	24	25	26	27	28	29	30	31	32	33	34	35	36	37	38	39	40	41	42	43	44	45	46	47	48	49	50	51	52	53	54	55	56	57	58	59	60	61	62	63	64	65	66	67	68	69	70	71	72	73	74	75	76	77	78	79	80	81	82	83	84	85	86	87	88	89	90	91	92	93	94	95	96	97	98	99	100	101	102	103	104	105	106	107	108	109	110	111	112	113	114	115	116	117	118	119	120	121	122	123	124	125	126	127	128	129	130	131	132	133	134	135	136	137	138	139	140	141	142	143	144	145	146	147	148	149	150	151	152	153	154	155	156	157	158	159	160	161	162	163	164	165	166	167	168	169	170	171	172	173	174	175	176	177	178	179	180	181	182	183	184	185	186	187	188	189	190	191	192	193	194	195	196	197	198	199	200	201	202	203	204	205	206	207	208	209	210	211	212	213	214	215	216	217	218	219	220	221	222	223	224	225	226	227	228	229	230	231	232	233	234	235	236	237	238	239	240	241	242	243	244	245	246	247	248	249	250	251	252	253	254	255	256	257	258	259	260	261	262	263	264	265	266	267	268	269	270	271	272	273	274	275	276	277	278	279	280	281	282	283	284	285	286	287	288	289	290	291	292	293	294	295	296	297	298	299	300	301	302	303	304	305	306	307	308	309	310	311	312	313	314	315	316	317	318	319	320	321	322	323	324	325	326	327	328	329	330	331	332	333	334	335	336	337	338	339	340	341	342	343	344	345	346	347	348	349	350	351	352	353	354	355	356	357	358	359	360	361	362	363	364	365	366	367	368	369	370	371	372	373	374	375	376	377	378	379	380	381	382	383	384	385	386	387	388	389	390	391	392	393	394	395	396	397	398	399	400	401	402	403	404	405	406	407	408	409	410	411	412	413	414	415	416	417	418	419	420	421	422	423	424	425	426	427	428	429	430	431	432	433	434	435	436	437	438	439	440	441	442	443	444	445	446	447	448	449	450	451	452	453	454	455	456	457	458	459	460	461	462	463	464	465	466	467	468	469	470	471	472	473	474	475	476	477	478	479	480	481	482	483	484	485	486	487	488	489	490	491	492	493	494	495	496	497	498	499	500	501	502	503	504	505	506	507	508	509	510	511	512	513	514	515	516	517	518	519	520	521	522	523	524	525	526	527	528	529	530	531	532	533	534	535	536	537	538	539	540	541	542	543	544	545	546	547	548	549	550	551	552	553	554	555	556	557	558	559	560	561	562	563	564	565	566	567	568	569	570	571	572	573	574	575	576	577	578	579	580	581	582	583	584	585	586	587	588	589	590	591	592	593	594	595	596	597	598	599	600	601	602	603	604	605	606	607	608	609	610	611	612	613	614	615	616	617	618	619	620	621	622	623	624	625	626	627	628	629	630	631	632	633	634	635	636	637	638	639	640	641	642	643	644	645	646	647	648	649	650	651	652	653	654	655	656	657	658	659	660	661	662	663	664	665	666	667	668	669	670	671	672	673	674	675	676	677	678	679	680	681	682	683	684	685	686	687	688	689	690	691	692	693	694	695	696	697	698	699	700	701	702	703	704	705	706	707	708	709	710	711	712	713	714	715	716	717	718	719	720	721	722	723	724	725	726	727	728	729	730	731	732	733	734	735	736	737	738	739	740	741	742	743	744	745	746	747	748	749	750	751	752	753	754	755	756	757	758	759	760	761	762	763	764	765	766	767	768	769	770	771	772	773	774	775	776	777	778	779	780	781	782	783	784	785	786	787	788	789	790	791	792	793	794	795	796	797	798	799	800	801	802	803	804	805	806	807	808	809	8010	8011	8012	8013	8014	8015	8016	8017	8018	8019	8020	8021	8022	8023	8024	8025	8026	8027	8028	8029	8030	8031	8032	8033	8034	8035	8036	8037	8038	8039	8040	8041	8042	8043	8044	8045	8046	8047	8048	8049	8050	8051	8052	8053	8054	8055	8056	8057	8058	8059	8060	8061	8062	8063	8064	8065	8066	8067	8068	8069	8070	8071	8072	8073	8074	8075	8076	8077	8078	8079	8080	8081	8082	8083	8084	8085	8086	8087	8088	8089	8090	8091	8092	8093	8094	8095	8096	8097	8098	8099	80100	80101	80102	80103	80104	80105	80106	80107	80108	80109	80110	80111	80112	80113	80114	80115	80116	80117	80118	80119	80120	80121	80122	80123	80124	80125	80126	80127	80128	80129	80130	80131	80132	80133	80134	80135	80136	80137	80138	80139	80140	80141	80142	80143	80144	80145	80146	80147	80148	80149	80150	80151	80152	80153	80154	80155	80156	80157	80158	80159	80160	80161	80162	80163	80164	80165	80166	80167	80168	80169	80170	80171	80172	80173	80174	80175	80176	80177	80178	80179	80180	80181	80182	80183	80184	80185	80186	80187	80188	80189	80190	80191	80192	80193	80194	80195	80196	80197	80198	80199	80200	80201	80202	80203	80204	80205	80206	80207	80208	80209	80210	80211	80212	80213	80214	80215	80216	80217	80218	80219	80220	80221	80222	80223	80224	80225	80226	80227	80228	80229	80230	80231	80232	80233	80234	80235	80236	80237	80238	80239	80240	80241	80242	80243	80244	80245	80246	80247	80248	80249	80250	80251	80252	80253	80254	80255	80256	80257	80258	80259	80260	80261	80262	80263	80264	80265	80266	80267	80268	80269	80270	80271	80272	80273	80274	80275	80276	80277	80278	80279	80280	80281	80282	80283	80284	80285	80286	80287	80288	80289	80290	80291	80292	80293	80294	80295	80296	80297	80298	80299	80300	80301	80302	80303	80304	80305	80306	80307	80308	80309	80310	80311	80312	80313	80314	80315	80316	80317	80318	80319	80320	80321	80322	80323	80324	80325	80326	80327	80328	80329	80330	80331	80332	80333	80334	80335	80336	80337	80338	80339	80340	80341	80342	80343	80344	80345	80346	80347	80348	80349	80350	80351	80352	80353	80354	80355	80356	80357	80358	80359	80360	80361	80362	80363	80364	80365	80366	80367	80368	80369	80370	80371	80372	80373	80374	80375	80376	80377	80378	80379	80380	80381	80382	80383	80384	80385	80386	80387	80388	80389	80390	80391	80392	80393	80394	80395	80396	80397	80398	80399	80400	80401	80402	80403	80404	80405	80406	80407	80408	80409	80410	80411	80412	80413	80414	80415	80416	80417	80418	80419	80420	80421	80422	80423	80424	80425	80426	80427	80428	80429	80430	80431	80432	80433	80434	80435	80436	80437	80438	80439	80440	80441	80442	80443	80444	80445	80446	80447	80448	80449	80450	80451	80452	80453	80454	80455	80456	80457	80458	80459	80460	80461	80462	80463	80464	80465	80466	80467	80468	80469	80470	80471	80472	80473	80474	80475	80476	80477	80478	80479	80480	80481	80482	80483	80484	80485	80486	80487	80488	80489	80490	80491	80492	80493	80494	80495	80496	80497	80498	80499	80500	80501	80502	80503	80504</

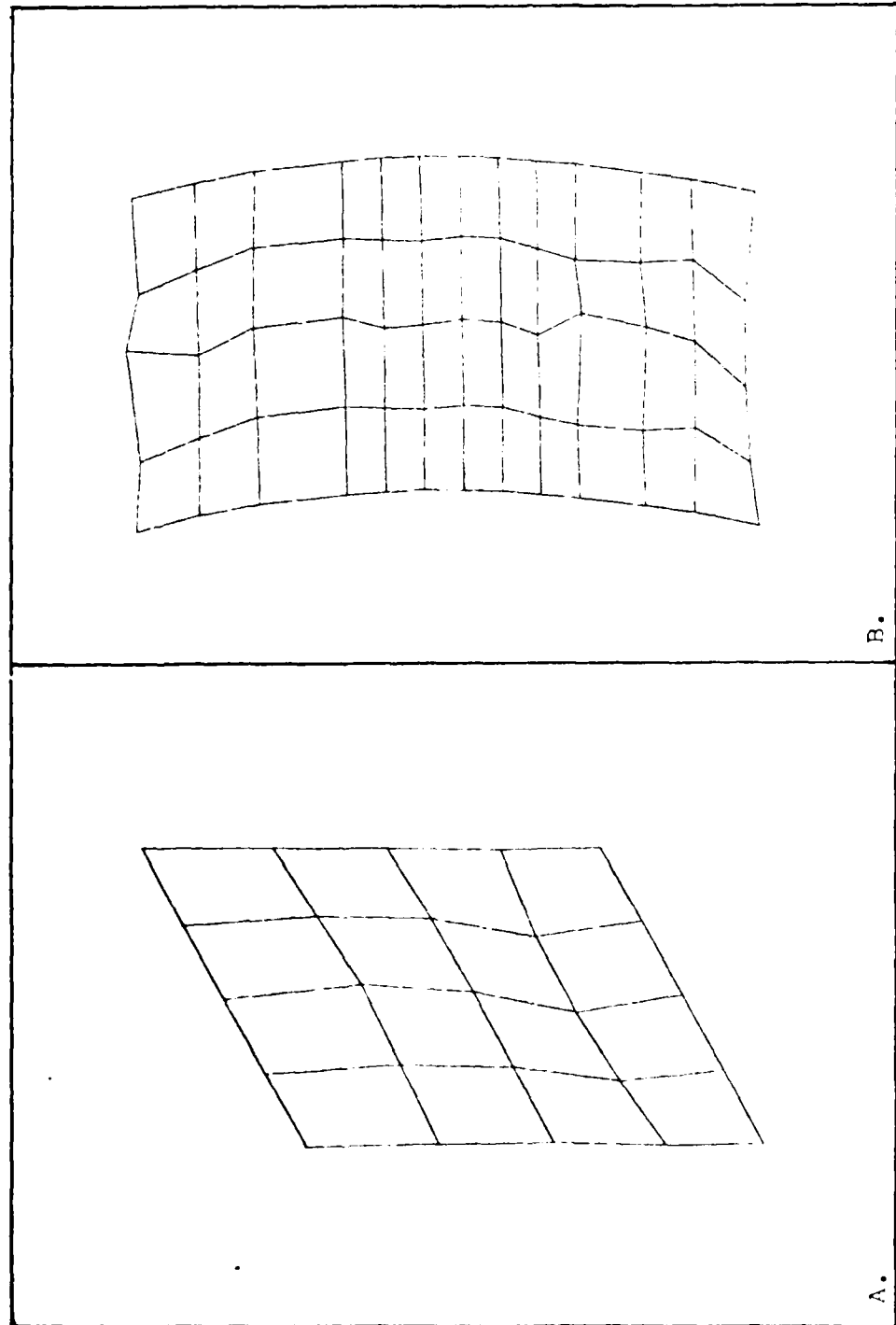


Figure 11. Sample Mode Shape Plots for A.) Smoother Stifferener Uniform Model (Discrete Stifferener Node Shapes Similar) and B.) Bay Nodes Model.

that the point did not lie on or near to a node line for any mode. Examination of the real and imaginary parts of the Transfer Function for that grid point revealed the natural frequencies for that particular model and configuration. Detailed modal analysis and test procedures are contained in Appendix B. Data acquisition programs for use in the Hewlett-Packard HP-5451B Fourier Analyser are presented in Appendix C.

Once the natural frequencies for a particular mode/configuration had been identified, the Transfer Function data from each point on the grid in question were reduced to yield mode shape vectors for each mode. For purposes of comparison with the finite element method the discrete mode shape vectors were converted to a format identical to NASTRAN output. NASTRAN data were processed using a standard graphics package, GCSNAST (Ref 6), which was used to display plots of the undeformed versus deformed mode shapes in both unloaded and mass-loaded configurations.

Results

Modal Assurance Criteria Function test results are presented in Table 2. Corresponding results from the Modal Analysis testing are shown in Table 3. Comparison of the data in these two tables reveals numerous areas of disagreement in the natural frequencies of each configuration. This apparent discrepancy can be explained

Table 3. Experimental Natural Frequencies Obtained Using Modal Analysis Software (Ref 2) and Bay Modes Model.

Mode Number	Unloaded	Configuration					7	% Chg
		2	% Chg	6	% Chg	7		
1	179.905	---	---	---	---	---	---	---
2	190.627	---	---	---	---	---	---	---
3	207.25	203.43	- 1.84	209.30	+ .99	---	---	---
4	238.63	---	---	239.65	+ .43	---	---	---
5	252.20	---	---	253.18	+ .39	255.91	+ 1.47	---
6	279.93	---	---	280.14	+ .08	---	---	---
7	292.69	273.25	- 6.64	294.16	+ .50	---	---	---
8	298.94	---	---	300.60	+ .56	---	---	---
9	311.67	326.04	- 4.29	340.82	+ .04	342.17	+ .44	---
10	311.50	363.79	+ .91	---	---	363.61	+ .86	---
11	376.16	---	---	369.01	- 1.90	371.89	- 1.14	---
12	383.87	---	---	383.65	- .06	383.22	- .17	---
13	425.12	---	---	425.26	+ .03	426.13	+ .24	---
14	454.09	454.63	+ .12	---	---	---	---	---

when one considers the test technique from which each set of data were obtained. The MAC testing used response data from a fixed reference accelerometer and a moveable accelerometer, and 15 impulse excitations which were randomly spaced over the entire panel. The spatial randomness of the excitations enhanced the probability that every mode in the structure would be excited in that not every excitation would lie on a node line. In contrast, the Modal Analysis testing used a fixed excitation point in conjunction with a moveable accelerometer to measure the structural forced response. Inherent in the latter technique is the assumption that the chosen excitation point never lies on or near to a node line and thus the mode shapes obtained from this technique represent a unique set of modal data. Therefore, if the chosen excitation point lies on or near to a node line, some modes may be "missed" during examination of Transfer Function data because these modes were never excited to begin with. In this respect it would appear that the MAC function data may be the more accurate data. Since a comparison of modal prediction techniques is the thrust of this report this comparison will be carried out only on those data for which corresponding results in the MAC Function data are available. This comparison method will be used throughout the remainder of this report.

III The Whaley Algorithm Method

Overview

The algorithm developed by Whaley (Ref 13) and subsequently used by Glenesk (Ref 3) substitutes suitable expressions for the kinetic and potential energy of a flat plate into Lagrange's equations of motion. Then, taking the first variation of the expression for the virtual work of the applied inertial loads with respect to the generalized coordinate, the expression for the generalized force, Q_i , is obtained. The final form of this expression is

$$Q_i = \frac{\delta P}{\delta q_i} = -M_o \phi_i(x_o, y_o) \sum_{j=1}^{\infty} \phi_j(x_o, y_o) \frac{d^2 q_j}{dt^2} - M_o R_x \frac{2 \partial \phi_i}{\partial x}(x_o, y_o) \sum_{j=1}^{\infty} \frac{\partial \phi_j}{\partial x}(x_o, y_o) \frac{d^2 q_j}{dt^2} - M_o R_y \frac{2 \partial \phi_i}{\partial y}(x_o, y_o) \sum_{j=1}^{\infty} \frac{\partial \phi_j}{\partial y}(x_o, y_o) \frac{d^2 q_j}{dt^2}. \quad (5)$$

Equation 5 contains the effects of the inertial forces due to the added lumped mass (M_o , R_x , R_y , x_o , and y_o) which are proportional to the second derivative of the generalized coordinate, $\frac{d^2 q_j}{dt^2}$ or \ddot{q}_j . These effects, in turn, become additions to the mass matrix when the eigenvalue problem is solved for natural frequencies and mode shapes.

Results

The results from Whaley's algorithm are summarized from Glenesk (Ref 3) in Tables 4, 5, and 6. The data generated using the MAC Function were merged with Whaley's algorithm (Ref 13) to yield the Whaley Algorithm results. Glenesk (Ref 3) noted that a comparison of unloaded versus mass-loaded mode shapes was the means of determining the unloaded/predicted mass-loaded frequency pairings.

Examination of the data in Tables 4, 5, and 6 reveals the largest percentage error between actual and predicted values occurred on Configuration 7 (Table 6, Mode 1) whereas the smallest percentage error value occurred on Configuration 2 (Table 4, Mode 9). With the exception of Mode 1, Configuration 7, all predicted frequency values were within $\pm 7.5\%$ of the experimentally measured values.

Table 7 presents a comparison of the absolute percentage in frequency shift from the unloaded panel to each of the three mass-loaded configurations. The largest percentage frequency shifts occur when the largest mass was located on an unsupported portion of the panel skin. With the exception of modes 8 and 9 for Configuration 6, all frequency shifts were within $\pm 3\%$ of the unloaded frequency.

Table 4. Data Results - Configuration 1 (Extracted from Ref 3).

Mode	Testing Techniques		Percent error
	Modal Assurance Criteria	Whaley Algorithm	
1	()	167.79	()
2	174.08	180.15	3.49
3	187.62	191.13	1.87
4	204.00	206.43	1.19
5	225.31	237.37	5.35
6	243.32	251.86	3.51
7	263.80	279.61	5.99
8	282.45	291.95	3.36
9	363.08	362.76	-0.09

Table 5. Data Results - Configuration 6 (Extracted from Ref 3).

Mode	Testing Techniques		Percent error
	Modal Assurance Criteria	Whaley Algorithm	
1	169.71	166.22	-2.06
2	180.72	175.34	-2.98
3	199.30	191.23	-4.05
4	208.27	205.63	-1.27
5	238.22	235.20	-1.27
6	252.20	251.18	-0.40
7	279.95	278.44	-0.54
8	292.20	271.14	-7.21
9	360.20	338.70	-6.11

Table 6. Data Results - Configuration 7 (Extracted from Ref 3).

Mode	Testing Techniques		Percent error
	Modal Assurance Criteria	Whaley Algorithm	
1	143.10	167.77	17.24
2	175.09	180.20	2.91
3	184.83	191.16	3.44
4	204.30	206.98	1.31
5	238.22	237.33	-0.37
6	257.50	250.45	-2.73
7	279.88	278.70	-0.42
8	292.76	292.48	-0.09
9	361.71	364.39	0.74

Table 7. Percentage of Frequency Shift Using Whaley's Algorithm versus Unloaded Measured Data (Extracted from Ref 3).

Mode Number	Unloaded Panel 1	Configuration 2 Predicted	Percent Change	Configuration 6 Predicted	Percent Change	Configuration 7 Predicted	Percent Change
1	167.93	167.79	-.0834	165.22	-1.0183	167.77	-.0953
2	180.50	180.15	-.1939	175.34	-2.8587	180.20	-.1662
3	191.22	191.13	-.0471	191.23	.0052	191.16	-.0313
4	207.31	206.43	-.4245	205.63	-.8104	206.98	-.1592
5	237.74	237.37	-.1556	235.20	-1.0684	237.33	-.1725
6	252.12	251.86	-.1031	251.18	-.3728	250.45	-.6624
7	280.02	279.61	-.1464	278.44	-.5642	278.70	-.4714
8	292.83	291.95	-.3005	271.14	7.4070	292.48	-.1195
9	365.00	362.76	-.6134	338.70	-7.2055	364.39	-.1671

IV The Finite Element Method

Overview

Several excellent finite element codes for structural analysis are presently in existence. One such widely used program, NASTRAN (NASA Structural ANalysis, Ref 9,11), was selected for use in the finite element modelling and modal analysis of the structure. This code includes the general 20 degree-of-freedom quadrilateral elements (CQUAD2) and 12 degree-of-freedom bar elements (CBAR) of which the test structure was constructed. NASTRAN also contains provisions to allow for the offset of the neutral axes of the bar elements from the grid points which were defined at the midsurface of the panel skin. Thus, the cross-sectional and spatial properties of each component stiffener could be included in the analysis. Only the out-of-plane component of the vibration (i.e. - radial component for curved models and z-component for the flat model) was investigated.

Finite Element Models

Three finite models were constructed to coincide with the test grids described in Section II. The Smear-ed Stiffener Uniform Model considered the panel to be a flat plate (Ref 3). This model did not extend to the panel extremities but was inset somewhat from the panel

edges (Figure 2) to coincide with the grid used by Glenesk (Ref 3). The mass of the entire panel including stiffeners was smeared over this grid to provide a uniform thickness model with homogeneous material properties. Although the mass of this model was identical to the overall structure mass, this model was more dense than had it been extended to the geometric test panel boundaries. It consisted of 25 grid points from which data were obtained and 16 quadrilateral elements.

The Discrete Stiffener Model (Figure 4) was constructed to allow for panel curvature, discrete stiffener geometries (i.e. - different cross-sections), and the offset of the stiffener neutral axes from the panel surface. This model was designed to faithfully represent the panel from a structural standpoint while maintaining the 25 grid points of the Smeared Stiffener Uniform Model. Forty-four bar elements, 25 grid points, and 16 quadrilateral elements were used in this model.

The Bay Modes Model (Figure 5) was included to investigate the motion of each of the four internal bays. This model was an extension of the Discrete Stiffener Model in that two extra sets of five grid points per bay were added to that model to derive this model. This model was constructed of 65 grid points, 48 quadrilateral elements, and 76 bar elements.

Appendix C contains a sample of the Bulk Data Decks

which were used to generate model data for these models.

Results

Only the Bay Modes Model results (Tables 8 through 11) will be discussed since this model yielded the best representation of the overall panel motion. As in the use of the Whaley Algorithm, a pairing of unloaded versus mass-loaded mode shapes (Figure 12) was used to track the change in natural frequency between the unloaded panel and each mass-loaded configuration. Upon observation of Figure 12 it is seen that this process is somewhat subjective in nature in that the mode shapes do not remain completely unaltered. It is left to the discretion of the engineer to properly select the mode pairings, and herein lies a potential source of error. In an attempt to have this mode pairing as unbiased as possible, the author consulted another engineer to independently aid him in this process. Mode pairings which were not in agreement between the author and the other engineer were discussed and a consensus of opinion arrived at. The results from this mode shape pairing exercise are presented in Table 12. Here absolute changes in natural frequency from the unloaded to mass-loaded panel range from essentially zero-% (Mode 20, Configuration 2) to -20.3-% (Mode 16, Configuration 6). Out of 57 such pairings, the frequency shift from the unloaded to the mass-loaded panel in was within $\pm 7.5\%$ of the unloaded panel in 79 percent of the pairings.

Table 8. NASTRAN Modal Data - Unloaded Panel.

Table 9. NASTRAN Modal Data - Configuration 2.

Table 10. NASTRAN Modal Data - Configuration 6.

Table 11. NASTRAN Modal Data - Configuration 7.

NODE NO.	EXTRACTION DEPTH	EIGENVALUE	REAL FITTING VALUES		GENERAL MASS
			ENHANCING FACTORY	CYCLIC FACTORY	
1	62	1.220412e-04	1.391316e-02	1.745430e-03	4.484316e-12
2	41	3.432165e-02	1.031827e-01	3.627685e-09	1.658388e-03
3	66	1.772425e-04	1.616427e-02	2.51331e-01	1.558327e-01
4	49	7.505610e-06	2.451414e-02	4.522561e-01	4.533543e-01
5	14	1.914810e-05	8.023434e-02	9.833067e-01	2.772244e-01
6	61	1.013540e-05	1.492150e-02	1.537370e-01	1.673130e-01
7	51	1.013540e-05	1.492150e-02	1.537370e-01	1.673130e-01
8	40	1.013540e-05	1.492150e-02	1.537370e-01	1.673130e-01
9	31	1.013540e-05	1.492150e-02	1.537370e-01	1.673130e-01
10	20	1.013540e-05	1.492150e-02	1.537370e-01	1.673130e-01
11	11	1.013540e-05	1.492150e-02	1.537370e-01	1.673130e-01
12	1	1.013540e-05	1.492150e-02	1.537370e-01	1.673130e-01
13	12	1.013540e-05	1.492150e-02	1.537370e-01	1.673130e-01
14	21	1.013540e-05	1.492150e-02	1.537370e-01	1.673130e-01
15	30	1.013540e-05	1.492150e-02	1.537370e-01	1.673130e-01
16	39	1.013540e-05	1.492150e-02	1.537370e-01	1.673130e-01
17	28	1.013540e-05	1.492150e-02	1.537370e-01	1.673130e-01
18	17	1.013540e-05	1.492150e-02	1.537370e-01	1.673130e-01
19	26	1.013540e-05	1.492150e-02	1.537370e-01	1.673130e-01
20	35	1.013540e-05	1.492150e-02	1.537370e-01	1.673130e-01
21	24	1.013540e-05	1.492150e-02	1.537370e-01	1.673130e-01
22	34	1.013540e-05	1.492150e-02	1.537370e-01	1.673130e-01
23	23	1.013540e-05	1.492150e-02	1.537370e-01	1.673130e-01
24	33	1.013540e-05	1.492150e-02	1.537370e-01	1.673130e-01
25	22	1.013540e-05	1.492150e-02	1.537370e-01	1.673130e-01
26	32	1.013540e-05	1.492150e-02	1.537370e-01	1.673130e-01
27	21	1.013540e-05	1.492150e-02	1.537370e-01	1.673130e-01
28	31	1.013540e-05	1.492150e-02	1.537370e-01	1.673130e-01
29	20	1.013540e-05	1.492150e-02	1.537370e-01	1.673130e-01
30	29	1.013540e-05	1.492150e-02	1.537370e-01	1.673130e-01
31	19	1.013540e-05	1.492150e-02	1.537370e-01	1.673130e-01
32	28	1.013540e-05	1.492150e-02	1.537370e-01	1.673130e-01
33	18	1.013540e-05	1.492150e-02	1.537370e-01	1.673130e-01
34	27	1.013540e-05	1.492150e-02	1.537370e-01	1.673130e-01
35	17	1.013540e-05	1.492150e-02	1.537370e-01	1.673130e-01
36	26	1.013540e-05	1.492150e-02	1.537370e-01	1.673130e-01
37	16	1.013540e-05	1.492150e-02	1.537370e-01	1.673130e-01
38	25	1.013540e-05	1.492150e-02	1.537370e-01	1.673130e-01
39	15	1.013540e-05	1.492150e-02	1.537370e-01	1.673130e-01
40	24	1.013540e-05	1.492150e-02	1.537370e-01	1.673130e-01
41	14	1.013540e-05	1.492150e-02	1.537370e-01	1.673130e-01
42	23	1.013540e-05	1.492150e-02	1.537370e-01	1.673130e-01

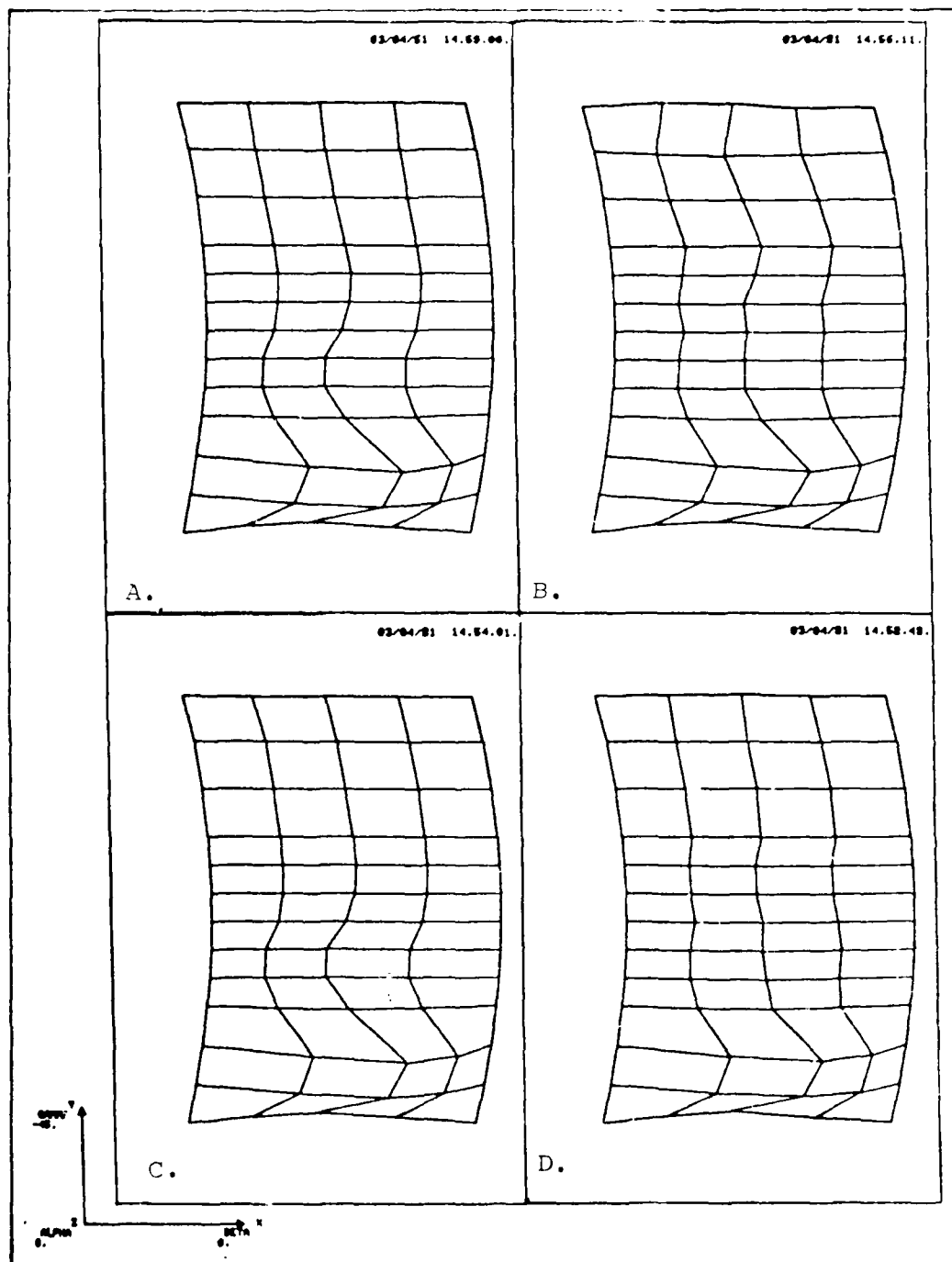


Figure 12. Mode shapes, Bay Modes Finite Element Model, for A.) Clean Panel (206.76 Hz), B.) Configuration 2 (208.11 Hz), C.) Configuration 6 (206.42 Hz), and D.) Configuration 7 (213.31 Hz).

Table 12. Natural Frequency Pairings Obtained Using NASTRAN (Ref 11).

Mode Number	Unloaded	2	% Chg	Configuration	6	% Chg	7	% Chg
1								
2	100.60	--		118.55	+17.84		--	+1.15
3	102.17	--		--			103.35	
4	169.27	174.36	+3.01	--			168.64	-.37
5	184.45	184.05	-.22	179.72	+ 2.56		184.47	+.01
6	190.38	190.53	+.08	190.45	+.04		190.45	+.04
7	198.67	219.90	+10.69	173.20	-12.82		197.47	-.60
8	206.56	208.14	+.76	206.42	-.07		213.84	+3.52
9	239.59	240.24	+.27	248.20	+ 3.59		239.61	+.00
10	244.67	249.73	+.02	249.70	+.01		249.81	+.01
11	250.38	285.99	+10.26	--			260.14	+.29
12	262.53	246.84	-5.98	217.53	-17.14		307.79	+17.24
13	307.55	353.52	+14.95	310.19	+.86		321.28	+4.46
14	328.18	328.86	+.21	316.72	-.349		328.80	+.19
15	333.66	--		310.34	+ 2.00		362.34	+8.60
16	346.52	369.17	+6.54	276.86	-20.30		353.48	+2.01
17	365.45	364.73	-.20	362.51	-.80		--	--
18	382.59	--		387.69	+ 1.33		--	--
19	388.56	381.98	-.92	--			--	--
20	403.10	403.07	+.00	--			402.28	-.20
21	418.59	418.76	+.00	418.53	+.00		422.93	+1.04
22	448.55	445.15	-.76	443.41	-.1.15		386.61	-13.81
23	466.20	456.04	-2.18	466.30	+.02		469.56	+ .72
24	472.36	472.04	-.07	469.64	-.58		472.32	-.01
25	478.33	--		478.10	-.05		--	--

and within \pm 3% of the unloaded panel 70 percent of the time.

V The Use of Pseudoinverses in the Recovery of the Discrete Mass, Stiffness, and Damping Matrices and Solution of the Mass-Loaded Problem

Overview

The method suggested by Briggs and Whaley (Ref 1) solves the general matrix-vector differential equation using generalized coordinates to obtain the definitions of equations 1 through 3. Then, using modal data obtained from standard vibration test methods, and suitable matrix manipulations (See Appendix A), equations 1 through 3 are solved for the mass, stiffness, and damping matrices. The usual method of solution requires a square modal matrix which is inverted in the solution for these matrices. However, in general, this matrix may be rectangular with more rows (grid points) than columns (mode vectors). Thus, one would like to have a means to solve equations 1 through 3 when the modal matrix is non-square. The pseudoinverse (Ref 8) presents such a method for inverting rectangular matrices and thus potentially for a more general solution to these equations.

Data Reduction

A computer program was developed to take the experimentally determined unloaded modal data, compute

the unloaded modal matrix and required inverses, and solve for the unloaded mass, stiffness, and damping matrices. Since only the natural frequencies and their resulting mode shapes were of interest in this study, the standard eigenvalue problem posed by equation 4 was solved with suitable additions of mass in the mass matrix for the mass-loaded natural frequencies and mode shapes. Appendix B contains a more detailed explanation of the data reduction process; Appendix C contains a copy of the program used for data reduction.

Results

An extremely simplified experimental set up consisting of nine grid points was used for each mass-loaded configuration (Figure 13) to demonstrate the validity of the computer program before extension to the more general pseudoinverse case was attempted. The structure was tested in both unloaded and three discrete mass-loaded configurations from which nine frequency/mode shape pairs were identified for each unloaded/mass-loaded configuration (Figure 14). The nine modal vectors were used to form a square 9 X 9 modal matrix; the nine natural frequencies were used to form the matrix on the right side of equation 2. Then, using the technique described in Appendix B, the unloaded mass and stiffness matrices were recovered, and a quantity of mass equal to the added mass

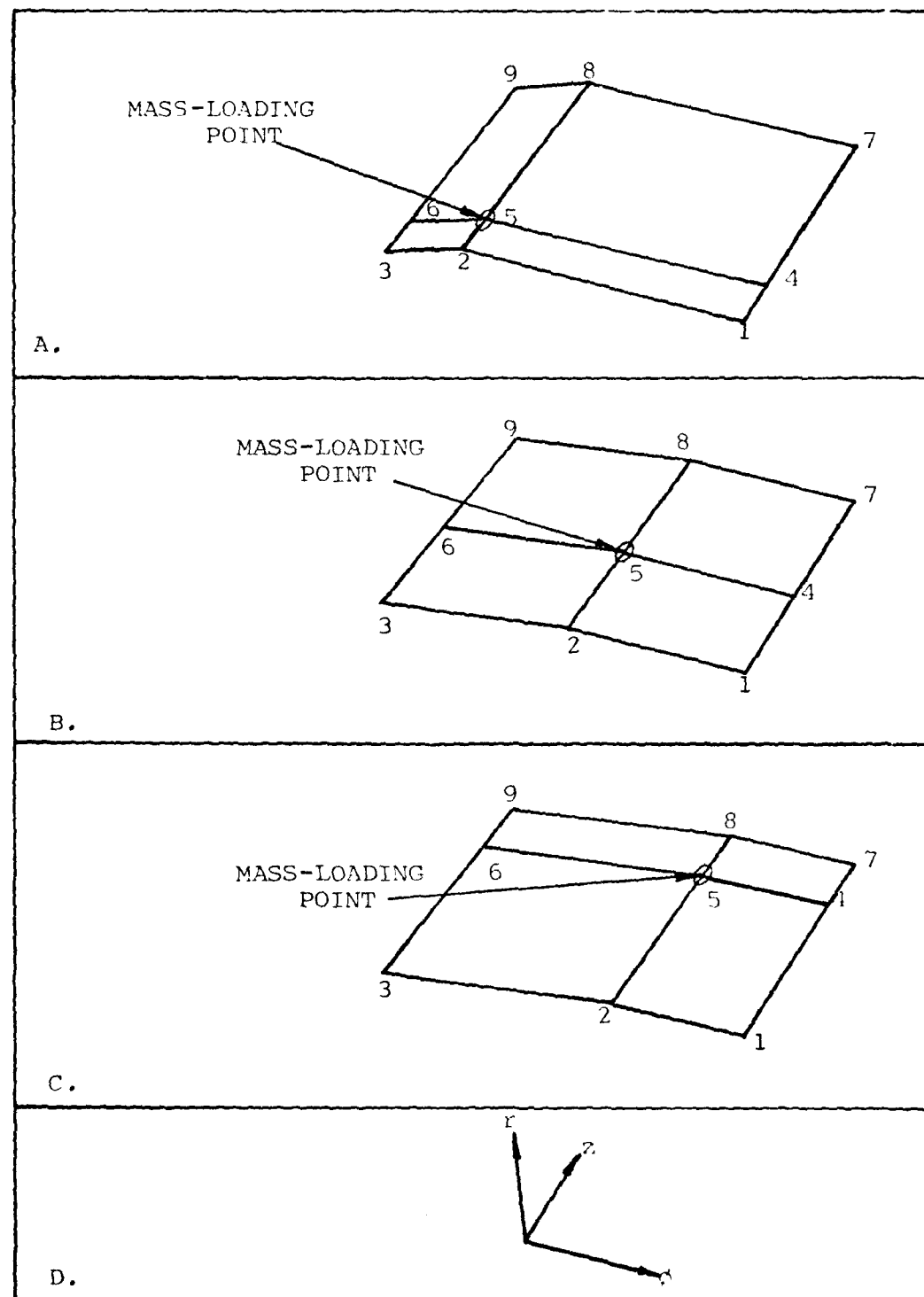


Figure 13. Nine point coarse grid (unloaded) for A.) Configuration 6, B.) Configuration 2, and C.) Configuration 7 with D.) Cylindrical Coordinate System.

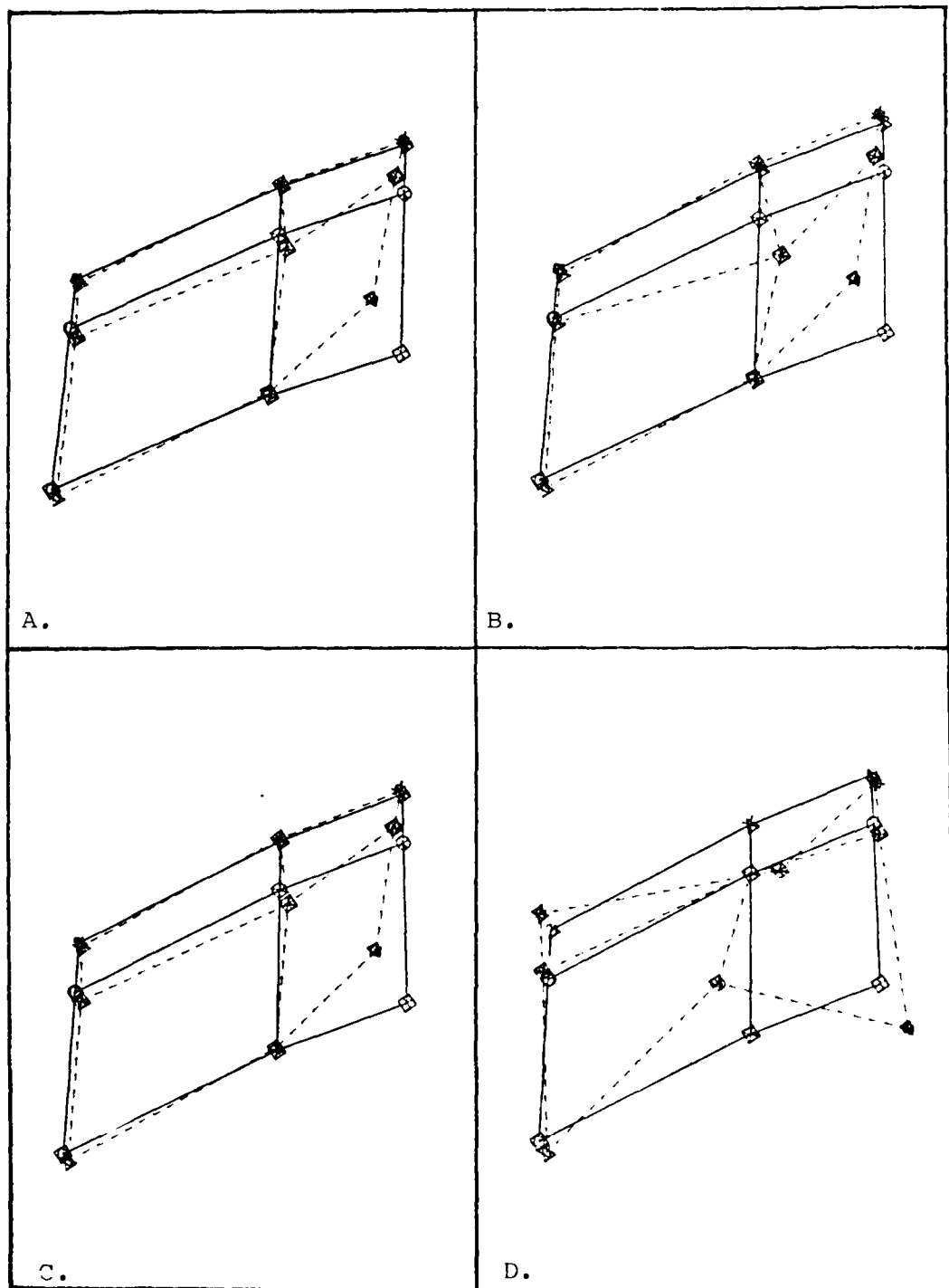


Figure 14. Nine point coarse grid mode shapes, Configuration 7, Mode 1, for A.) Unloaded Panel (169.437 Hz), B.) Loaded Panel (139.975 Hz), C.) Square Modal Matrix Prediction (168.847 Hz) and D.) Pseudoinverse Prediction (169.437 Hz). (Deformed panel denoted by dotted lines)

was added to the 5,5 term (i.e., the mass loading point, See Figure 13) of the mass matrix. Finally, equation 4 was solved using a generalized eigenvalue routine, EIGZF (Ref 5), for the mass-loaded natural frequencies and mode shapes. These predicted mode shapes were then compared to the actual measured mode shapes to verify that the program had successfully predicted both the correct natural frequency and its corresponding mode shape. From this mode shape comparison (Tables 13, 14, and 15) it was determined that the program using a square modal matrix had correctly predicted the frequency within $\pm 5\%$ error 24 out of 27 times, and with $\pm 10\%$ error 26 out of 27 times. These data are presented in Tables 13, 14, and 15.

Next, the last column of the modal matrix and the last row and column of the matrix of natural frequencies squared were deleted to simulate a case where fewer than "n" modes were measured where "n" is the number of grid points (or rows in the modal matrix). The modified 9 X 8 modal matrix was then inverted, and 9 X 9 mass and stiffness matrices were generated. The mass matrix was perturbed by addition of a quantity of mass equal to the mass loading configuration at the 5,5 location, and the general eigenvalue problem was again solved using EIGZF. Upon examination of the actual unloaded and predicted mass-loaded pseudoinverse frequency data, it was found

Table 13. Frequency Prediction - Square and Rectangular Modal Matrix, Configuration 2.

UNLOADED EXPERIMENTAL DATA	PREDICTED MASS-LOADED USING SQUARE MODAL MATRIX	ACTUAL MASS-LOADED EXPERIMENTAL DATA	PERCENT ERROR PREDICTED VERSUS ACTUAL	PREDICTED MASS-LOADED USING PSEUDOINVERSE (494.881, 803.553)	PERCENT ERROR PREDICTED VERSUS ACTUAL
137.275	137.201	144.672	+6.41	137.275	+6.41
207.085	205.117	202.548	-1.24	207.085	-2.01
239.182	237.659	238.515	+0.36	239.182	+0.36
280.553	277.785	276.142	-0.50	280.553	-2.06
294.848	290.891	301.519	+3.22	294.848	+2.21
327.881	327.649	325.245	-1.36	327.881	-1.43
394.224	394.041	401.578	+1.88	394.224	+1.53
414.164	414.102	414.504	+0.90	414.164	+0.68
453.688	453.645	456.524	+0.63	453.688	100.00

Table 14. Frequency Prediction - Square and Rectangular Modal Matrix, Configuration 6.

UNLOADED EXPERIMENTAL DATA	PREDICTED MASS-LOADED USING SQUARE MODAL MATRIX	ACTUAL MASS-LOADED EXPERIMENTAL DATA	PERCENT ERROR PREDICTED VERSUS ACTUAL	PREDICTED MASS-LOADED USING PSEUDOINVERSE (494.881, 803.553)	PERCENT ERROR PREDICTED VERSUS ACTUAL
167.266	158.593	165.205	+5.73	167.266	+6.1
180.424	180.083	180.711	+0.35	180.424	+0.16
207.288	204.739	208.393	+1.75	207.288	+0.93
228.543	220.920	220.976	+0.33	228.543	+0.43
238.530	230.224	238.062	+0.4	238.530	+0.14
279.684	275.747	279.764	+1.44	279.684	+0.9
299.232	295.634	293.175	-0.91	299.232	-2.07
303.621	301.653	300.294	-0.52	303.621	-1.11
328.523	327.008	324.819	-0.97	328.523	100.00

Table 15. Frequency Prediction - Square and Rectangular Modal Matrix, Configuration 7.

UNLOADED EXPERIMENTAL DATA	PREDICTED MASS-LOADED USING SQUARE MODAL MATRIX	ACTUAL MASS-LOADED EXPERIMENTAL DATA	PERCENT ERROR PREDICTED VERSUS ACTUAL	PREDICTED MASS-LOADED USING PSEUDOINVERSE (494.881, 803.553)	PERCENT ERROR PREDICTED VERSUS ACTUAL
169.437	169.497	170.671	+7.03	169.437	+7.03
181.251	180.970	179.532	-2.42	181.251	-2.79
206.396	205.147	204.455	-0.59	206.396	-1.05
206.643	206.507	206.605	+0.71	206.643	+0.97
238.039	237.175	239.030	+0.61	238.039	+0.5
238.212	238.153	238.000	-0.21	238.212	+0.19
279.993	279.777	280.656	+0.30	279.993	+0.23
451.669	451.673	453.664	+0.88	451.669	+0.58
484.487	484.487	486.076	+1.24	484.487	100.00

that these data are identical to six decimal places. Of even more concern is the fact that the predicted mode shapes were quite different from the measured mode shapes. Thus, from this preliminary investigation, it did not appear that the method employing pseudoinverses would yield valid results and further attempts at its use were abandoned.

However, it was demonstrated that the method using square modal matrices will yield valid results. One drawback in the use of square modal matrices in this method is that when one increases the dimension of the modal matrix (i.e. - the number of grid points or rows), a corresponding number of mode shape vectors and natural frequencies must be generated. At the outset of this report it was pointed out that for larger numbers of grid points this may be both undesirable and that it may not be possible to obtain a large number of natural frequencies. Thus, there is a need to limit the number of grid points when one models the structure in question. Unfortunately, there is at present no general method to predict the number of natural frequencies/modes within a given frequency range. The solution to this problem may be to initially begin with a simplified nine point grid, test the unloaded structure and reduce the Transfer Function data to obtain the number of natural frequencies/modes in the specific frequency range of interest.

This number of natural frequencies/modes will give an indication of the maximum number of grid points available if one wishes to refine this grid and use the square modal matrices. Since the Transfer Function data theoretically contain the same information for any grid point unless the response accelerometer for a particular grid point was situated on a node line, it is not required to initially increase the number of grid points above nine. During data reduction to determine the maximum number of natural frequencies (or grid points), it will thus be advantageous to reduce the data from more than one grid point to insure that no modes were "missed" due to a given accelerometer being inadvertently placed on a discrete node line.

VI Discussion of the Method

General

As with any endeavour of this type, a learning curve is associated with one's ability to use unfamiliar equipment, software, and testing/modelling techniques. This was especially true for the author who had no previous experience in modal analysis testing, with the associated data reduction techniques, nor with finite element modelling procedures. Thus, the author was in a unique position to be able to evaluate the three modal analysis techniques which are the subject of this report. Admittedly this assessment of the three methods will be only one person's viewpoint and, as such, is somewhat subjective in nature. However, it represents the viewpoint of one who was previously uninitiated in this area of expertise. The evaluation of each method will be presented separately in the successive paragraphs of this section.

At the outset of this investigation it was cited that the Modal Analysis Software developed by Brown (Ref 2) would be used as a datum for comparing the methods. However, because the mode shapes from Brown's software and NASTRAN were quite different, such a comparison between experimental data and NASTRAN data was not possible. Furthermore, since the method using pseudoinverses was abandoned in favor of square, invertible 9×9 modal

matrices, and extension to either 25- or 65- grid points was not possible due to a lack of a sufficient number of natural frequencies in the specific range from 0-500 Hz, a comparison of this method to Brown's software was likewise not possible. Neither was it possible to tie Glenesk's modal data to corresponding modal data generated by Brown's software due to lack of sufficient modal data in Glenesk's report (Ref 2). Thus, each method will be discussed as fully as possible while keeping these limitations in mind.

The Whaley Algorithm

The results obtained from use of the Whaley Algorithm were extracted directly from Reference 3 and are presented in Tables 4 through 6. Because the author did not directly use this algorithm, the author is unable to present an evaluation of the difficulties encountered in obtaining results from this method. However, when one considers the modes which were predicted by the algorithm when modal testing did not reveal such a mode, one can envision serious limitations to its use. As previously noted, Glenesk reported a degradation in algorithm performance as the size of the added lumped mass increased relative to the overall structure mass. Thus, an as yet undetermined upper bound exists, beyond which the predicted mode shapes and natural frequencies will cease to have an acceptable degree of accuracy.

The use of this algorithm requires one to obtain modal data on the unloaded structure before the mass-loaded modal quantities can be predicted. This requires modal testing facilities, test hardware, and the necessary software for conducting the required Fourier analysis on the Transfer Function data. This can mean a significant commitment in terms of resources (manpower, money, testing facility, etc). However, with the advent of portable modal analysis equipment, this investment in resources is expected to decline rapidly. One factor not as easily evaluated is the level of expertise required to successfully conduct the required modal testing and subsequent data reduction in order to obtain valid results. It was the author's experience that one must rely heavily upon "experts" in this field to avoid the pitfalls of questionable test procedures or of an invalid data analysis. The knowledge required to successfully conduct the testing and data analysis is one of those intangible factors upon which it is extremely difficult to place an evaluation.

The one serious limitation inherent in the use of this algorithm is that it will not predict mass-loaded mode shapes. Instead, it considers the mode shapes to be unaltered by the addition of mass to the structure. Although unaltered mode shapes were observed, they were

randomly scattered throughout the experimental data. It is the opinion of the author upon review of the experimental data that even with a frequency shift the mode shapes were altered far more often than not. This is not believed to be a function of experimental methodology or questionable data, but rather an actual occurrence in nature.

The Finite Element Method

Again, as in the case of the modal analysis testing, a learning curve was associated with the use of the finite element method as presented in NASTRAN. Unlike modal analysis testing where the methodology used to obtain and reduce the data is all important, the author found the structural modelling technique, especially modelling of the boundary conditions, to be critical in obtaining good results. Since the structure was supported by bungy cords, the support conditions fell somewhere between the "free-free" case and the "clamped-clamped" case at the panel boundaries. Thus, it was not possible to clamp the finite element model at the edges, nor was it possible to allow the panel to be totally unrestrained. Several methods of modelling the boundary conditions were used to determine the model which most closely approximated the actual boundary conditions. Among the methods tried were the restraint of rigid body modes by

modelling the bungey cords as long slender rods with small stiffness, the use of the SUPPORT card or SPC1 cards to restrain suitable degrees-of-freedom at three non-collinear grid points on the panel edges, and the use of the SUPPORT card to restrain all six degree-of-freedom at one selected grid point. In the latter case a CONM2 card was used with small mass and inertia values at the selected grid point to alleviate the singularity in the mass matrix imposed by restraining six degrees-of-freedom at the same grid point. The technique using SPC1 cards was chosen as the best method to model the supports.

In general, each finite element model generated a greater number of natural frequencies (Tables 8 through 12) than the MAC function test results (Tables 2, 4, 5, and 6) indicated were present in the frequency range from 0-500 Hz. However, when the finite element results (Table 12) were compared to Modal Analysis test results (Table 7), approximately the same number of natural frequencies were obtained using these two methods. Although the quantity of frequencies obtained using the finite element method was approximately the same as those obtained from Modal Analysis results and the frequencies were numerically similar, it became apparent upon comparison of the mode shapes from numerically similar frequencies that mere numerical similarity of the natural frequencies was inadequate by itself as a criterion for comparing the

Modal Analysis test results with similar results from NASTRAN. As the desired means of comparison of these two sets of data was a "pairing" of "like" mode shapes, it was unfortunate that this was not possible due to the large discrepancy in mode shape versus natural frequency when the two sets of data were compared. Thus, a better means of comparing analytical to experimental data is needed and should be the subject of further research.

This failure in ability to compare experimental to analytical data presents a perplexing problem for the designer who wishes to minimize the vibrational effects on the hardware to be installed by placing the associated attachment hardware at points of minimum vibration. Which mode shapes does the designer believe? Even more distressing are the "additional" modes which were computed by NASTRAN. Do these modes really exist? Are they heavily damped modes which exist not far from the noise floor? Were these modes missed in the experimental testing due to an inadequate sampling bandwidth? Or are these "additional" modes purely "synthetic" modes generated by the solution software in NASTRAN but not actually existing in nature? These questions remain unanswered and are seen as a severe limitation of the "state-of-the-art" in vibration analysis.

Although a pairing of experimental versus analytical (finite element, NASTRAN-generated) mode shapes was not successful, no such lack of success was encountered when

pairing either NASTRAN-generated uncalled data to NASTRAN-generated mass-loaded data (Table 12 and Figure 12) or when corresponding Modal Analysis Software data (Table 3) were compared. Thus, both methods appear to be internally consistent when data generated by a particular method are compared.

Since the thrust of this investigation has been the comparison of techniques for predicting mass-loaded natural frequencies and mode shapes, and not to argue the validity of the experimental baseline data versus NASTRAN data, one would be inclined to agree that NASTRAN presents the easiest technique for the experienced designer to predict mass-loaded modal data. The basis for this is that if all the NASTRAN-predicted modal quantities really do exist, the designer has at his disposal all such data without the need for testing which might lead to incomplete results.

One area which has not been explored is the fact that the Modal Analysis Software uses a least-squares algorithm to fit the Transfer Functions for residues and phase angles in a given frequency range. In the generation of the Modal Analysis Software mode shapes, any phase angles generated due to a frequency shift between Transfer Functions were ignored. This, by itself, will result in non-orthogonal modal vectors. Since NASTRAN generates a set of mutually orthogonal modal vectors, it may be possible to compare the Modal Analysis data to the NASTRAN data if the effect

of phase angle (i.e. - frequency shift with grid point within a given mode) is included in the display of the Modal Analysis mode shapes. This capability is not presently available on the HP5451B Fourier Analyser used in the experimental phase of this effort. Should this capability be added in the future, the apparent discrepancy between the Modal Analysis and NASTRAN results may be eliminated.

The percentage in absolute frequency shift from the unloaded panel to the mass-loaded data are presented in Table 12. Unlike Whaley's Algorithm where all but two cases were within $\pm 3\%$ of the unloaded panel results, 17 out of 58 (29.3%) were greater than this $\pm 3\%$ frequency shift. Even more disturbing is the wide range of frequency shift indicated by mass-loading for some configurations (refer to Table 12, Modes 12, 16, and 22). Thus, it would appear that at least part of the NASTRAN data may be questionable.

A considerable expenditure of the author's time and computer resources was made in obtaining these results. For comparison purposes, the author kept records of the computer resources used to obtain the modal data for each of the three finite element models as well as for designing, debugging, and running the pseudoinverse program. These data are presented in Table 16. It should be emphasized that the author was totally inexperienced in the use of

NASTRAN at the outset of this effort; thus, the expenditure of resources for the finite element data using NASTRAN can be expected to be reduced by up to 75% by an engineer who is more experienced in the use of NASTRAN.

In view of the fact that the finite element method results did not compare favorably with the experimental results, one must answer the question whether the time and effort invested in obtaining these data was commensurate with comparable investments from the other two methods vis-a-vis their respective results. The answer lies in the accuracy required by the structural modification, and by the vibration sensitivity of the hardware to be installed. In the case of electro-optical devices which are known to be inherently vibration sensitive, it would appear that, time permitting, this investment of resources would be justified. However, one must weigh the desired/required results with the method used in each individual case. Thus, one of the other two methods (Whaley Algorithm or Matrix Recovery) may, with other less vibration sensitive installations, be optimal when all factors are considered.

Table 16. Computer Resources Used to Obtain Modal Results.

Parameter	Finite Element Models ¹		Pseudoinverse Matrix Recovery ²	
	Total	Average Per Run	Total	Average Per Run
Central Processor Unit Time (sec)	37590	178.16	3660	19.26
Input/Output Time (sec)	75155	356.18	4640	24.56
Computer Cost	\$4461.46	\$21.14	\$280.92	\$ 1.49

¹These data include post-processor time using GCSNAST for models up to 158 grid points.
²The data are for primarily nine grid point models and include post-processor time using DISSPLA.

The Use of Pseudoinverses In the Recovery of the Discrete Mass, Stiffness, and Damping Matrices, and Solution of the Eigenvalue Problem

The recovery of the mass and stiffness matrices and solution of the eigenvalue problem was considered by Whaley (Ref 16) for a two degree-of-freedom system and the case of a square modal matrix. When one extends this procedure to the case of a non-square modal matrix, the problem becomes more complicated because the mass matrix will in general be fully populated and thus the problem becomes a generalized eigenvalue problem (Ref. 8). A simple example for a three degree-of-freedom system is

presented in Appendix A. There it is shown that, when only two mode shapes and corresponding natural frequencies are considered, the resulting mass-loaded natural frequency and mode shape do not closely approximate the analytical solution. Thus, it does not presently appear that this method will yield accurate results for the case of a non-square modal matrix. Further research into this area is needed as an algorithm (technique) for predicting mass-loaded natural frequencies and shapes for the general (non-square modal matrix) case would be extremely useful.

Summary

The time invested in each method (including the use of Brown's software, Ref 2) was approximately equal. Although the author does not have such data on Whaley's method, it is assumed since Glenesk completed an independent study effort leading to a Master's degree that the effort expended in the use of Whaley's Algorithm would be comparable to the other methods. Each method has both drawbacks and good points, and the use of any one method over another will have to be seasoned with a great amount of engineering judgment.

VII Recommendations

In retrospect, it appears that the test item selected was much too ambitious for the comparison of the three modal analysis techniques. One suggested test item would be a uniform thickness flat plate. Many experiments have been performed on such an item and analysis of the uniform flat plate is included in many elementary vibrations textbooks (Ref 5). Once the methods have been tied together using this simplified model, modifications to the structure could be added one at a time and the process would be repeated. Thus one would gain faith in the three methods and, at the same time, gain valuable experience concerning the interactions between the various structural components.

Along the same line of the gradual increase in structural complexity is the incremental increase in the added point masses. It is envisioned that this small incremental change in added mass would significantly aid in tracking frequency shifts during the method comparison phase by allowing better visual comparison of the various unloaded and mass-loaded mode shapes.

The fact that phase angles different from zero were present in the experimental data gives rise to the question "Were these real modes?" Specifically, this question is precipitated because a mode shape which can be visually

observed is inherently real-valued with no phase angle between the peaks in the Transfer Functions at a given frequency. If, in fact, a complex mode did exist, a complex display would be necessary to properly observe the behaviour of the structure. Further research on the subject of complex-valued mode shapes is beyond the scope of this report but should be pursued in the future.

One area using the square/rectangular modal matrix which has not as yet been investigated is the addition of a structure such as a tripod which connects three or more grid points. Hence, off-diagonal terms are generated in the mass and stiffness matrices which further complicate the issue because the subject of finite element modelling of the tripod structure (or any other added structure) enters the picture. It is the author's opinion that this would be an interesting problem for one who is interested in furthering the research in this area.

Bibliography

1. Briggs, H.C., and Whaley, P.W., "Theis Topic Proposal," Air Force Institute of Technology, Wright-Patterson AFB, Ohio, January 1980.
2. Brown, D. Modal Analysis Software, User Program Nine, Hewlett-Packard 4451 Fourier Analysis System, Modal Analysis User's Guide, (Rough Draft), Cincinnati, Ohio: University of Cincinnati, September, 1980.
3. Glenesk, Larry D. The Prediction of Mass Loaded Natural Frequencies and Forced Response of Complex, Fib-Stiffened Structures. M.S. Thesis. Wright-Patterson AFB, Ohio: School of Engineering, Air Force Institute of Technology, December 1979.
4. HP5451B Fourier Analyser, Operating and Service Manuals, Volumes 1-8., Hewlett-Packard Company, January 1974.
5. International Mathematical and Scientific Library, IMSI LIB-0008, Houston, Texas: June 1980.
6. Mierovitch, Leonard. Analytical Methods in Vibrations. New York: The MacMillan Company, 1967.
7. McVinnie, W. and Verhelle, R. GCSNAST Manual. Graphics manual for NASTRAN output. Wright-Patterson AFB, Ohio: Engineering Systems Development Department, Technical Computer and Information Center, November 1978.
8. Moler, C.B. and Stewart, G.W. "An Algorithm for Generalized Matrix Eigenvalue Problems," SIAM Journal on Numerical Analysis, Volume 10, No. 2, April 1973, 241-256.
9. Noble, Ben. Applied Linear Algebra Englewood Cliffs, New Jersey: Prentice-Hall, Incorporated, 1969, 142-146.
10. Penrose, R. "A Generalized Inverse for Matrices," Proceedings of the Cambridge Philosophical Society, Volume 51, 406-413.
11. Schaeffer, Harry L. MSC/NASTRAN Static and Normal Modes Analysis. Millford, New Hampshire: Wallace Press, Incorporated, April 1979.
12. Strang, Gilbert. Linear Algebra and Its Applications. New York: Academic Press, Incorporated, 1980.

13. The Nastran User's Modal Model (V1.0). NASA-SP-221 (05). Washington, D.C.: Scientific and Technical Information Office, National Aeronautics and Space Administration, December 1978.
14. Whaley, P.W. "Calculations of Natural Frequencies and Mode Shapes of Mass Loaded Aircraft Structures," The Shock and Vibration Bulletin, No. 48, Part 3, 13-20.
15. Whaley, P.W. "Prediction of the Change in Natural Frequency of a Cantilevered Flat Plate With Added Lumped Mass," Journal of Sound and Vibration, Volume 69, Part 4, 519-529.
16. Whaley, P.W. "On Complex Valued Mode Shapes, Models For Structural Damping, and Mini-Computer Modal Analysis Techniques", Unpublished paper submitted to the 51st Shock and Vibration Symposium, San Diego, CA, June 1980.

APPENDICES

APPENDIX A

APPENDIX A

Mathematical Considerations and Example Problem In the Calculation and Use of the Pseudoinverse

Mathematical Considerations

In the paper by Penrose (Ref. 8) it is shown that for any matrix A there is one and only one matrix A^+ satisfying the four conditions:

$$(1) \quad AA^+A = A \quad (A-1a)$$

$$(2) \quad A^+AA^+ = A^+ \quad (A-1b)$$

$$(3) \quad (AA^+)^* = AA^+ \quad (A-1c)$$

$$(4) \quad (A^+A)^* = A^+A \quad (A-1d)$$

The matrix A^+ , called the pseudoinverse of A , is the matrix such that for the inconsistent set of equations $A \bar{x} = \bar{b}$, the solution $\bar{x} = A^+ \bar{b}$ represents the optimal solution to the least squares problem $A \bar{x} = \bar{b}$.

Now, consider the problem (posed by Noble, Ref. 7) $A \bar{x} = \bar{b}$ where $A = BC$, and A , B , C are, respectively, $m \times n$, $m \times k$, and $k \times n$, and all three matrices are of rank k , then the solution of $A \bar{x} = \bar{b}$ which minimizes

a) the sum of the squares of the residuals $\bar{r}^T \bar{r}$, where $\bar{r} = \bar{b} - A \bar{x}$, and

b) the sum of the squares of the unknowns $\bar{x}^T \bar{x}$, is given by $\bar{x} = A^+ \bar{b}$, where

$$A^+ = C^T (CCT)^{-1} (B^T B)^{-1} B^T. \quad (A-2)$$

When one accomplishes a decomposition of the matrix A

in the form $A = LU$ where A is an $m \times n$ matrix, L is an $m \times m$ matrix, and U is an $m \times n$ matrix, B , B^T , C , and C^T in equation A-2 can be replaced by L , L^T , U , and U^T respectively, Equation A-2 then becomes (Ref 10)

$$A^+ = U^T (UU^T)^{-1} (L^T L)^{-1} L^T \quad (A-3)$$

Example Problem 1. Calculation of Pseudoinverse

Armed with equation A-3, let us consider an example problem. Let the matrix A be represented by

$$A = \begin{bmatrix} 1.0 & 0.5 \\ 2.0 & 1.0 \\ 3.0 & 0.0 \end{bmatrix} .$$

Following the procedure of Strang (Ref 10), the following procedure is used to decompose A into L and U factors. Using an elementary matrix, E , to accomplish multiplication/addition of rows in matrix A , and a permutation matrix, P , to interchange rows to achieve non-zero pivot elements in U as needed,

$$PEA = U, \text{ and} \quad (A-4)$$

$$A = (PE)^{-1} U = LU. \quad (A-5)$$

The LU decomposition of the given matrix will now be calculated.

$$A = \begin{bmatrix} 1.0 & 0.5 \\ 2.0 & 1.0 \\ 3.0 & 0.0 \end{bmatrix} \longrightarrow \begin{bmatrix} 1 & 0 & 0 \\ -2 & 1 & 0 \\ -3 & 0 & 1 \end{bmatrix} \begin{bmatrix} 1.0 & 0.5 \\ 2.0 & 1.0 \\ 3.0 & 0.0 \end{bmatrix} = EA = \begin{bmatrix} 1.0 & 0.5 \\ 0.0 & 0.0 \\ 0.0 & -1.5 \end{bmatrix} .$$

Noting that the second row of EA contains a non-zero pivot element, a row exchange with the third row of

EA is accomplished using a permutation matrix as

$$\begin{bmatrix} 1 & 0 & 0 \\ 0 & 0 & 1 \\ 0 & 1 & 0 \end{bmatrix} \begin{bmatrix} 1.0 & 0.5 \\ 0.0 & 0.0 \\ 0.0 & -1.5 \end{bmatrix} = P(EA) = \begin{bmatrix} 1.0 & 0.5 \\ 0.0 & -1.5 \\ 0.0 & 0.0 \end{bmatrix} = U.$$

To get L, augment the $m \times m$ PE matrix with an $m \times m$ identity matrix on the right side and perform elementary row operations until an identity matrix is obtained in place of the original position of PE. The matrix now occupying the previous location of the original identity matrix is the inverse, $(PE)^{-1}$.

$$\begin{bmatrix} PE & I \end{bmatrix} = \begin{bmatrix} 1 & 0 & 0 & 1 & 0 & 0 \\ -3 & 0 & 1 & 0 & 1 & 0 \\ -2 & 1 & 0 & 0 & 0 & 1 \end{bmatrix} \xrightarrow{\quad} \begin{bmatrix} 1 & 0 & 0 & 1 & 0 & 0 \\ 0 & 0 & 1 & 3 & 1 & 0 \\ 0 & 1 & 0 & 2 & 0 & 1 \end{bmatrix} \\ \xrightarrow{\quad} \begin{bmatrix} 1 & 0 & 0 & 1 & 0 & 0 \\ 0 & 1 & 0 & 2 & 0 & 1 \\ 0 & 0 & 1 & 3 & 1 & 0 \end{bmatrix}.$$

Thus, $A = LU$ becomes

$$A = LU = \begin{bmatrix} 1 & 0 & 0 \\ 2 & 0 & 1 \\ 3 & 1 & 0 \end{bmatrix} \begin{bmatrix} 1.0 & 0.5 \\ 0.0 & -1.5 \\ 0.0 & 0.0 \end{bmatrix} = \begin{bmatrix} 1.0 & 0.5 \\ 2.0 & 1.0 \\ 3.0 & 0.0 \end{bmatrix}.$$

According to Reference 10, if the matrix U contains rows consisting of all zero elements, one can delete those rows in U and the corresponding columns of L to obtain new factors \bar{L} and \bar{U} such that

$$A = \bar{L}\bar{U} \quad (A-6)$$

Thus,

$$A = \bar{L}\bar{U} = \begin{bmatrix} 1 & 0 \\ 2 & 0 \\ 3 & 1 \end{bmatrix} \begin{bmatrix} 1.0 & 0.5 \\ 0.0 & -1.5 \end{bmatrix} = \begin{bmatrix} 1.0 & 0.5 \\ 2.0 & 1.0 \\ 3.0 & 0.0 \end{bmatrix}.$$

The pseudoinverse of A becomes

$$A^+ = \bar{U}^T (\bar{U}\bar{U}^T)^{-1} (\bar{L}^T\bar{L})^{-1} \bar{L}^T. \quad (A-7)$$

Continuing to obtain A^+ ,

$$\begin{aligned} A^+ &= \bar{U}^T \left(\begin{bmatrix} 1.0 & 0.5 \\ 0.0 & -1.5 \end{bmatrix} \begin{bmatrix} 1.0 & 0.0 \\ 0.5 & -1.5 \end{bmatrix} \right)^{-1} \left(\begin{bmatrix} 1 & 2 & 3 \\ 0 & 0 & 1 \end{bmatrix} \begin{bmatrix} 1 & 0 \\ 2 & 0 \\ 3 & 1 \end{bmatrix} \right)^{-1} \bar{L}^T \\ &= \begin{bmatrix} 1.0 & 0.0 \\ 0.5 & -1.5 \end{bmatrix} \begin{bmatrix} 1.25 & -0.75 \\ -0.75 & 2.25 \end{bmatrix}^{-1} \begin{bmatrix} 1.4 & 3 \\ 3 & 1 \end{bmatrix}^{-1} \begin{bmatrix} 1 & 2 & 3 \\ 0 & 0 & 1 \end{bmatrix} \\ &= \frac{1}{45} \begin{bmatrix} 0 & 0 & 15 \\ 18 & 36 & -30 \end{bmatrix}. \end{aligned}$$

Once the matrix A^+ has been calculated, one must verify that equations A-1a and A-1b hold. Since A and A^+ contain only real numbers, conditions A-1c and A-1d need not be checked. In general, all four of conditions A-1a through A-1d must be checked. Checking,

$$AA^+A = \begin{bmatrix} 1.0 & 0.5 \\ 2.0 & 1.0 \\ 3.0 & 0.0 \end{bmatrix} \frac{1}{45} \begin{bmatrix} 0 & 0 & 15 \\ 18 & 36 & -30 \end{bmatrix} \begin{bmatrix} 1.0 & 0.5 \\ 2.0 & 1.0 \\ 3.0 & 0.0 \end{bmatrix} = \begin{bmatrix} 1.0 & 0.5 \\ 2.0 & 1.0 \\ 3.0 & 0.0 \end{bmatrix} = A.$$

Similarly,

$$\begin{aligned} A^+AA^+ &= \frac{1}{45} \begin{bmatrix} 0 & 0 & 15 \\ 18 & 36 & -30 \end{bmatrix} \begin{bmatrix} 1.0 & 0.5 \\ 2.0 & 1.0 \\ 3.0 & 0.0 \end{bmatrix} \frac{1}{45} \begin{bmatrix} 0 & 0 & 15 \\ 18 & 36 & -30 \end{bmatrix} \\ &= \frac{1}{45} \begin{bmatrix} 0 & 0 & 15 \\ 18 & 36 & -30 \end{bmatrix} = A^+. \end{aligned}$$

Thus, the matrix A^+ represents the pseudoinverse of the

original matrix A.

If we take $B = A^T$ and compute B^+ , we find

$$B^+ = \frac{1}{45} \begin{bmatrix} 0 & 18 \\ 0 & 36 \\ 15 & -30 \end{bmatrix} = (A^+)^T.$$

If we let $A = U$, $B = U^T$, equation 3-a becomes

$$U^T M U = B M A = I. \quad (A-8)$$

Premultiplication of equation A-8 by B^+ and postmultiplication by A^+ yields

$$B^+ B M A A^+ = B^+ I A^+ = B^+ A^+. \quad (A-9)$$

The solution to equation A-9 is

$$M = B^+ I A^+ \quad (A-10)$$

provided the consistency condition

$$B B^+ I A^+ A = I \quad (A-11)$$

holds. The reader can verify equation A-11 is valid.

Thus, the mass matrix becomes

$$\begin{aligned} M &= B^+ I A^+ = B^+ A^+ = \frac{1}{45} \begin{bmatrix} 0 & 18 \\ 0 & 36 \\ 15 & -30 \end{bmatrix} \frac{1}{45} \begin{bmatrix} 0 & 0 & 15 \\ 18 & 36 & -30 \end{bmatrix} \\ &= \frac{1}{45^2} \begin{bmatrix} 324 & 648 & -540 \\ 648 & 1296 & -1080 \\ -540 & -1080 & 1125 \end{bmatrix} \\ &= \begin{bmatrix} 0.16 & 0.32 & -0.267 \\ 0.32 & 0.64 & -0.533 \\ -0.267 & -0.533 & 0.556 \end{bmatrix}. \end{aligned} \quad (A-12)$$

Before one can be sure equation A-12 represents the least squares solution to the mass matrix, one final check must

be made;

$$BMA^2 = I. \quad (A-13)$$

The reader can verify that equation A-13 holds. A similar procedure is followed to calculate the unloaded stiffness and damping matrices using equations 2 and 3, respectively.

Example Problem 2. Calculation of Mass-Loaded Mass and Stiffness Matrices

Following the procedure of Example Problem A-1, consider the three degree-of-freedom system of Figure A-1. Let $M_1 = M_2 = M_3 = 1$ and $K_1 = K_2 = K_3 = 100$. Neglecting damping and the forcing functions, the equations of motion become:

$$\begin{bmatrix} 1 & 0 & 0 \\ 0 & 1 & 0 \\ 0 & 0 & 1 \end{bmatrix} \begin{Bmatrix} \ddot{x}_1 \\ \ddot{x}_2 \\ \ddot{x}_3 \end{Bmatrix} + \begin{bmatrix} 200 & -100 & 0 \\ -100 & 200 & -100 \\ 0 & -100 & 100 \end{bmatrix} \begin{Bmatrix} x_1 \\ x_2 \\ x_3 \end{Bmatrix} = \begin{Bmatrix} 0 \\ 0 \\ 0 \end{Bmatrix}. \quad (A-14)$$

These equations are the three degree-of-freedom eigenvalue problem for this system. Upon solving equation A-14 for its eigenvalues (natural frequencies) and eigenvectors (mode shapes), the results in column two of Table A-1 are obtained.

Table A-1. Analytical Data From Three Degree-of-Freedom Spring-Mass-Damper-System

Parameter	$M_1 = M_2 = M_3 = 1$ $K_1 = K_2 = K_3 = 100$	$M_1 = M_3 = 1, M_2 = 2$ $K_1 = K_2 = K_3 = 100$
Unnormalized Modal Matrix	$\begin{bmatrix} 1. & -.802 & .445 \\ .445 & 1. & .802 \\ -.802 & .445 & 1. \end{bmatrix}$	$\begin{bmatrix} 1. & -.675 & .461 \\ -.452 & -.403 & .855 \\ .311 & 1. & 1. \end{bmatrix}$
Natural Frequencies	$\omega_1 = 4.45$ $\omega_2 = 12.47$ $\omega_3 = 18.019$	$\omega_1 = 3.813$ $\omega_2 = 11.845$ $\omega_3 = 15.648$

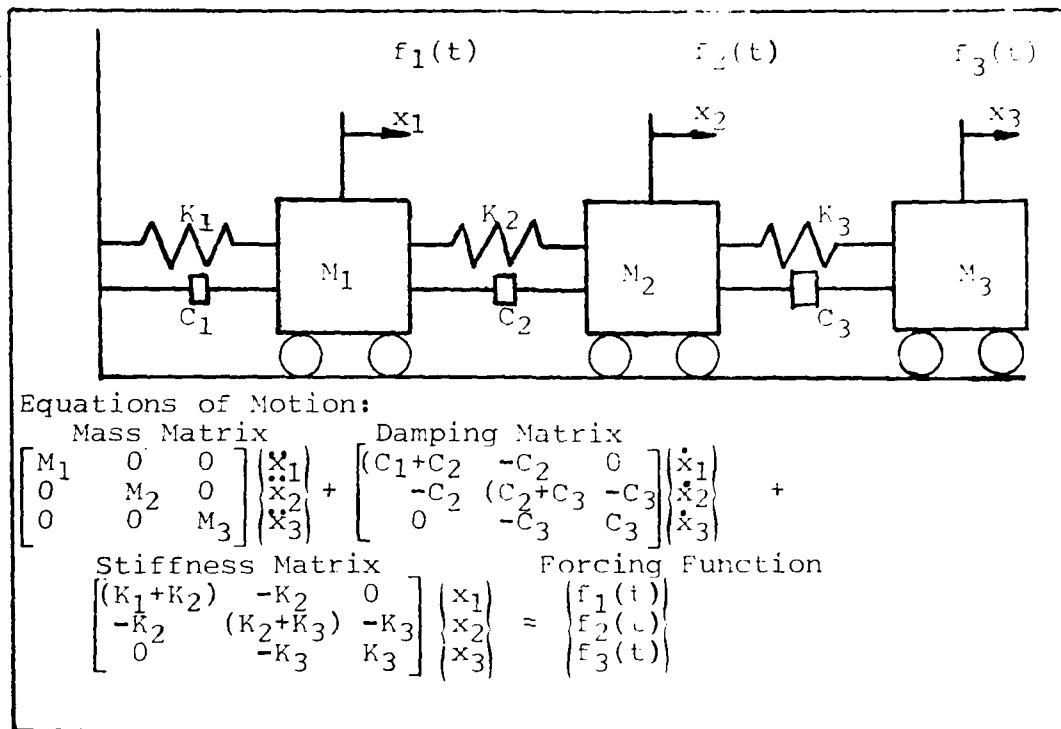


Figure A-1. Three Degree of Freedom System

Next, let a mass of magnitude one be added to mass M_2 such that M_2 is now equal to two. This will simulate a mass-loaded configuration. Data for this configuration are listed in column three of Table A-1. Note that the mass addition lowered the natural frequencies and modified the mode shapes.

Now, consider the first two natural frequencies and corresponding mode shapes (Table A-1, column 2) to be the measured modal data in the frequency range of interest. Using the procedure of Example Problem A-1 to recover the mass and stiffness matrices, the "generalized inverse" equations of motion become:

$$\begin{bmatrix} .485 & -.105 & -.131 \\ -.105 & .353 & -.237 \\ -.131 & -.237 & .249 \end{bmatrix} \begin{bmatrix} \dot{x}_1 \\ \dot{x}_2 \\ \dot{x}_3 \end{bmatrix} + \begin{bmatrix} 35.359 & -.112 & 11.719 \\ -34.212 & 47.009 & -22.523 \\ 11.719 & -22.523 & 12.871 \end{bmatrix} \begin{bmatrix} x_1 \\ x_2 \\ x_3 \end{bmatrix} = \begin{bmatrix} 0 \\ 0 \\ 0 \end{bmatrix} \quad (A-15)$$

After adding a unit of mass to the M_{22} term, and resolving the eigenvalue problem, the following results were obtained:

$$\omega_1 = 0.02$$

$$\omega_2 = 4.45$$

$$\omega_3 = 12.46$$

Comparison of these results with column two of Table A-1 reveals that, with the exception of ω_1 , the values are nearly identical with the unloaded results, and that the magnitude of the frequency shift was nowhere near that which was encountered in column three of Table A-1.

APPENDIX B

APPENDIX B

Detailed Modal Analysis and Test Procedures

Modal Assurance Criteria (MAC) Function Testing

The test panel was suspended from a ceiling-mounted conduit in the Structural Vibrations Branch (Bldg 24C) of the Air Force Wright Aeronautical Laboratories (FBG/AFWAL) by bungy cords which were approximately four feet in length. These bungy cords were attached to the panel through holes in the skin located near each of the four edges. The test grid used by Glenesk (Ref 3) was marked on the upper surface, and a reference accelerometer was mounted on the skin (see "x" on Fig 2) using double-backed tape. The reference accelerometer and moveable accelerometer responses were individually amplified and filtered through a pair of matched filters before their signals were input to the HP-5451B Fourier Analyser (Ref 4). The reference accelerometer was used to provide the trigger signal for data sampling.

With the panel configured as described, the moveable accelerometer was mounted at grid point number one. The panel was then excited (tapped) 15 times at randomly selected locations. Following each tap, and prior to computations using these data in the Fourier Analyser, each data sample was viewed separately on a refresh-trace

oscilloscope to insure the tapping is not overloaded the internal electronics, or that multiple excitations had not occurred during the data sample. Assuming an acceptable data sample had been obtained, these data were stored in the Fourier Analyser. Each time a good data sample was processed, the response data for that sample was averaged with the previous sample(s) such that after 15 iterations the stable average for each channel was computed. Using these average response data with the reference accelerometer as the input and the moveable accelerometer as the system forced response, the Fourier Analyser calculated both the MAC and Transfer Functions for that grid point and displayed the Transfer Function on the oscilloscope. At this point the user had the option to either accept the data, or reject the data and reaccomplish this process for that grid point. If accepted, hard copies, including plots and digital information, were made of Transfer Function and MAC Function data. The Transfer Function data were stored for later use.

The next step was to successively mount the moveable accelerometer at each of the remaining grid points and repeat this procedure. Once the entire grid had been surveyed, the MAC Function data were examined to determine candidate frequencies for which a curve fit

of the Transfer Function data would be made. Prior to curve-fitting the Transfer Function data, each discrete Transfer Function was examined at the given frequency range to determine the data with the "cleanest" spike. This spike was fit first using a least-squares algorithm to determine the natural frequency and damping ratio to be used in each of remaining Transfer Functions to determine the mode shape at that frequency. This process was repeated for each candidate frequency range identified by the MAC Function data in the range of 0-500 Hz.

Modal Analysis Test Procedure

Several grid sets were used in this testing: the 25 grid point scheme of Glenesk (Ref 3, Figure 2), a 25 grid point scheme (Figure 5) to coincide with the addition of structural components, and a 65 grid point model with fine meshes superimposed on each of the four internal bays (Figure 6) to investigate the modes of vibration of each of these bays. Since the test procedure is identical for each grid set, it will only be discussed for the 25 grid point scheme.

This testing used a moveable accelerometer to survey the grid. However, unlike the MAC function testing, a second stationary accelerometer was not used. Instead, one grid point was selected (number one for this grid) at which the structure would be excited by an impact hammer configured with a load cell to measure the amplitude

of the impact. The output from the load cell was used as the trigger source with the moveable accelerometer measuring the forced system response. Again, unlike the MAC function testing, the structure was excited only five times at each grid point. The number five was chosen for two reasons: first, it was noticed during the MAC function testing that more than five data samples had no significant impact on increasing the accuracy of the average PSD; and second, due to the large number of grid points used in the larger models, including more than five iterations per grid point would cause excessively long testing while providing little, if any, improvement in the quality of the data.

The process began by mounting the accelerometer at grid point number one and exciting the structure using the impact hammer five times at the selected excitation point. As in the MAC function testing, the data were examined following each discrete sample to determine if an overload of the internal electronics or a multiple excitation had occurred. Assuming acceptable data were obtained, the discrete force input was multiplied a force window (Figure B-1) to artificially force it to die out rapidly as would be the case for an impulse excitation. Similarly, the structural forced response was multiplied by an exponentially decaying window (Figure B-2) to simulate the effect of damping on the structural

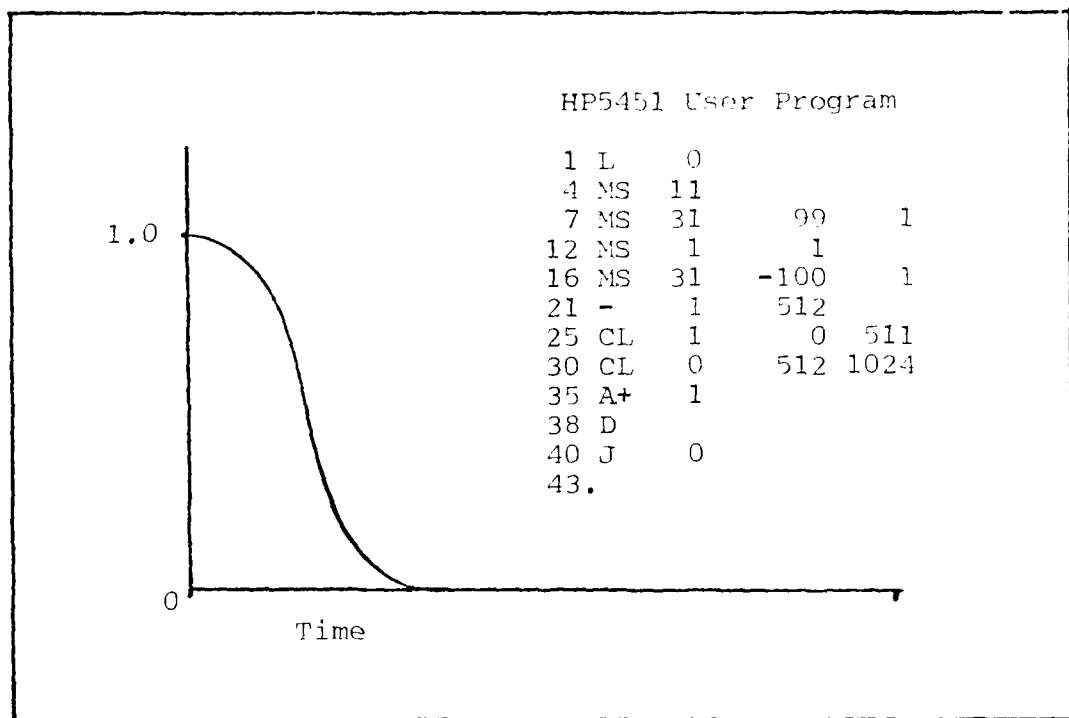


Figure B-1. Force Window.

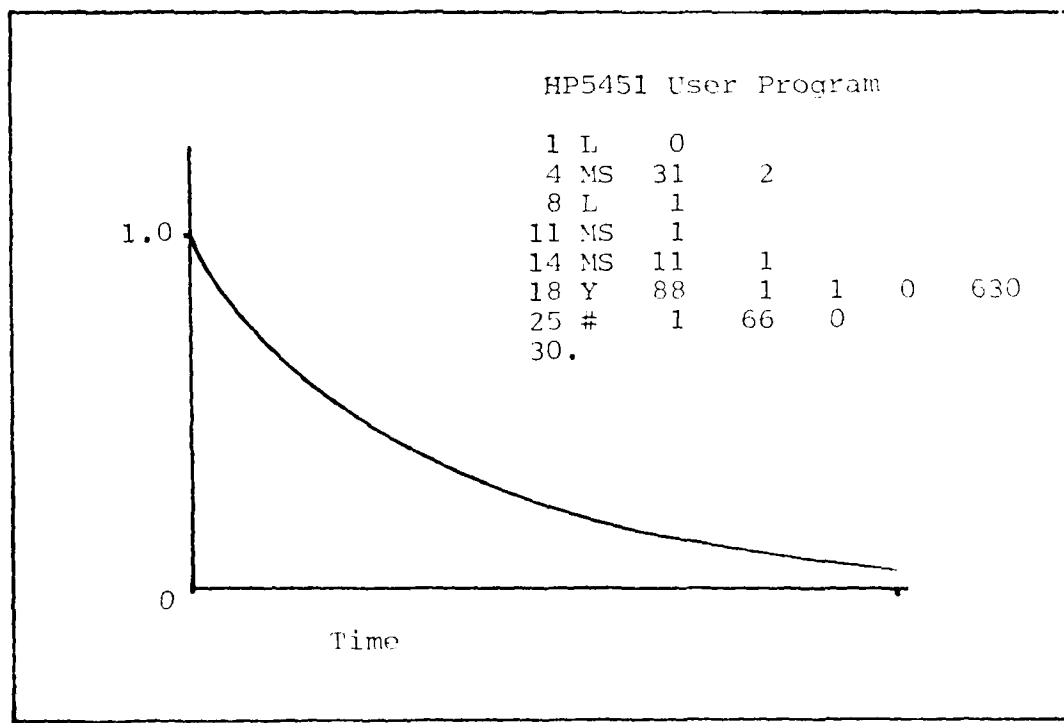


Figure B-2. Exponential Decay Window

response. The average of each sample with preceeding samples was computed after each of the five discrete data samples was accepted. As before, a Transfer Function was computed for each point. Upon completion of the fifth iteration, the average Transfer Function and a Coherence Function were computed and individually displayed. A decision whether to accept the data was based on a Coherence Function with many of its values at or near one in the 0-500 Hz range. This process was repeated until the entire grid had been surveyed.

Once the survey was complete, a grid point was selected which was believed to contain all the modes of the structure. Several methods for examining the Transfer Function data at that grid point were available in the software. Among these methods were a Kennedy-Planck Circle fit, a least-squares algorithm, and an option which merely computed the magnitude of the Transfer Function at selected frequencies where the real and imaginary parts of the Transfer Function were 90 degrees out of phase with each other. Initially the author selected the magnitude option as it ignores damping. However, the least-squares algorithm was eventually used to analyse the data.

Mathematical-Experimental Procedure

This procedure uses the experimentally determined modal data for the unloaded panel gathered in the Modal

AD-A100 820

AIR FORCE INST OF TECH WRIGHT-PATTERSON AFB OH SCHO0--ETC F/6 12/1
A COMPARISON OF VARIOUS TECHNIQUES FOR THE PREDICTION OF MASS-L--ETC(U)
MAR 81 F B ATKINSON

UNCLASSIFIED AFIT/GAE/A/80D-1

NL

2 OF 2
40 A
100 4-20

END
DATE FILMED
7-81
DTIC

Analysis Section presented earlier in this Appendix. The mathematical portion of this procedure begins with the general matrix-vector differential equation used in modal analysis,

$$[M] \ddot{x} + [C] \dot{x} + [K] x = f(t), \quad (B-1)$$

where $[M]$ is the mass matrix, $[C]$ is the damping matrix, and $[K]$ is the stiffness matrix, all of which are square and symmetric matrices. A generalized coordinates solution to this equation results in "n" uncoupled equations. Assuming the solution to equation 1 can be written in the form

$$x(t) = [U] q(t), \quad (B-2)$$

where $[U]$ is a square matrix consisting of mode shape vectors as its columns (i.e.-the modal matrix), then it follows that $q(t)$ is the generalized coordinate. Following the derivation of Meirovich (Ref 5) after substitution of equation B-2 into equation B-1 and premultiplication of equation B-1 by $[U]^T$, the following definitions are made:

$$[U]^T [M] [U] = [I] \quad (B-3a)$$

$$[U]^T [K] [U] = \begin{bmatrix} \ddots & & 0 \\ & \omega_n^2 & \\ 0 & & \ddots \end{bmatrix} \quad (B-3b)$$

$$[U]^T [C] [U] = \begin{bmatrix} \ddots & & 0 \\ & 2\xi_n\omega_n & \\ 0 & & \ddots \end{bmatrix} . \quad (B-3c)$$

With these definitions equation B-1 becomes

$$\ddot{q}_r + 2\xi_r \omega_r q_r + \omega_r^2 q_r = f_r, \quad r = 1, 2, 3, \dots \quad (B-4)$$

where $f_r(t) = [U]^T f(t)$ is the generalized force.

Equation B-4 can be solved for at most "n" natural frequencies. However, there are often less than "n" natural frequencies in the frequency range of interest such that the modal matrix contains fewer columns than it contains rows. It is proposed to premultiply each of the equations B-3 by $([U]^T)^{-1}$ and postmultiply each of these equations by $[U]^{-1}$ in such a way as to isolate the mass, damping, and stiffness matrices on the left side of equations B-3 which involve these respective matrices. In general, $[U]^T$ and $[U]$ will be non-square (rectangular) matrices necessitating the use of the pseudoinverse developed by Penrose (Ref 8) to find their inverses. Using a superscript "+" to indicate a pseudoinverse and after the previously mentioned pre- and post-multiplications, equations B-3 become

$$([U]^T)^+ [U]^T [M] [U] [U]^+ = ([U]^T)^+ [I] [U]^+ \quad (B-5a)$$

$$([U]^T)^+ [U]^T [K] [U] [U]^+ = ([U]^T)^+ \begin{pmatrix} -\omega_n^2 & 0 \\ 0 & \dots \end{pmatrix} [U]^+ \quad (B-5b)$$

$$([U]^T)^+ [U]^T [C] [U] [U]^+ = ([U]^T)^+ \begin{pmatrix} -2\xi_n \omega_n & 0 \\ 0 & \dots \end{pmatrix} [U]^+ \quad (B-5c)$$

Equations B-5 can be further reduced using standard linear algebra matrix manipulations (Noble, Ref 7) to yield the mass, stiffness, and damping matrices respectively as

$$[M] = \left([U]^T \right)^+ [I] [U]^+ \quad (B-6a)$$

$$[K] = \left([U]^T \right)^+ \begin{pmatrix} -\omega_n^2 & 0 \\ 0 & \end{pmatrix} [U]^+ \quad (B-6b)$$

$$[C] = \left([U]^T \right)^+ \begin{pmatrix} -2\xi_n\omega_n & 0 \\ 0 & \end{pmatrix} [U]^+ \quad (B-6c)$$

Reference 8 (Penrose) contains the basic theory of the pseudoinverse.

With these definitions for the mass, damping, and stiffness matrices, and the experimentally determined modal data for the unloaded panel gathered in the Modal Analysis Section presented earlier in this report, one can calculate the mass, damping, and stiffness matrices. Appendix A contains a simple example of the technique.

Since the thrust of this procedure is to accurately predict the mass-loaded natural frequencies and mode shapes of a complex structure when only the unloaded modal data are known, the procedure must be continued to recover mass-loaded modal data (ω_n , ξ_n , U_n). For example, consider the mass matrix. When the designer has made his decision regarding the placement of the additional mass (hardware) in the structure in question, he need only add an appropriate

mass in the mass matrix at the proper grid location to obtain the modified mass matrix. A similar procedure is followed to obtain the modified stiffness and damping matrices. Assuming one is only interested in mode shapes and natural frequencies, the modified mass and stiffness matrices are substituted into equation 4. Equation 4 is then solved for the mass-loaded natural frequencies and mode shapes.

Finite Element Modelling Procedure

Finite Element Models. The three finite element models used in this analysis were described in Section II. Because the development of a finite element model is described in Reference 11, the main question became how to add a quantity of mass to the mass matrix which would be used to solve for the modified natural frequencies and mode shapes.

NASTRAN provides this capability in the form of a CONM2 card which adds a finite-valued point mass, including its inertia properties and neutral axes offset, to a particular location in the mass matrix. Another card, the ASET1 card, was used to discard all but the out-of-plane translation from the analysis set in the solution for mode shapes and natural frequencies. Appendix C contains listings of a sample NASTRAN deck used in the modal analysis of each configuration.

Analytical Procedures. NASTRAN (Ref 11) uses several

rigid formats to provide flexibility to the user in the analysis at hand. Rigid Format 3 was chosen for the modal analysis of the test panel. This format neglects damping and solves equation B-1 with the forcing function and damping matrices set equal to zero. The output from this Format is a table of the "n" natural frequencies and tables of the "n" eigenvectors (mode shapes). These data were then post-processed using GCSNAST to be displayed on a standard computer terminal.

APPENDIX C

Figure C-1. Program Matrix Listing.

```

CNRD = NUMERICAL ROW DIMENSION
CNR = NUMBER OF ROWS
CNC = NUMBER OF COLUMNS
CINITIALIZE THE MATRICES:
C*****+
      DIMENSION UU(9,9),U1(9,9),U2(9,9),U3(9,9)
      DIMENSION XA(3),YA(3),ZA(3),XA(9),YA(9),ZA(9)
      DIMENSION XXX(9),YYY(9),ZZZ(9)
      DIMENSION AALP(9)
      DIMENSION U5(9,9),U6(9,9),U7(9,9),U8(9,9)
      DIMENSION WMRDA(9),WALP(9),U4(9,9),ERROR(9)
      DIMENSION AAI(9,9),F1(9,9),C(9,9),H(9,9),OMEGA(9,9),U(9,9),UT(9,9)
      DIMENSION AC(9,9),AI(9,9),ZETA(9,9),FF(9,9),GG(9,9),HH(9,9),HA(9,9)
      L,FFF(9,9),GGG(9,9),C1(9,9),D1(9,9),E1(9,9),ZETAS(9),OMEGAS(9),AL(9)
      DIMENSION EROR(9)
      DIMENSION WMRDA(9),UGITN(9,9)
      DIMENSION SUM1(9),SUM1(9),SUM2(9),SUM3(9)
      DIMENSION SUM4(9)
      REAL A(9,9),U3P(8,9),S3P(8,9),WK3(161),U3(9,9),RETAZ(9),WK4(162)
      REAL A(9,9),UGIN(9,9),TOL(9,9),WK(162),AM(9,9),AK(9,9),BETA(9),U2(9,9),
      WK2(162),AM(9,9),AAK(9,9),RETA(9),WK1(162),U1(9,9),MEGA(9)
      COMPLEX ALFA(9,7),ALFA(9,7),ALFA(9,7),ALFA(9,7),ALFA(9,7),ALFA(9,7)
      COMPLEX ALFA(9,7),Z3(9,9),ALP(9)
      DIMENSION OMEG1(8,8),OMEGAL(8),AI(8,8),CC(9,8),U3TP(9,8),AMA(9,9),
      10010,81
      NR=9
      NC=9
      ND=8
      CALL COMPRS
      NCASES=3
      DO 6 KK=1,NCASES
C*****+
C*
C* READ STRUCTURAL GRID POINTS
C*
C* INITIALIZE THE MATRICES
C*
C*****+
      DO 111 I=1,NR
      RFAD(1),X(1),Y(1),Z(1)
      IF(EOP(5)INPUT).NE.01 STOP
      202 PRINT*,X(1),Y(1),Z(1)
C*****+
C*
C* INITIALIZE THE MATRICES
C*
C*****+
      DO 111 I=1,NR
      DO 111 J=1,NC
      AI(I,J)=0.0
      U(I,J)=0.0
      U2(I,J)=0.0
      U4(I,J)=0.0
      UT(I,J)=0.0
      UGIN(J,I)=0.0
      UGITN(I,J)=0.0
      ZETAS(J)=0.0
      AL(I,J)=1.0
      111 OMEGAS(I)=0.0
      DO 2 I=1,NC
      DO 2 J=1,NC
      AT(I,J)=C.0
      OMEGA(I,J)=0.0
      2 ZETA(I,J)=0.0
      DO 333 I=1,NR
      AM(I,J)=0.0
      AK(I,J)=0.0
      333 AC(I,J)=0.0
      DO 70 I=1,ND
      DO 70 J=1,ND
      AI(I,J)=0.0
      70 OMEGAI(I,J)=0.0
      PRINT*, "THE INITIALIZED MATRICES ARE:"
      PRINT*, " THE MODAL MATRIX:"
      DO 61 I=1,NR
      62 PRINT*,(U(I,J),J=1,NC)

```

Figure C-1. Program Matrix Listing (Continued).

```

PRINT*, " THE MODAL MATRIX TRANSPOSE:"*
DO 62 J=1,NC
62 PRINT*,(UTIJ,I,J=1,1,1=1,NR)
PRINT*, " THE GENERALIZED INVERSE:"*
DO 63 J=1,NC
63 PRINT*,(UGINIJ,I,J=1,1,T=1,NR)
PRINT*, " THE GENERALIZED INVERSE TRANSPOSE:"*
DO 64 I=1,NR
64 PRINT*,(UGITNIE,I,J=1,1,NC)
PRINT*, " THE ZETA MATRIX:"*
DO 65 I=1,NC
65 PRINT*,(ZETAI,I,J=1,NC)
PRINT*, " THE OMEGA MATRIX:"*
DO 66 I=1,NC
66 PRINT*,(OMEGAI,I,J=1,NC)
PRINT*, " THE "DUMMY" MATRICES:"*
PRINT*, " THE AL MATRIX:"*
DO 131 I=1,NC
131 PRINT*,AL(I)
PRINT*, " THE MASS MATRIX:"*
DO 132 I=1,NR
132 PRINT*,(AM(I,J),J=1,1,1=1,NR)
PRINT*, " THE DAMPING MATRIX:"*
DO 133 I=1,NR
133 PRINT*,(AK(I,J),J=1,NR)
PRINT*, " THE STIFFNESS MATRIX:"*
DO 134 I=1,NR
134 PRINT*,(AK(I,J),J=1,NR)
PRINT*, " THE IDENTITY MATRIX:"*
DO 135 I=1,NC
135 PRINT*,(AI(I,J),J=1,NC)
C*****
C
C READ ZETA AND OMEGA VALUES FOR UNLOADED PANEL
C
C
C***** READ ZETA AND OMEGA VALUES FOR UNLOADED PANEL
C
C
C***** OPTIONS: LLL=1; THIS OPTION WILL ALLOW THE PREDICTED MODE SHAPES FROM THE
C           SQUARE MODAL MATRIX TO BE PLOTTED.
C           LLL=2; THIS OPTION REQUIRES THAT THE USER ORDER THE ACTUAL MASS-
C           LOADED FREQUENCIES AND MODE SHAPES WITH THEIR CORRESPON-
C           DING UNLOADED DATA TO PLOT THE ACTUAL DATA.
C           LLL=3; THIS OPTION ALLOWS PLOTS FOR THE PSEUDOUNVERSE MODE SHAPES.
C
C***** LLL=1
1FLLL.EQ.2) GO TO 258
00 1016 I=1,NC
1016 READ(5,1017) OMEGAS(I),ZETAS(I)
1017 FORMAT(27X,FR.3,FR.3)
00 80 I=1,ND
80  OMEGAI(I)=OMEGAS(I)/100.
PRINT*, "THESE ARE THE VALUES OF OMEGA:"*
PRINT*,(OMEGAI(I),I=1,ND)
C*****
C
C READ MODE SHAPE VECTORS AND NORMALIZE
C
C
C***** READ MODE SHAPE VECTORS AND NORMALIZE
00 1018 J=1,NC
00 1019 I=1,NR
1018 READ(5,1019) A(I,J)
1019 FORMAT(13X,FI0.2)
00 411 I=1,NC
00 411 J=1,NR
411 A(I,J)=A(I,J)/100.
00 218 J=1,NC
SUM(J)=0.0
00 219 I=1,ND
219 SUM(I)=SUM(J)+A(I,J)***7

```

Figure C-1. Program Matrix Listing (Continued).

```

PRINT*,SUM(JJ)
SUM(JJ)=SUM(SUM(JJ))
DO 210 I=1,NR
210 AII,JJ=AII,JJ/SUM(JJ)
DO 220 I=1,NR
220 PRINT*,(AII,JJ,J=1,NC)
DO 220 I=1,NR
DO 220 J=1,NC
UII,JJ=AII,JJ
220 UII,JJ=AII,JJ
C*****
C*
C* DELETE THE LAST COLUMN FROM THE MODAL MATRIX U TO FORM THE RECTANGULAR
C* MATRIX U3.
C*
C*****
DO 81 I=1,NR
DO 81 J=1,ND
81 UIII,JJ=AII,JJ
PRINT*, "THIS IS THE U MATRIX"
DO 911 I=1,NR
911 PRINT*,(UII,JJ,J=1,NR)
PRINT*, "THIS IS THE A MATRIX"
DO 91 I=1,NR
91 PRINT*,(AII,JJ,J=1,NR)
PRINT*, "THIS IS THE UT MATRIX"
DO 92 I=1,NR
92 PRINT*,(UTI,JJ,J=1,NR)
PRINT*, "THIS IS THE U3 MATRIX"
DO 82 I=1,NR
82 PRINT*,(U3I,JJ,J=1,ND)
DO 71 I=1,NR
71 ALPII=0.0
DO 83 I=1,ND
83 OMEGAII,I=0.0
83 ALII,I=1.0
PRINT*, "THIS IS THE OMEGI MATRIX"
DO 84 I=1,ND
84 PRINT*,(OMEGAII,JJ,J=1,ND)
PRINT*, "THIS IS THE AI MATRIX"
DO 85 I=1,ND
85 PRINT*,(ALII,JJ,J=1,ND)
C*****
C*
C*
C*COMPUTE THE GENERALIZED INVERSE OF THE MODAL MATRIX AND ITS TRANSPOSE
C*
C*
C*****
NRN1=9
NRD=9
NC=9
NR=9
TOL=0.0
20 CALL LGINFLA,NRD,NR,NC,TOL,UGIN,NRD1,S,WK,IER
PRINT*, "THIS IS THE MATRIX UGIN"
DO 77 I=1,NC
77 PRINT*,(UGINII,JJ,J=1,NR)
DO 1235 I=1,ND
DO 1235 J=1,NC
1235 UGITTII,JJ=UGINII,JJ
PRINT*, "THIS IS THE MATRIX UGITN"
DO 410 I=1,NC
410 PRINT*,(UGITTII,JJ,J=1,NC)
PRINT*, "THE VALUES OF ZETA AND OMEGA ARE, RESPECTIVELY"
DO 15 I=1,NC
15 OMEGASII=OMEGASII/100.
15 PRINT*,ZETASII,OMEGASII
C*****
C*
C* COMPUTE THE GENERALIZED INVERSE OF THE MATRIX U3. THIS IS THE MATRIX U3P.
C*
C*****
NRD1=9

```

Figure C-1. Program Matrix Listing (Continued).

```

NR3=0
NC3=R
TOL=0.0
NRD4=0
CALL LGINF(U3,NRD3,NR3,NC3,TOL,U3P,NRD4,S3,WK3,IER3)
PRINT*, "THIS IS THE MATRIX U3P:"
DO 30 I=1,ND
30 PRINT*,(U3P(I,J),J=1,NC)
C*****TRANPOSE U3 TO FORM U3T. ALSO TRANPOSE U3P TO FORM U3TP.
C
C*****FORM THE ZETA, OMEGA, AND AI MATRICES:
C
C*****THE ACTUAL MATRICES ARE:
DO 5 I=1,NC
  ETAE(I,I)=2*ZETAE(I,I)*0*MEGAE(I,I)
  MEGAI(I,I)=0*MEGAI(I,I)*2
  AII(I,I)=1.0
5 CONTINUE
PRINT*, " THE ZETA MATRIX:"
DO 25 I=1,NC
25 PRINT*,(ZETAI(I,I),I=1,NC)
PRINT*, " THE OMEGA MATRIX:"
DO 26 I=1,NC
26 PRINT*,(MEGAI(I,I),I=1,NC)
PRINT*, " THE IDENTITY MATRIX:"
DO 27 I=1,NC
27 PRINT*,(AI(I,J),J=1,NC)
DO 41 I=1,NR
  DO 41 II=1,NC
    CII,II=0.0
    DO 41 K=1,NC
      CII,II=CII,II+UGITN(I,K)*AI(K,II)
41 CONTINUE
DO 42 I=1,NR
  DO 42 II=1,NC
    AMII,II=0.0
    DO 42 K=1,NC
      AMII,II=AMII,II+CII,K*UGINEK,II
      AMII,II=AMII,II
42 CONTINUE
DO 43 I=1,NC
  DO 43 II=1,NC
    DII,II=0.0
    DO 43 K=1,NC
      DII,II=DII,II+UGITN(I,K)*ZETAK,II
43 CONTINUE
DO 44 I=1,NR
  DO 44 II=1,NC
    ACII,II=0.0
    DO 44 K=1,NC
      ACII,II=ACII,II+DII,K*UGINEK,II
44 CONTINUE
DO 45 I=1,NC
  DO 45 II=1,NC
    EII,II=0.0
    DO 45 K=1,NC
      EII,II=EII,II+UGITN(I,K)*OMEGAII,K
45 CONTINUE
DO 46 I=1,NR
  DO 46 II=1,NC
    AKII,II=0.0

```

Figure C-1. Program Matrix Listing (Continued) .

```

DO 46 K=1,NC
AK(I,J)=AK(I,J)+E(I,K)*UGIN(K,J)
46 CONTINUE
DO 1 I=1,NR
DO 1 J=1,NC
IF(ABS(AK(I,J)).LE.10.E-8) AK(I,J)=0.0
IF(ABS(AK(I,J)).LE.10.E-8) AK(I,J)=0.0
1 IF(ABS(AK(I,J)).LE.10.E-8) AK(I,J)=0.0
PRINT*, " THE DAMPING MATRIX:"
DO 48 I=1,NR
48 PRINT*,(AK(I,J),J=1,NR)
PRINT*, " THE STIFFNESS MATRIX:"
DO 49 I=1,NR
49 PRINT*,(AK(I,J),J=1,NR)
PRINT*, "CHECK CONSISTENCY CONDITION FOR THE IDENTITY MATRIX:"
DO 990 I=1,NR
DO 990 J=1,NR
F(I,J)=0.0
DO 990 K=1,NC
990 F(I,J)=F(I,J) + UGIN(K,J)*UGIN(K,J)
DO 992 I=1,NR
DO 992 J=1,NC
H(I,J)=0.0
DO 992 K=1,NC
992 H(I,J)=H(I,J) + F(I,K)*U(I,K)
DO 993 I=1,NC
DO 993 J=1,NC
AA(I,J)=0.0
DO 993 K=1,NC
993 AA(I,J)=AA(I,J) + U(I,K)*H(K,J)
DO 9993 I=1,NC
DO 9993 J=1,NC
9993 IF(ABS(AA(I,J)).LE.10.E-8) AA(I,J)=0.0
DO 994 I=1,NC
994 PRINT*,(AA(I,J),J=1,NC)
PRINT*, "CHECK CONSISTENCY CONDITION FOR THE ZETA MATRIX:"
DO 995 I=1,NC
DO 995 J=1,NC
FF(I,J)=0.0
DO 995 K=1,NC
995 FF(I,J)=FF(I,J) + U(I,K)*UGIN(K,J)
DO 996 I=1,NC
DO 996 J=1,NC
GG(I,J)=0.0
DO 996 K=1,NC
996 GG(I,J)=GG(I,J) + FF(I,K)*ZETA(K,J)
DO 997 I=1,NC
DO 997 J=1,NC
HH(I,J)=0.0
DO 997 K=1,NC
997 HH(I,J)=HH(I,J) + UGIN(I,K)*U(I,K)
DO 998 I=1,NC
DO 998 J=1,NC
HA(I,J)=0.0
DO 998 K=1,NC
998 HA(I,J)=HA(I,J) + GG(I,K)*HH(K,J)
DO 9994 I=1,NC
DO 9994 J=1,NC
9994 IF(ABS(HA(I,J)).LE.10.E-8) HA(I,J)=0.0
999 PRINT*,(HA(I,J),J=1,NC)
PRINT*, "CHECK CONSISTENCY CONDITION FOR THE OMEGA MATRIX:"
DO 1003 I=1,NC
DO 1003 J=1,NC
FFF(I,J)=0.0
DO 1003 K=1,NC
1003 FFF(I,J)=FFF(I,J) + FFF(I,K)*OMEGA(K,J)
DO 1001 I=1,NC
DO 1001 J=1,NC
GGG(I,J)=0.0
DO 1001 K=1,NC
1001 GGG(I,J)=GGG(I,J) + FFF(I,K)*HH(K,J)
DO 9995 I=1,NC
DO 9995 J=1,NC
9995 IF(ABS(GGG(I,J)).LE.10.E-8) GGG(I,J)=0.0

```

Figure C-1. Program Matrix Listing (Continued).

```

      DO 1002 I=1,NC
1002 PRINT*,IGGG(I,J),J=1,NC1
      PRINT*, "THE MASS MATRIX: "
      DO 1004 I=1,NR
1004 PRINT*,(AMEI,I,J),J=1,NC1
C*=====
C*
C*
C* SINCE THE MASS WAS ADDED TO GRID POINT NUMBER FIVE ON THE ACTUAL PANEL, THE
C* MASS MATRIX WILL BE PERTURBED IN THE 5,5 POSITION BY ADDING A QUANTITY OF
C* MASS EQUAL TO THE MASS LOADING ON THE ACTUAL PANEL. THIS WILL SIMULATE THE
C* "REAL WORLD" CASE. NOTE THAT THE MASS WAS PLACED ON ONLY ONE GRID POINT. IF
C* THE MASS WAS A STRUCTURE SUCH AS A TRIPOD WHICH CONNECTED TO THREE GRID
C* POINTS, THE ADDED STRUCTURE WOULD HAVE TO BE MODELLED IN THAT IT WOULD ADD
C* BOTH MASS AND STIFFNESS TO THE PANEL. THIS ADDED MASS AND STIFFNESS WOULD
C* GENERATE ADDITIONS TO OFF DIAGONAL TERMS OF LIKE NUMBER TO THE TWO CONNECT-
C* ED GRID POINTS. AS PREVIOUSLY NOTED, THIS PROGRAM SOLVES THE GENERALIZED
C* EIGENVALUE PROBLEM. THUS, THERE IS NO NEED TO CREATE A SIMILAR MODEL FOR
C* ANY ADDITIONAL DAMPING INCURRED BY THE ADDITIONAL STRUCTURE.
C*
C*
C*=====
      PRINT*, "ENTER THE LOOP TO PERTURB THE MASS MATRIX: "
      IF(EKK.F0.1F AM(5,5)=AA(5,5)+0.1144
      IF(EKK.E0.21 AM(5,5)=AA(5,5)+0.2420
      IF(EKK.F0.3F AM(5,5)=AA(5,5)+0.4158
      PRINT*, " THE MASS MATRIX: "
      DO 50 I=1,NR
50   PRINT*,(AMEI,I,J),J=1,NC1
      PRINT*, "THE MODIFIED MASS MATRIX: "
      DO 47 I=1,NR
47   PRINT*,(AMEI,I,J),J=1,NC1
      PRINT*, "THE STIFFNESS MATRIX: "
      DO 58 I=1,NR
58   PRINT*,(AKI,I,J),J=1,NC1
C*=====
C*
C* SOLVE THE GENERALIZED EIGENVALUE PROBLEM FOR THE MASS-LOADED NATURAL FRE-
C* QUENCIES AND MODE SHAPES WITH THE SQUARE MODAL MATRIX U.
C*
C*=====
      IAM=9
      IAK=9
      NAMAK=9
      IZ=9
      IJOB=2
      CALL EIGZFEAK,IAK,AM,IAM,NAMAK,I JOB,ALFA,BETA,Z,IZ,WK2,IER2
      N=9
      PRINT*, "THESE ARE THE VALUES OF RALAMBDA: "
      DO 1234 I=1,N
      RALAMBDAI(I)=CSORT(REALFA(I)/BETA(I))
      PRINT*,RALAMBDAI(I)
1234  CONTINUE
      PRINT*, "THESE ARE THE VALUES OF THE Z MATRIX: "
      DO 1009 I=1,N
1009  PRINT*,(Z(I,J),J=1,NC)
      PRINT*, "THE PREDICTED MODE SHAPES AND NATURAL FREQUENCIES FOR AM(5
      1,5)=AM(5,5),ARE: "
      DO 21 I=1,NC
21   WAMBDAI(I)=CSORT(RALAMBDAI(I)**2)
      PRINT*,(WAMBDAI(I),I=1,NC1)
      LA=9
      CALL VSRT(WAMBDAI,LA)
      PRINT*,(WAMBDAI(I),I=1,NC1)
      DO 22 I=1,NC
      DO 22 J=1,NC
      IF(ABS(WAMBDAI(I)-REAL(RALAMBDAI(J))) .LE. 10.E-8) GO TO 23
      IF(ABS(WAMBDAI(I)-REAL(RALAMBDAI(J))) .GT. 10.E-8) GO TO 22
23   DO 24 K=1,NR
      U2IK,IJ=0.0
24   U2IK,IJ=U2IK,IJ+REAL(Z(K,J))
      CONTINUE
      DO 152 J=1,NC
      SUM4(J)=0.0
      DO 153 I=1,NR
153  SUM4(J)=SUM4(J)+U2(I,J)**2

```

Figure C-1. Program Matrix Listing (Continued) .

```

      SUM4(JJ)=SORT(SUM4(JJ))
      DO 152 I=1,NR
      U2(I,JI)=U2(I,JI)/SUM4(JJ)
      PRINT*, "COMPUTE SUM OF SQS OF DIFFERENCES BETWEEN LOADED ACTUAL AND
      LO LOADED PREDICTED MODAL VECTORS?"
      C*****
      C*
      C* READ MASS-LOADED MODAL VECTORS
      C*
      C*****
      DO 250 J=1,NC
      DO 250 I=1,NC
      UU(I,JI)=0.0
      READ(5,251) UU(I,JI)
      251 FORMAT(10X,E15.4)
      250 PRINT*,UU(I,JI)
      DO 252 I=1,NC
      DO 252 J=1,NC
      UU(I,JI)=UU(I,JI)+UU(I,JI)/100.
      252 DO 263 J=1,NC
      SUM1(JJ)=0.0
      DO 264 I=1,NC
      264 SUM1(JJ)=SUM1(JJ)+UU(I,JI)**2
      SUM1(JJ)=SORT(SUM1(JJ))
      DO 263 J=1,NC
      UU(I,JI)=UU(I,JI)/SUM1(JJ)
      C*****
      C*
      C* COMPUTE THE SUM OF THE SQUARES OF THE DIFFERENCES BETWEEN ACTUAL AND PRE-
      C* DICTED LOADED MODAL VECTORS
      C*
      C*****
      DO 253 J=1,NC
      DIF(JJ)=0.0
      DO 253 I=1,NC
      DIF1(I)=0.0
      253 DIF(JJ)=DIF(JJ)+UU(I,JI)-U2(I,JI)**2
      DO 259 I=1,NC
      DIF1(I)=DIF(I)
      259 CONTINUE
      DO 261 I=1,NC
      261 DIF1(I)=SORT(DIF1(I))
      PRINT*, "THESE ARE THE VALUES OF THE MODE SHAPE VECTORS:"
      DO 245 I=1,NC
      245 PRINT*,U2(I,JI),J=1,NC)
      DO 86 I=1,NC
      DO 86 J=1,ND
      CC(I,JI)=0.0
      DO 86 K=1,ND
      86 CC(I,JI)=CC(I,JI)+U3TP(I,K)*A1(I,K,JI)
      DO 87 I=1,NC
      DO 87 J=1,ND
      AM(I,J)=0.0
      AM(I,J)=0.0
      DO 87 K=1,ND
      AM(I,J)=AM(I,J)+CC(I,K)*U3PT(K,JI)
      87 AM(I,J)=AM(I,J)
      DO 88 I=1,NC
      DO 88 J=1,ND
      DD(I,J)=0.0
      DO 88 K=1,ND
      88 DD(I,J)=DD(I,J)+U3TP(I,K)*OMEG1(K,JI)
      DO 89 I=1,NC
      DO 89 J=1,ND
      AAK(I,J)=0.0
      DO 89 K=1,ND
      89 AAK(I,J)=AAK(I,J)+DD(I,K)*U3PT(K,JI)
      DO 72 I=1,NC
      DO 72 J=1,NC
      IF(ABSA(AAK(I,J)),1.E-10,F-89) AM(I,J)=0.0
      IF(ABSA(AAK(I,J)),1.E-10,F-89) AM(I,J)=0.0
      72 IF(ABSA(AAK(I,J)),1.E-10,F-89) AAK(I,J)=0.0
      C*****
      C*
      C* THIS IS THE LEAST-SQUARES SOLUTION TO THE MASS MATRIX BEFORE THE MASS HAS
      C* BEEN ADDED TO THE 5,5 TERM.
      C*****

```

Figure C-1. Program Matrix Listing (Continued).

```

PRINT*, "THIS IS THE MATRIX AMM"
DO 73 I=1,NR
 73 PRINT*, (AMM(I,J), J=1,NC)
C* PRINT*, "THIS IS THE MATRIX AAK"
DO 74 I=1,NR
 74 PRINT*, (AAK(I,J), J=1,NC)
C*
C* SOLVE THE GENERALIZED EIGENVALUE PROBLEM FOR THE MASS-LOADED NATURAL FRE-
C* QUENCIES AND MODE SHAPES USING THE RECTANGULAR MODAL MATRIX U3.
C*
C*
IF (KK.EQ.1) AMM(5,5)=AMM(5,5)+0.1144
IF (KK.EQ.2) AMM(5,5)=AMM(5,5)+0.242
IF (KK.EQ.3) AMM(5,5)=AMM(5,5)+0.4158
I2=9
IJOR=2
IA=9
IB=9
N=9
PRINT*, "THE MODIFIED MASS MATRIX AMM"
DO 67 I=1,NR
 67 PRINT*, (AMM(I,J), J=1,NC)
  CALL EIGZFAAK,IA,AMM,IR,N,IJOR,ALFA2,BETA2,Z3,IK4,IER4
C*
C* THESE ARE THE LEAST-SQUARES SOLUTIONS FOR THE NATURAL FREQUENCIES WITH THE
C* THE ADDED MASS IN THE 5,5 POSITION OF THE MASS MATRIX.
C*
C*
PRINT*, "THESE ARE THE VALUES OF THE Z3 MATRIX"
DO 246 I=1,NR
 246 PRINT*, (Z3(I,J), J=1,NC)
PRINT*, "THESE ARE THE VALUES OF ALP"
DO 33 I=1,NR
 33 ALP(I)=CSORT(ALFA2(I)/BETA2(I))
  WALP(I)=CSORT(ALP(I)**2)
  PRINT*, ALP(I), WALP(I)
  CALL VSRTA(WALP,IA)
PRINT*, "THESE ARE THE VALUES OF WALP"
PRINT*, (WALP(I), I=1,NC)
DO 265 I=1,NC
  IF (I.EQ.1) AALP(9)=WALP(I)
  IF (I.GT.1) GO TO 266
  GO TO 265
266 K=I-1
  AALP(K)=WALP(I)
265 PRINT*, AALP(K)
  DO 198 I=1, R
  DO 198 J=1,NC
  IF (ARS(AALP(I))-REAL(ALP(J))) .LE. 10.E-8) GO TO 197
  IF (ARS(AALP(I))-REAL(ALP(J))) .GT. 10.E-8) GO TO 198
197 DO 196 K=1,NR
  U4(K,I)=0.0
196 U4(K,I)=U4(K,I)+REAL(Z3(K,J))
198 PRINT*, U4(I,J)
  DO 150 J=1,NC
  SUM3(J)=C.0
  DO 151 I=1,NR
  SUM3(J)=SUM3(J)+U4(I,J)**2
  SUM3(J)=SORT(SUM3(J))
  DO 150 I=1,NR
  U4(I,J)=U4(I,J)/SUM3(J)
150 PRINT*, "COMPUTE THE SUM OF SQS OF DIFFERENCES BETWEEN LOADED ACTUA-
IL AND PREDICTED LOADED MODAL VECTORS USING THE GENERALIZED INVERSE
25"
  DO 255 J=1,NC
  DIFF(J)=0.0
  DO 255 I=1,NR
  255 DIFF(J)=DIFF(J)+U4(I,J)-U4(I,J)**2
  DO 256 I=1,NC
  256 DIFF(I)=DIFF(I)
  CONTINUE
  DO 262 I=1,NR
  262 DIFF(I)=SCRT(DIFF(I))

```

Figure C-1. Program Matrix Listing (Continued).

Figure C-1. Program Matrix Listing (Continued).

```

      DO 140 J=1,NC
      SUM2(J)=0.0
      DO 141 I=1,NR
141  SUM2(J)=SUM2(J)+U2(I,J)*92
      SUM2(J)=SORT(SUM2(J))
      DO 140 I=1,NR
      U2(I,J)=U2(I,J)/SUM2(J)
269  CONTINUE
      DO 211 LL=1,NR
      CALL BCNPL(I)
      CALL TITL3D("MODE", "CONFIGURATION", "S", 100, 8, 0, 0, 0)
      CALL AXES3D("THETAS", 100, "ZS", 100, "RADIALS", 100, 15., 15., 15., 1)
      CALL VUARSI(-20., 70., 50.)
      CALL GRAF3D(-20., 10., 50., -1., 10., 50., -0.5, 10., 50.)
      LK=LL
      CALL NEWPEN(I)
      DO 212 KL=1,2
      IF(KL, EQ, 1) GO TO 204
      IF(KL, GT, 1) GO TO 201
204  DO 206 I=1,3
      K=3*(I-1)+1
206  CALL CURV3D(X(IK), Y(IK), Z(IK), 3, 1)
      DO 207 J=1,3
      K=J
      XX(1)=X(K)
      YY(1)=Y(K)
      ZZ(1)=Z(K)
      XX(2)=X(K+3)
      YY(2)=Y(K+3)
      ZZ(2)=Z(K+3)
      XX(3)=X(K+6)
      YY(3)=Y(K+6)
      ZZ(3)=Z(K+6)
      PRINT*, XX(1), YY(1), ZZ(1), XX(2), YY(2), ZZ(2), XX(3), YY(3), ZZ(3)
207  CALL CURV3D(XX, YY, ZZ, 3, 1)
      IF(KL, EQ, 1) GO TO 208
201  DO 203 L=1,NR
      XXX(L)=X(L)
      YYY(L)=Y(L)
      IF(LLL, EQ, 1) GO TO 199
      IF(LLL, EQ, 2) GO TO 199
      IF(LLL, EQ, 3) ZZ(L)=Z(L)+U4(L, LL)*5.
      GO TO 203
199  ZZZ(L)=Z(L)+U2(L, LL)*5.
203  PRINT*, XXX(L), YYY(L), ZZZ(L)
205  DO 209 I=1,3
      K=3*(I-1)+1
209  CALL CURV3D(XXX(K), YYY(K), ZZZ(K), 3, 1)
      DO 210 J=1,3
      K=J
      XA(1)=XXX(K)
      YA(1)=YYY(K)
      ZA(1)=ZZZ(K)
      XA(2)=XXX(K+3)
      YA(2)=YYY(K+3)
      ZA(2)=ZZZ(K+3)
      XA(3)=XXX(K+6)
      YA(3)=YYY(K+6)
      ZA(3)=ZZZ(K+6)
      PRINT*, XA(1), YA(1), ZA(1), XA(2), YA(2), ZA(2), XA(3), YA(3), ZA(3)
210  CALL CURV3D(XA, YA, ZA, 3, 1)
      IF(KL, GT, 1) GO TO 216
208  CALL N7H1DF
      CALL NEWPEN(I)
      IF(KL, EQ, 1) GO TO 217
216  CALL NEWPEN(I)
217  CONTINUE
      CALL DASH
212  CONTINUE
211  CALL FNDPL(I)
6   CONTINUE
      CALL DONEPL
215  STOP
      END
*   END OF RECORD

```

Figure C-1. Program Matrix Listing (Continued).

-19.	24.375	12.5						
-5.5	24.375	12.5						
19.	24.375	10.5						
-19.	6.	12.5						
-5.5	6.	12.5						
19.	6.	10.5						
-19.	0.	12.5						
-5.5	0.	12.5						
19.	0.	10.5						
1	84	1	169.437	2.1589694	5	1		
2	90	2	181.251	2.2807813	5	2		
1	103	0	206.396	.7570244	5	1		
4	103	0	206.643	.7313859	5	4		
2	119	0	234.039	.6190009	5	2		
5	119	0	234.212	.7674094	5	5		
4	139	1	279.993	.7539196	5	4		
2	225	1	451.669	.7763402	5	2		
3	242	1	484.487	.7087252	5	3		
1	1	168.	.000E+00	.000E+00	30.5	.0	.0	
1	2	7.69	.000E+00	.000E+00	72.6	.0	.0	
1	3	-24.6	.000E+00	.000E+00	94.5	.0	.0	
1	4	53.3	.000E+00	.000E+00	63.1	.0	.0	
1	5	-44.2	.000E+00	.000E+00	69.5	.0	.0	
1	6	-31.2	.000E+00	.000E+00	22.7	.0	.0	
1	7	10.5	.000E+00	.000E+00	108.9	.0	.0	
1	8	5.30	.000E+00	.000E+00	55.1	.0	.0	
1	9	-11.3	.000E+00	.000E+00	90.7	.0	.0	
2	1	132.	.000E+00	.000E+00	121.4	.0	.0	
2	2	2.41	.000E+00	.000E+00	.3	.0	.0	
2	3	-27.6	.000E+00	.000E+00	165.7	.0	.0	
2	4	127.	.000E+00	.000E+00	105.1	.0	.0	
2	5	-48.9	.000E+00	.000E+00	122.5	.0	.0	
2	6	-23.5	.000E+00	.000E+00	28.1	.0	.0	
2	7	5.41	.000E+00	.000E+00	172.1	.0	.0	
2	8	8.39	.000E+00	.000E+00	4.3	.0	.0	
2	9	-19.5	.000E+00	.000E+00	139.2	.0	.0	
1	1	80.8	.000E+00	.000E+00	127.3	.0	.0	
1	2	-14.6	.000E+00	.000E+00	122.1	.0	.0	
1	3	153.	.000E+00	.000E+00	121.5	.0	.0	
1	4	790.	.000E+00	.000E+00	141.6	.0	.0	
1	5	202.	.000E+00	.000E+00	140.4	.0	.0	
1	6	-280.	.000E+00	.000E+00	135.8	.0	.0	
1	7	-142.	.000E+00	.000E+00	132.3	.0	.0	
1	8	-24.1	.000E+00	.000E+00	120.3	.0	.0	
1	9	143.	.000E+00	.000E+00	120.6	.0	.0	
4	1	48.9	.000E+00	.000E+00	45.2	.0	.0	
4	2	-11.0	.000E+00	.000E+00	110.5	.0	.0	
4	3	145.	.000E+00	.000E+00	108.5	.0	.0	
4	4	737.	.000E+00	.000E+00	134.5	.0	.0	
4	5	228.	.000E+00	.000E+00	131.5	.0	.0	
4	6	-275.	.000E+00	.000E+00	126.7	.0	.0	
4	7	-121.	.000E+00	.000E+00	122.6	.0	.0	
4	8	-25.4	.000E+00	.000E+00	119.2	.0	.0	
4	9	140.	.000E+00	.000E+00	113.4	.0	.0	
2	1	264.	.000E+00	.000E+00	64.5	.0	.0	
2	2	-14.0	.000E+00	.000E+00	150.2	.0	.0	
2	3	142.	.000E+00	.000E+00	141.9	.0	.0	
2	4	77.2	.000E+00	.000E+00	98.5	.0	.0	
2	5	-131.	.000E+00	.000E+00	145.9	.0	.0	
2	6	-502.	.000E+00	.000E+00	140.0	.0	.0	
2	7	-96.4	.000E+00	.000E+00	148.7	.0	.0	
2	8	-30.8	.000E+00	.000E+00	149.7	.0	.0	
2	9	112.	.000E+00	.000E+00	142.6	.0	.0	
5	1	346.	.000E+00	.000E+00	56.8	.0	.0	
5	2	8.51	.000E+00	.000E+00	29.0	.0	.0	
5	3	87.7	.000E+00	.000E+00	161.5	.0	.0	
5	4	33.6	.000E+00	.000E+00	96.7	.0	.0	
5	5	-101.	.000E+00	.000E+00	150.6	.0	.0	
5	6	-437.	.000E+00	.000E+00	137.6	.0	.0	
5	7	61.6	.000E+00	.000E+00	13.5	.0	.0	
5	8	-29.6	.000E+00	.000E+00	153.4	.0	.0	
5	9	83.3	.000E+00	.000E+00	160.3	.0	.0	
4	1	421.	.000E+00	.000E+00	22.1	.0	.0	
4	2	-13.9	.000E+00	.000E+00	123.9	.0	.0	
4	3	125.	.000E+00	.000E+00	174.4	.0	.0	
4	4	80.8	.000E+00	.000E+00	21.1	.0	.0	

Figure C-1. Program Matrix Listing (Continued).

4	5	-60.8	.000E+00	.000E+00	64.9	.0	.0
4	6	232.	.000E+00	.000E+00	169.8	.0	.0
4	7	82.8	.000E+00	.000E+00	11.4	.0	.0
4	8	-64.0	.000E+00	.000E+00	175.8	.0	.0
4	9	107.	.000E+00	.000E+00	174.7	.0	.0
2	1	-724.	.000E+00	.000E+00	177.7	.0	.0
2	2	-27.7	.000E+00	.000E+00	88.0	.0	.0
2	3	201.	.000E+00	.000E+00	36.3	.0	.0
2	4	33.7	.000E+00	.000E+00	116.8	.0	.0
2	5	68.0	.000E+00	.000E+00	155.6	.0	.0
2	6	-50.8	.000E+00	.000E+00	2.9	.0	.0
2	7	-89.3	.000E+00	.000E+00	94.7	.0	.0
2	8	-18.0	.000E+00	.000E+00	6.5	.0	.0
2	9	18.0	.000E+00	.000E+00	14.6	.0	.0
3	1	979.	.000E+00	.000E+00	11.1	.0	.0
3	2	-16.9	.000E+00	.000E+00	57.6	.0	.0
3	3	185.	.000E+00	.000E+00	42.8	.0	.0
3	4	-81.6	.000E+00	.000E+00	91.8	.0	.0
3	5	64.5	.000E+00	.000E+00	53.9	.0	.0
3	6	-68.2	.000E+00	.000E+00	44.9	.0	.0
3	7	119.	.000E+00	.000E+00	60.8	.0	.0
3	8	-61.5	.000E+00	.000E+00	42.7	.0	.0
3	9	124.	.000E+00	.000E+00	47.6	.0	.0
1	1	156.	.000E+00	.000E+00	118.6	.0	.0
1	2	5.86	.000E+00	.000E+00	112.0	.0	.0
1	3	-25.0	.000E+00	.000E+00	118.9	.0	.0
1	4	47.8	.000E+00	.000E+00	111.8	.0	.0
1	5	-115.	.000E+00	.000E+00	82.5	.0	.0
1	6	-13.2	.000E+00	.000E+00	125.1	.0	.0
1	7	22.9	.000E+00	.000E+00	125.7	.0	.0
1	8	16.6	.000E+00	.000E+00	109.9	.0	.0
1	9	-14.9	.000E+00	.000E+00	125.8	.0	.0
2	1	167.	.000E+00	.000E+00	99.0	.0	.0
2	2	-9.11	.000E+00	.000E+00	88.4	.0	.0
2	3	-44.0	.000E+00	.000E+00	92.3	.0	.0
2	4	146.	.000E+00	.000E+00	62.7	.0	.0
2	5	-20.9	.000E+00	.000E+00	147.0	.0	.0
2	6	-26.0	.000E+00	.000E+00	122.7	.0	.0
2	7	37.6	.000E+00	.000E+00	151.4	.0	.0
2	8	-5.06	.000E+00	.000E+00	32.9	.0	.0
2	9	-46.0	.000E+00	.000E+00	85.9	.0	.0
4	1	67.1	.000E+00	.000E+00	47.3	.0	.0
4	2	34.1	.000E+00	.000E+00	114.6	.0	.0
4	3	118.	.000E+00	.000E+00	93.9	.0	.0
4	4	576.	.000E+00	.000E+00	126.4	.0	.0
4	5	186.	.000E+00	.000E+00	123.7	.0	.0
4	6	-238.	.000E+00	.000E+00	118.6	.0	.0
4	7	-140.	.000E+00	.000E+00	119.9	.0	.0
4	8	-9.84	.000E+00	.000E+00	145.6	.0	.0
4	9	136.	.000E+00	.000E+00	122.2	.0	.0
1	1	97.7	.000E+00	.000F+00	110.0	.0	.0
1	2	32.4	.000E+00	.000E+00	104.1	.0	.0
1	3	136.	.000E+00	.000E+00	80.3	.0	.0
1	4	664.	.000E+00	.000E+00	116.5	.0	.0
1	5	215.	.000E+00	.000E+00	114.2	.0	.0
1	6	-275.	.000E+00	.000E+00	113.6	.0	.0
1	7	-151.	.000E+00	.000E+00	103.3	.0	.0
1	8	-8.25	.000E+00	.000E+00	101.7	.0	.0
1	9	155.	.000E+00	.000F+00	112.2	.0	.0
3	1	202.	.000E+00	.000E+00	71.6	.0	.0
3	2	-1.11	.000E+00	.000E+00	41.2	.0	.0
3	3	116.	.000E+00	.000F+00	145.6	.0	.0
3	4	103.	.000E+00	.000E+00	105.2	.0	.0
3	5	34.8	.000F+00	.000E+00	154.3	.0	.0
3	6	-449.	.000E+00	.000E+00	134.0	.0	.0
3	7	-65.2	.000E+00	.000E+00	159.0	.0	.0
3	8	-27.6	.000F+00	.000E+00	152.1	.0	.0
3	9	92.4	.000E+00	.000E+00	149.0	.0	.0
6	1	296.	.000F+00	.000E+00	55.5	.0	.0
6	2	8.24	.000E+00	.000E+00	81.7	.0	.0
6	3	115.	.000E+00	.000E+00	174.4	.0	.0
6	4	45.4	.000E+00	.000E+00	85.1	.0	.0
6	5	37.9	.000E+00	.000E+00	180.0	.0	.0
6	6	-395.	.000E+00	.000E+00	132.6	.0	.0
6	7	73.6	.000E+00	.000E+00	13.9	.0	.0
6	8	-31.3	.000E+00	.000E+00	167.9	.0	.0

Figure C-1. Program Matrix Listing (Continued).

6	9	84.9	.000E+00	.000E+00	175.4	.0	.0
5	1	360.	.000E+00	.000E+00	44.0	.0	.0
5	2	15.1	.000E+00	.000E+00	83.3	.0	.0
5	3	-90.1	.000E+00	.000E+00	14.1	.0	.0
5	4	121.	.000E+00	.000E+00	69.0	.0	.0
5	5	-21.2	.000E+00	.000E+00	168.6	.0	.0
5	6	148.	.000E+00	.000E+00	179.9	.0	.0
5	7	63.3	.000E+00	.000E+00	50.4	.0	.0
5	8	-35.5	.000E+00	.000E+00	177.6	.0	.0
5	9	-82.1	.000E+00	.000E+00	13.3	.0	.0
2	1	-393.	.000E+00	.000E+00	136.0	.0	.0
2	2	-22.0	.000E+00	.000E+00	20.8	.0	.0
2	3	-197.	.000E+00	.000E+00	130.4	.0	.0
2	4	57.9	.000E+00	.000E+00	118.0	.0	.0
2	5	-11.6	.000E+00	.000E+00	174.9	.0	.0
2	6	29.7	.000E+00	.000E+00	177.9	.0	.0
2	7	-88.1	.000E+00	.000E+00	90.6	.0	.0
2	8	17.8	.000E+00	.000E+00	152.1	.0	.0
2	9	-34.8	.000E+00	.000E+00	165.8	.0	.0
3	1	483.	.000E+00	.000E+00	3.4	.0	.0
3	2	-33.6	.000E+00	.000E+00	104.3	.0	.0
3	3	-258.	.000E+00	.000E+00	177.2	.0	.0
3	4	-42.2	.000E+00	.000E+00	107.6	.0	.0
3	5	29.4	.000E+00	.000E+00	115.0	.0	.0
3	6	27.8	.000E+00	.000E+00	41.8	.0	.0
3	7	20.8	.000E+00	.000E+00	26.7	.0	.0
3	8	-44.6	.000E+00	.000E+00	129.0	.0	.0
3	9	31.9	.000F+00	.000E+00	85.2	.0	.0
1	69	1	139.975	2.0175486	5	1	
2	89	2	179.832	3.0957055	5	2	
4	102	0	204.245	.7355951	5	4	
1	102	0	204.655	.6540350	5	1	
3	119	0	238.630	.6101121	5	3	
6	119	0	238.660	.6657898	5	6	
5	140	0	280.646	.7069019	5	5	
2	226	2	453.668	1.0136778	5	2	
3	233	2	466.076	1.1651139	5	3	
-19.	24.375	12.5					
-1.	24.375	12.5					
19.	24.375	10.5					
-19.	14.	12.5					
-1.	14.	12.5					
19.	14.	10.5					
-19.	0.	12.5					
-1.	0.	12.5					
19.	0.	10.5					
1	69	3	137.275	4.7611160	5	1	
5	103	0	207.085	.7830667	5	5	
3	119	0	239.182	.7887224	5	3	
5	140	1	280.553	.9846845	5	5	
6	147	4	294.848	2.7664447	5	6	
3	163	2	327.881	1.2368145	5	3	
7	197	4	394.224	2.2474298	5	7	
4	207	2	414.164	1.0396776	5	4	
6	226	2	453.688	1.2814689	5	6	
1	1	214.	.000E+00	.000E+00	97.4	.0	.0
1	2	1.49	.000E+00	.000E+00	22.1	.0	.0
1	3	-37.9	.000E+00	.000F+00	103.5	.0	.0
1	4	-37.5	.000E+00	.000E+00	56.9	.0	.0
1	5	-6.65	.000E+00	.000E+00	133.3	.0	.0
1	6	45.1	.000E+00	.000E+00	132.1	.0	.0
1	7	41.5	.000E+00	.000E+00	111.7	.0	.0
1	8	2.71	.000E+00	.000E+00	78.2	.0	.0
1	9	-24.5	.000E+00	.000E+00	110.8	.0	.0
5	1	-61.8	.000E+00	.000E+00	96.6	.0	.0
5	2	-17.7	.000E+00	.000E+00	117.4	.0	.0
5	3	150.	.000E+00	.000E+00	100.8	.0	.0
5	4	810.	.000E+00	.000E+00	86.1	.0	.0
5	5	276.	.000E+00	.000E+00	120.4	.0	.0
5	6	-487.	.000E+00	.000E+00	111.0	.0	.0
5	7	-143.	.000E+00	.000E+00	116.0	.0	.0
5	8	-39.9	.000E+00	.000E+00	118.3	.0	.0
5	9	172.	.000E+00	.000E+00	108.2	.0	.0
3	1	61.9	.000E+00	.000E+00	159.6	.0	.0
3	2	-24.4	.000E+00	.000E+00	117.3	.0	.0
3	3	139.	.000E+00	.000E+00	116.5	.0	.0

Figure C-1. Program Matrix Listing (Continued).

3	4	82.1	.000E+00	.000E+00	91.9	.0	.0
3	5	153.	.000F+00	.000F+00	20.1	.0	.0
3	6	-611.	.000E+00	.000E+00	88.2	.0	.0
3	7	-112.	.000E+00	.000E+00	132.8	.0	.0
3	8	-31.1	.000E+00	.000E+00	127.7	.0	.0
3	9	128.	.000E+00	.000E+00	118.3	.0	.0
5	1	-266.	.000F+00	.000F+00	176.7	.0	.0
5	2	-11.8	.000E+00	.000E+00	62.6	.0	.0
5	3	117.	.000E+00	.000F+00	137.7	.0	.0
5	4	107.	.000E+00	.000E+00	.3	.0	.0
5	5	124.	.000F+00	.000F+00	111.9	.0	.0
5	6	310.	.000E+00	.000E+00	148.8	.0	.0
5	7	-103.	.000E+00	.000F+00	110.0	.0	.0
5	8	-42.8	.000E+00	.000E+00	148.6	.0	.0
5	9	109.	.000E+00	.000F+00	134.0	.0	.0
6	1	509.	.000E+00	.000F+00	41.3	.0	.0
6	2	-41.0	.000F+00	.000E+00	166.0	.0	.0
6	3	-180.	.000F+00	.000E+00	16.6	.0	.0
6	4	145.	.000E+00	.000F+00	162.7	.0	.0
6	5	278.	.000E+00	.000F+00	169.8	.0	.0
6	6	-72.0	.000F+00	.000E+00	24.7	.0	.
6	7	321.	.000E+00	.000F+00	2.3	.0	.0
6	8	26.8	.000F+00	.000E+00	.8	.0	.0
6	9	-163.	.000E+00	.000E+00	9.7	.0	.0
3	1	320.	.000E+00	.000E+00	118.1	.0	.0
3	2	-15.5	.000E+00	.000E+00	50.2	.0	.0
3	3	-4.53	.000E+00	.000E+00	137.2	.0	.0
3	4	48.5	.000E+00	.000E+00	32.7	.0	.0
3	5	-28.7	.000E+00	.000E+00	94.7	.0	.0
3	6	20.9	.000F+00	.000E+00	97.9	.0	.0
3	7	32.3	.000E+00	.000E+00	104.4	.0	.0
3	8	20.0	.000E+00	.000F+00	29.4	.0	.0
3	9	27.8	.000E+00	.000E+00	179.8	.0	.0
7	1	432.	.000E+00	.000E+00	67.9	.0	.0
7	2	-9.72	.000F+00	.000E+00	98.1	.0	.0
7	3	41.9	.000E+00	.000E+00	42.7	.0	.0
7	4	28.5	.000E+00	.000E+00	82.3	.0	.0
7	5	-29.2	.000E+00	.000E+00	26.4	.0	.0
7	6	-22.1	.000E+00	.000E+00	50.3	.0	.0
7	7	18.4	.000E+00	.000E+00	96.2	.0	.0
7	8	-9.62	.000E+00	.000E+00	143.7	.0	.0
7	9	-24.5	.000E+00	.000E+00	147.0	.0	.0
4	1	437.	.000E+00	.000E+00	25.4	.0	.0
4	2	-12.3	.000E+00	.000E+00	24.2	.0	.0
4	3	114.	.000E+00	.000E+00	63.0	.0	.0
4	4	43.1	.000E+00	.000E+00	40.2	.0	.0
4	5	-17.4	.000E+00	.000E+00	145.9	.0	.0
4	6	-51.0	.000E+00	.000E+00	68.5	.0	.0
4	7	15.7	.000E+00	.000E+00	157.5	.0	.0
4	8	13.0	.000E+00	.000E+00	128.2	.0	.0
4	9	28.6	.000E+00	.000E+00	64.0	.0	.0
6	1	-390.	.000F+00	.000E+00	169.3	.0	.0
6	2	-24.3	.000E+00	.000E+00	7.7	.0	.0
6	3	87.3	.000E+00	.000E+00	64.2	.0	.0
6	4	42.0	.000F+00	.000E+00	3.5	.0	.0
6	5	16.1	.000E+00	.000E+00	3.6	.0	.0
6	6	350.	.000E+00	.000E+00	50.3	.0	.0
6	7	-85.2	.000E+00	.000E+00	84.4	.0	.0
6	8	33.9	.000E+00	.000E+00	131.9	.0	.0
6	9	-23.1	.000E+00	.000E+00	166.9	.0	.0
1	1	155.	.000E+00	.000E+00	98.2	.0	.0
1	2	-2.83	.000E+00	.000E+00	151.2	.0	.0
1	3	-9.09	.000E+00	.000E+00	67.7	.0	.0
1	4	-27.2	.000F+00	.000E+00	86.1	.0	.0
1	5	18.9	.000F+00	.000E+00	64.2	.0	.0
1	6	-19.7	.000E+00	.000E+00	132.2	.0	.0
1	7	5.23	.000E+00	.000E+00	88.4	.0	.0
1	8	-578	.000F+00	.000E+00	136.4	.0	.0
1	9	-6.20	.000E+00	.000F+00	86.2	.0	.0
4	1	-112.	.000E+00	.000E+00	160.9	.0	.0
4	2	-41.4	.000E+00	.000E+00	139.2	.0	.0
4	3	161.	.000E+00	.000E+00	133.8	.0	.0
4	4	1030.	.000E+00	.000E+00	103.8	.0	.0
4	5	163.	.000E+00	.000E+00	117.1	.0	.0
4	6	-828.	.000F+00	.000E+00	125.5	.0	.0
4	7	-147.	.000E+00	.000E+00	134.2	.0	.0

Figure C-1. Program Matrix Listing (Continued).

4	8	-56.1	.000E+00	.000E+00	.25.8	.0	.0
4	9	191.	.000E+00	.000E+00	11.4	.0	.0
5	1	282.	.000E+00	.000E+00	34.5	.0	.0
5	2	16.3	.000E+00	.000E+00	175.5	.0	.0
5	3	169.	.000E+00	.000E+00	174.2	.0	.0
5	4	226.	.000E+00	.000E+00	160.2	.0	.0
5	5	-84.4	.000E+00	.000E+00	144.2	.0	.0
5	6	-716.	.000E+00	.000E+00	141.3	.0	.0
5	7	113.	.000E+00	.000E+00	2.6	.0	.0
5	8	31.9	.000E+00	.000E+00	149.8	.0	.0
5	9	175.	.000E+00	.000E+00	158.6	.0	.0
1	1	-485.	.000E+00	.000E+00	172.8	.0	.0
1	2	-38.1	.000E+00	.000E+00	144.4	.0	.0
1	3	284.	.000E+00	.000E+00	176.8	.0	.0
1	4	365.	.000E+00	.000E+00	145.5	.0	.0
1	5	197.	.000E+00	.000E+00	152.4	.0	.0
1	6	518.	.000E+00	.000E+00	143.9	.0	.0
1	7	-410.	.000E+00	.000E+00	162.8	.0	.0
1	8	-99.5	.000E+00	.000E+00	159.6	.0	.0
1	9	307.	.000E+00	.000E+00	153.0	.0	.0
3	1	294.	.000E+00	.000E+00	70.7	.0	.0
3	2	-12.7	.000E+00	.000E+00	165.2	.0	.0
3	3	96.5	.000E+00	.000E+00	159.7	.0	.0
3	4	185.	.000E+00	.000E+00	34.2	.0	.0
3	5	-7.66	.000E+00	.000E+00	125.9	.0	.0
3	6	68.3	.000E+00	.000E+00	14.9	.0	.0
3	7	140.	.000E+00	.000E+00	4.6	.0	.0
3	8	4.84	.000E+00	.000E+00	145.1	.0	.0
3	9	162.	.000E+00	.000E+00	174.1	.0	.0
4	1	305.	.000E+00	.000E+00	71.2	.0	.0
4	2	-23.1	.000E+00	.000E+00	68.3	.0	.0
4	3	99.1	.000E+00	.000E+00	141.6	.0	.0
4	4	136.	.000E+00	.000E+00	22.7	.0	.0
4	5	-32.3	.000E+00	.000E+00	165.1	.0	.0
4	6	-123.	.000E+00	.000E+00	18.4	.0	.0
4	7	-72.4	.000E+00	.000E+00	138.4	.0	.0
4	8	9.92	.000E+00	.000E+00	144.4	.0	.0
4	9	107.	.000E+00	.000E+00	148.4	.0	.0
4	1	560.	.000E+00	.000E+00	53.7	.0	.0
4	2	-14.9	.000E+00	.000E+00	78.8	.0	.0
4	3	29.5	.000E+00	.000E+00	72.3	.0	.0
4	4	54.4	.000E+00	.000E+00	58.1	.0	.0
4	5	8.63	.000E+00	.000E+00	75.7	.0	.0
4	6	5.37	.000E+00	.000E+00	132.4	.0	.0
4	7	-27.5	.000E+00	.000E+00	34.1	.0	.0
4	8	-9.25	.000E+00	.000E+00	144.2	.0	.0
4	9	18.1	.000E+00	.000E+00	52.5	.0	.0
6	1	563.	.000E+00	.000E+00	75.5	.0	.0
6	2	-11.9	.000E+00	.000E+00	151.7	.0	.0
6	3	98.0	.000E+00	.000E+00	31.4	.0	.0
6	4	50.2	.000E+00	.000E+00	103.1	.0	.0
6	5	4.46	.000E+00	.000E+00	92.4	.0	.0
6	6	-115.	.000E+00	.000E+00	56.4	.0	.0
6	7	-29.0	.000E+00	.000E+00	89.8	.0	.0
6	8	-16.1	.000E+00	.000E+00	151.5	.0	.0
6	9	41.9	.000E+00	.000E+00	106.9	.0	.0
7	1	-305.	.000E+00	.000E+00	157.5	.0	.0
7	2	43.7	.000E+00	.000E+00	170.9	.0	.0
7	3	107.	.000E+00	.000E+00	7.0	.0	.0
7	4	36.9	.000E+00	.000E+00	101.0	.0	.0
7	5	-11.6	.000E+00	.000E+00	168.3	.0	.0
7	6	130.	.000E+00	.000E+00	15.9	.0	.0
7	7	-50.0	.000E+00	.000E+00	24.2	.0	.0
7	8	17.1	.000E+00	.000E+00	64.8	.0	.0
7	9	-11.9	.000E+00	.000E+00	37.3	.0	.0
1	74	1	149.872	1.7321522	5	1	
4	101	0	202.598	.6890111	5	4	
5	119	1	239.415	1.2039478	5	5	
1	138	1	276.142	.7430311	5	1	
3	150	0	301.519	.5816044	5	3	
4	161	2	323.245	1.7030649	5	4	
4	200	1	401.578	.9915557	5	4	
6	217	2	436.504	1.0381837	5	6	
7	229	1	456.524	.5899760	5	7	
			-19. 24.375	12.5			
			11. 24.375	12.5			

Figure C-1. Program Matrix Listing (Continued).

19.	24.375	10.5						
-19.	20.	12.5						
11.	20.	12.5						
19.	20.	10.5						
-19.	0.	12.5						
11.	0.	12.5						
19.	0.	10.5						
1	83	1	167.266	1.3821552	5	1		
2	90	0	190.424	.6090055	5	2		
4	103	0	297.288	.6091039	5	4		
5	114	4	229.543	3.7508655	5	5		
6	119	0	238.530	.5621688	5	6		
8	139	0	279.684	.5192603	5	8		
1	149	1	299.232	.6977379	5	1		
2	151	2	303.621	1.7963026	5	2		
3	164	0	328.523	.5889673	5	3		
1	1	12.2	.000E+00	.000E+00	128.9	.0	.0	
1	2	42.7	.000E+00	.000E+00	149.4	.0	.0	
1	3	-33.8	.000F+00	.000E+00	132.5	.0	.0	
1	4	13.3	.000E+00	.000E+00	116.7	.0	.0	
1	5	34.5	.000E+00	.000E+00	47.1	.0	.0	
1	6	-8.16	.000F+00	.000E+00	78.9	.0	.0	
1	7	7.55	.000F+00	.000E+00	125.5	.0	.0	
1	8	-10.5	.000E+00	.000E+00	99.6	.0	.0	
1	9	-13.4	.000F+00	.000E+00	139.7	.0	.0	
2	1	24.2	.000E+00	.000F+00	163.0	.0	.0	
2	2	62.8	.000E+00	.000E+00	150.9	.0	.0	
2	3	-30.4	.000F+00	.000E+00	124.9	.0	.0	
2	4	34.6	.000E+00	.000E+00	86.6	.0	.0	
2	5	-10.9	.000E+00	.000E+00	149.0	.0	.0	
2	6	29.0	.000F+00	.000E+00	39.4	.0	.0	
2	7	-19.6	.000E+00	.000E+00	35.5	.0	.0	
2	8	-7.19	.000E+00	.000E+00	87.8	.0	.0	
2	9	-14.2	.000E+00	.000E+00	165.5	.0	.0	
4	1	60.4	.000E+00	.000E+00	59.9	.0	.0	
4	2	60.7	.000E+00	.000E+00	123.6	.0	.0	
4	3	-79.3	.000E+00	.000E+00	60.3	.0	.0	
4	4	-102.	.000E+00	.000E+00	44.9	.0	.0	
4	5	-54.9	.000E+00	.000E+00	62.8	.0	.0	
4	6	42.5	.000E+00	.000E+00	49.9	.0	.0	
4	7	66.0	.000E+00	.000E+00	62.4	.0	.0	
4	8	-24.9	.000E+00	.000E+00	51.4	.0	.0	
4	9	-83.0	.000E+00	.000E+00	39.1	.0	.0	
5	1	4.54	.000E+00	.000E+00	92.0	.0	.0	
5	2	107.	.000E+00	.000E+00	103.0	.0	.0	
5	3	-17.7	.000E+00	.000E+00	98.4	.0	.0	
5	4	-76.9	.000E+00	.000E+00	22.4	.0	.0	
5	5	-8.47	.000E+00	.000F+00	106.1	.0	.0	
5	6	-14.0	.000F+00	.000E+00	90.9	.0	.0	
5	7	2.35	.000E+00	.000E+00	97.7	.0	.0	
5	8	8.65	.000E+00	.000E+00	112.4	.0	.0	
5	9	9.09	.000E+00	.000E+00	120.9	.0	.0	
6	1	65.5	.000E+00	.000E+00	65.4	.0	.0	
6	2	-110.	.000E+00	.000E+00	20.5	.0	.0	
6	3	-104.	.000F+00	.000F+00	67.9	.0	.0	
6	4	23.1	.000E+00	.000E+00	63.1	.0	.0	
6	5	-21.1	.000E+00	.000E+00	91.9	.0	.0	
6	6	137.	.000E+00	.000E+00	56.4	.0	.0	
6	7	62.7	.000E+00	.000E+00	62.3	.0	.0	
6	8	-57.9	.000F+00	.000E+00	59.2	.0	.0	
6	9	-112.	.000E+00	.000E+00	49.9	.0	.0	
8	1	89.6	.000E+00	.000E+00	100.7	.0	.0	
8	2	55.8	.000E+00	.000E+00	65.7	.0	.0	
8	3	-107.	.000E+00	.000E+00	101.1	.0	.0	
8	4	75.3	.00 E+00	.000E+00	96.4	.0	.0	
8	5	-64.5	.000E+00	.000E+00	80.0	.0	.0	
8	6	-144.	.000E+00	.000E+00	88.5	.0	.0	
8	7	48.4	.000E+00	.000E+00	106.1	.0	.0	
8	8	-50.4	.000E+00	.000E+00	110.2	.0	.0	
8	9	-62.8	.000E+00	.000E+00	124.2	.0	.0	
1	1	218.	.000E+00	.000E+00	157.4	.0	.0	
1	2	85.9	.000E+00	.000E+00	13.8	.0	.0	
1	3	-290.	.000E+00	.000E+00	58.9	.0	.0	
1	4	66.4	.000E+00	.000E+00	100.9	.0	.0	
1	5	100.	.000E+00	.000E+00	141.5	.0	.0	
1	6	-18.6	.000E+00	.000E+00	125.7	.0	.0	

Figure C-1. Program Matrix Listing (Continued).

1	7	185.	.000E+00	.000E+00	144.7	.0	.0
1	6	-79.0	.000E+00	.000E+00	88.5	.0	.0
1	9	-100.	.000E+00	.000E+00	84.2	.0	.0
2	1	103.	.000E+00	.000E+00	24.9	.0	.0
2	2	141.	.000E+00	.000E+00	163.1	.0	.0
2	3	-85.6	.000E+00	.000E+00	119.8	.0	.0
2	4	109.	.000E+00	.000E+00	38.1	.0	.0
2	5	68.0	.000E+00	.000E+00	7.3	.0	.0
2	6	-24.1	.000E+00	.000E+00	63.2	.0	.0
2	7	98.0	.000E+00	.000E+00	42.9	.0	.0
2	8	8.73	.000E+00	.000E+00	117.1	.0	.0
2	9	24.1	.000E+00	.000E+00	168.1	.0	.0
3	1	33.2	.000E+00	.000E+00	70.9	.0	.0
3	2	26.8	.000E+00	.000E+00	112.4	.0	.0
3	3	-111.	.000E+00	.000E+00	94.7	.0	.0
3	4	368.	.000E+00	.000E+00	69.2	.0	.0
3	5	-89.0	.000E+00	.000E+00	91.0	.0	.0
3	6	155.	.000E+00	.000E+00	104.1	.0	.0
3	7	-92.7	.000E+00	.000E+00	81.5	.0	.0
3	8	-27.6	.000E+00	.000E+00	90.1	.0	.0
3	9	-155.	.000E+00	.000E+00	84.2	.0	.0
3	1	98.8	.000E+00	.000E+00	164.2	.0	.0
3	2	5.22	.000E+00	.000E+00	11.1	.0	.0
3	3	-24.3	.000E+00	.000E+00	175.7	.0	.0
3	4	12.1	.000E+00	.000E+00	138.7	.0	.0
3	5	6.46	.000E+00	.000E+00	106.6	.0	.0
3	6	-9.28	.000E+00	.000E+00	151.2	.0	.0
3	7	13.3	.000E+00	.000E+00	126.0	.0	.0
3	8	9.55	.000E+00	.000E+00	36.4	.0	.0
3	9	13.0	.000E+00	.000E+00	9.6	.0	.0
4	1	-151.	.000E+00	.000E+00	41.9	.0	.0
4	2	-101.	.000F+00	.000F+00	111.2	.0	.0
4	3	-68.6	.000F+00	.000F+00	144.4	.0	.0
4	4	195.	.000E+00	.000E+00	98.1	.0	.0
4	5	12.9	.000E+00	.000E+00	74.0	.0	.0
4	6	185.	.000E+00	.000E+00	88.0	.0	.0
4	7	-104.	.000E+00	.000E+00	59.0	.0	.0
4	8	-90.2	.000E+00	.000E+00	90.0	.0	.0
4	9	-52.4	.000E+00	.000F+00	105.7	.0	.0
5	1	-223.	.000E+00	.000E+00	139.4	.0	.0
5	2	66.6	.000E+00	.000E+00	131.3	.0	.0
5	3	207.	.000E+00	.000E+00	114.2	.0	.0
5	4	285.	.000E+00	.000E+00	117.3	.0	.0
5	5	-35.7	.000E+00	.000E+00	112.9	.0	.0
5	6	-121.	.000E+00	.000E+00	120.0	.0	.0
5	7	-121.	.000E+00	.000E+00	117.2	.0	.0
5	8	51.0	.000E+00	.000E+00	128.1	.0	.0
5	9	178.	.000E+00	.000E+00	119.6	.0	.0
6	1	188.	.000E+00	.000E+00	93.8	.0	.0
6	2	-15.8	.000E+00	.000E+00	115.7	.0	.0
6	3	-45.6	.000E+00	.000E+00	114.1	.0	.0
6	4	-19.5	.000E+00	.000E+00	58.6	.0	.0
6	5	1.62	.000E+00	.000E+00	16.2	.0	.0
6	6	-13.6	.000E+00	.000E+00	59.7	.0	.0
6	7	40.4	.000E+00	.000F+00	116.6	.0	.0
6	8	-21.6	.000E+00	.000E+00	126.2	.0	.0
6	9	-39.6	.000E+00	.000E+00	117.3	.0	.0
7	1	129.	.000E+00	.000E+00	74.2	.0	.0
7	2	31.9	.000E+00	.000E+00	168.8	.0	.0
7	3	63.1	.000E+00	.000E+00	136.9	.0	.0
7	4	-37.5	.000E+00	.000E+00	156.8	.0	.0
7	5	7.96	.000E+00	.000F+00	121.6	.0	.0
7	6	-133.	.000E+00	.000E+00	144.4	.0	.0
7	7	-21.4	.000E+00	.000E+00	158.4	.0	.0
7	8	41.5	.000E+00	.000E+00	151.0	.0	.0
7	9	55.4	.000E+00	.000E+00	138.2	.0	.0
5	1	246.	.000E+00	.000E+00	31.8	.0	.0
5	2	-64.0	.000E+00	.000E+00	7.6	.0	.0
5	3	-96.8	.000E+00	.000F+00	6.7	.0	.0
5	4	-103.	.000F+00	.000E+00	168.8	.0	.0
5	5	-19.6	.000E+00	.000E+00	167.5	.0	.0
5	6	144.	.000E+00	.000F+00	173.6	.0	.0
5	7	-84.5	.000E+00	.000E+00	174.2	.0	.0
5	8	-72.1	.000E+00	.000F+00	.8	.0	.0
5	9	-96.2	.000E+00	.000E+00	.1	.0	.0
6	1	577.	.000E+00	.000F+00	51.7	.0	.0

Figure C-1. Program Matrix Listing (Continued).

6	2	28.3	.000E+00	.000E+00	176.9	.0	.0
6	3	-33.8	.000E+00	.000E+00	106.3	.0	.0
6	4	-42.2	.000E+00	.000E+00	109.1	.0	.0
6	5	5.72	.000E+00	.000E+00	29.5	.0	.0
6	6	-51.1	.000E+00	.000E+00	29.1	.0	.0
6	7	-148.	.000E+00	.000E+00	178.1	.0	.0
6	8	-25.2	.000E+00	.000E+00	52.6	.0	.0
6	9	-76.0	.000E+00	.000E+00	72.2	.0	.0
7	1	432.	.000E+00	.000E+00	6.6	.0	.0
7	2	-274.	.000E+00	.000E+00	28.1	.0	.0
7	3	-564.	.000E+00	.000E+00	.7	.0	.0
7	4	44.	.000E+00	.000E+00	15.5	.0	.0
7	5	-15.4	.00 E+00	.000E+00	15.8	.0	.0
7	6	-130.	.000E+00	.000E+00	15.3	.0	.0
7	7	562.	.000E+00	.000E+00	27.3	.0	.0
7	8	-223.	.000E+00	.000E+00	1.1	.0	.0
7	9	520.	.000E+00	.000E+00	147.3	.0	.0
3	1	364.	.000E+00	.000E+00	112.0	.0	.0
3	2	7.72	.000E+00	.000E+00	18.3	.0	.0
3	3	53.8	.000E+00	.000E+00	98.3	.0	.0
3	4	-88.3	.000E+00	.000E+00	162.1	.0	.0
3	5	-3.97	.000E+00	.000E+00	35.5	.0	.0
3	6	14.4	.000E+00	.000E+00	34.9	.0	.0
3	7	-55.0	.000E+00	.000E+00	21.4	.0	.0
3	8	20.6	.000E+00	.000E+00	50.0	.0	.0
3	9	26.1	.000E+00	.000E+00	73.2	.0	.0
3	84	2	164.285	2.8288817	5	3	
4	90	0	180.711	.6866900	5	4	
5	104	0	208.393	.7893097	5	5	
6	110	5	220.972	4.8140106	5	6	
7	119	1	238.822	1.0497084	5	7	
5	139	0	279.764	.5510013	5	5	
6	146	1	293.175	1.0753403	5	6	
7	150	0	300.294	.5929505	5	7	
3	162	4	324.819	2.8444567	5	3	
" END OF RECORD							
DRAW=1-END\$							

Figure C-1. Program Matrix Listing (Concluded).

280.646									
453.668									
466.076									
-2.619	-.202	1.755	1.407	-.633	.240	.853	-.251	-.114	
-.346	-.012	1.843	1.043	-.059	-.157	-.043	-.022	.040	
-.4310	-.067	1.824	1.027	-.011	-.143	-.070	-.040	-.021	
2.562	-.014	-.991	2.815	-.752	.231	.127	.106	-.206	
-.793	-.025	1.244	1.242	-.462	.003	-.115	-.038	.152	
.607	-.181	.804	-.025	-.213	-.1.097	-1.124	-.185	.658	
-.732	-.039	.437	-.054	-.217	-.351	.187	-.081	.032	
.162	.008	-.099	-.007	-.050	-.136	-.091	.026	-.015	
-.851	.026	.120	-.055	.409	-.001	.049	.001	.008	
52.106	2.665	22.903	4.431	.409	-.6.920	10.783	-2.448	4.353	
2.665	.173	1.405	-.100	.090	-.253	.590	-.117	.265	
22.903	1.605	12.534	2.957	1.103	-.3.789	4.842	-1.107	2.625	
-.431	-.300	2.957	4.262	.190	-.1.681	-1.821	.173	-.207	
.909	.090	1.108	-.190	.863	-.865	-.1.0	-.134	.512	
-.6.920	-.253	3.789	-.1.681	-.865	7.531	-.173	.565	-1.941	
10.783	.580	4.842	-.1.821	-.010	-.173	2.697	-.426	.614	
-.2.448	-.117	1.107	.173	-.184	.565	-.456	.155	-.270	
4.353	.265	2.625	-.207	.512	-.1.941	.614	-.270	.904	

THE EIGENVALUES ARE:

THE COMPARISON OF EIGENVALUES:

UNLOADED	PREDICTED	ACTUAL	PERCENT	SQUARE	PREDICTED	PERCENT	SQUARE	
EXPERIMENTAL	MASS-LOADED	MASS-LOADED	ERROR	ROOT	MASS-LOADED	ERROR	ROOT	
DATA	USING	EXPERIMENTAL	PREDICTED	OF	USING	PREDICTED	OF	
SQUARE MODAL			DATA			VERSUS		
MATRIX			DIFF'S			VERSUS		
			ACTUAL			50*0 (9ROWS,8COLS)		
169.437	159.454	139.975	-13.92	.39	169.437	-21.05	2.59	
181.251	176.554	179.832	1.82	.85	181.251	-.79	2.65	
206.396	197.687	204.245	3.21	.39	206.396	-1.05	1.44	
206.643	206.499	204.655	-.90	.42	206.643	-.97	1.49	
238.039	233.101	238.630	2.32	3.87	238.039	.25	3.80	
238.212	238.144	238.660	.22	1.31	238.212	.19	3.27	
279.993	278.872	280.646	.63	.84	279.993	.23	1.26	
451.669	450.286	453.668	.75	8.65	451.669	.44	8.71	
484.487	483.779	466.076	-3.80	.72	0.000	100.00	1.79	

1.
 .03935263276104
 -.175363006526
 .2073197035749
 -.3763924572951
 -.1670133446116
 .09739424924915
 .03701173773741
 -.1063298400954
 .6241900775484
 -.04570486746359
 -.35858313139561
 1.
 -.8188571713628
 .02468098086104
 .1414912860321
 .1121140266862
 -.3764636974775
 .2970937382057
 -.002409682492266
 .06594301379177
 1.
 .1533587683567
 -.2440583475722
 -.1182601321003
 -.000614223666287

Figure C-2. Edited Output From Program Matrix.

Sample output from DIS3DPA graphics, 1 page:

```
.....  
WORKBOX-DIMENSIONS  
.....  
X3DAXIS= 15.00  
Y3DAXIS= 15.00  
Z3DAXIS= 15.00  
IN ABS. 3-D UNITS  
.....  
VIEWPOINT  
.....  
XVU=-2.000E+01  
YVU= 7.000E+01  
ZVU= 5.000E+01  
IN ABS. 3-D UNITS  
.....  
GRAPH SET-UP 1 GRAF3D  
.....  
ORIGIN  
.....  
X3DORIGIN=-2.000E+01  
Y3DORIGIN=-1.000E+00  
Z3DORIGIN=-5.000E-01  
.....  
STEP SIZE  
.....  
X3DSTP= 1.000E+01  
Y3DSTP= 1.000E+01  
Z3DSTP= 1.000E+01  
.....  
MAXIMUM  
.....  
X3DMAX= 5.000E+01  
Y3DMAX= 5.000E+01  
Z3DMAX= 5.000E+01  
.....  
LOCATION OF CURRENT PHYSICAL ORIGIN  
X= .50 Y= 1.12 INCHES  
FROM LOWER LEFT CORNER OF PAGE
```

Figure C-2. Edited Output From Program Matrix (Continued).

276.142
301.519
323.245
401.578
434.504
456.524

2.406	-.151	.167	1.012	-.074	1.474	.203	.479	-.018
.137	.036	-.071	-.036	-.066	-.274	.025	-.033	.025
1.409	.058	-.442	.562	-.087	.083	.524	.012	-.163
1.088	-.015	-.343	1.605	.350	.142	.495	.049	-.160
-.005	-.041	.055	-.116	.282	.082	.339	-.032	.008
1.213	-.128	-.151	-2.930	.861	-2.019	.571	-.217	-.037
-.282	.044	-.152	.081	-.374	-.139	.007	.118	-.234
.109	.024	-.054	.029	-.115	-.164	.005	.004	.001
-.632	-.001	-.363	.652	-.042	.873	.654	.118	-.320
12.391	-.843	-1.041	.453	-.450	-6.227	2.236	-.010	1.229
-.843	.132	.222	-.013	-.075	.175	.041	.065	-.098
-1.041	.222	1.611	1.639	-.067	-.358	-.473	.073	.962
.453	-.013	1.639	2.862	.078	-1.879	-.349	-.040	1.594
-.450	-.075	-.067	.076	.294	.943	.400	-.132	.022
-.6222	.125	-.353	-1.879	.943	9.367	-1.835	-.307	-1.247
2.236	-.041	-.473	-.349	-.400	-1.835	1.257	.159	-.047
-.010	.065	.073	-.040	-.132	-.307	.154	.072	-.048
1.229	-.098	.962	1.594	.022	-1.247	-.047	-.048	1.214

THE EIGENVALUES ARE:

THE COMPARISON OF EIGENVALUES:

UNLOADED	PREDICTED	ACTUAL	PERCENT	SQUARE	PREDICTED	PERCENT	SQUARE	
EXPERIMENTAL	MASS-LOADED	MASS-LOADED	ERROR	ROOT	MASS-LOADED	ERROR	ROOT	
DATA	USING	EXPERIMENTAL	PREDICTED	OF	USING	PREDICTED	OF	
SQUARE	MODAL	DATA	PREDICTED	VERSUS	DIFF'S	PSEUDOINVERSE	VERSUS	DIFF'S
MATRIX			ACTUAL	SO'D	19ROWS,8CQLS1	ACTUAL	SO'D	
137.275	137.085	149.872	8.53	.45	137.275	8.41	.43	
207.085	181.200	202.598	10.56	.44	207.085	2.21	2.57	
239.182	227.943	238.415	4.39	3.96	239.182	.32	4.28	
280.553	260.788	276.142	5.56	1.85	280.553	1.60	3.04	
294.848	286.278	301.519	5.05	1.62	294.848	2.21	2.53	
327.881	327.150	323.245	-1.21	.77	327.881	1.43	.89	
394.224	393.434	401.578	2.03	.17	394.224	1.83	.35	
414.164	413.894	434.506	4.74	.16	414.164	4.68	.26	
453.688	453.491	456.524	.66	4.08	.001	100.00	2.99	

1.
.008457103552768
-.1817037949291
-.1973675842973
-.04608525837128
.2268198035452
-.1959742337667
.01445647102725
-.1195120692267
.03897282641439
-.0513527429702
.2057647600871
1.
.5553119430493
-.7256695747228
-.1291540476511
-.07121916674448
.23037773737547
-.3241635862971
.09265044877094
-.2005212367571
.7396044777757
-.4413760844472

Figure C-2. Edited Output From Program Matrix (Continued).

279.764
293.175
300.294
324.819

-.628 2.866 737 -.368 1.065 .240 .100 .968 1.043
-.500 -1.662 .454 -.209 .061 -.556 -.326 .001 .156
-.749 -1.814 .722 -.117 -.277 -.625 -.455 -.021 .261
-.131 .606 .701 1.012 .175 -.278 -.751 .324 .951
-.053 .236 -.149 -.053 .038 -.107 .022 -.054 -.039
1.167 .071 -1.453 -.019 -.115 1.304 .707 -.764 -1.570
-.333 1.094 -.019 .179 .040 -.929 .714 .178 .293
-.397 -.729 .751 -.176 .082 -.649 -.255 .009 .181
-.611 .352 1.510 1.142 .216 -1.229 -.422 .747 1.544
7.803 -.170 -1.371 -1.050 .081 -1.241 .877 -.064 .458
-.130 .702 1.072 -.629 -.011 -.887 -.292 .645 .142
-1.371 1.072 2.177 -.439 -.046 -1.093 -1.154 .979 .072
-1.950 -.620 -.439 2.985 -.056 .347 .086 -.557 1.010
.041 -.011 -.046 -.056 .036 .004 .017 .005 -.049
-1.241 -.887 -1.093 .387 .004 2.563 -.592 -.921 -1.535
.877 -.292 -1.150 .086 .017 -.592 1.803 -.184 .954
-.064 .645 .979 -.557 .005 -.921 -.184 .621 .251
.458 .142 .072 1.010 -.069 -1.535 .954 .241 1.849

THE EIGENVALUES ARE:

THE COMPARISON OF EIGENVALUES:

UNLOADED EXPERIMENTAL DATA	PREDICTED MASS-LOADED USING SQUARE MODAL MATRIX	ACTUAL MASS-LOADED EXPERIMENTAL DATA	PERCENT ERROR VERSUS ACTUAL	SQUARE ROOT OF DIFF'S VERSUS 50'D	PREDICTED MASS-LOADED USING PSFUDINV OFROWS,BCOLS)	PREDICTED VERSUS ACTUAL	PERCENT ERROR VERSUS 50'D	SQUARE ROOT OF DIFF'S
167.266	105.091	169.285	37.55	1.47	167.266	.61	1.53	
180.424	179.656	180.711	.58	2.14	180.424	.16	2.21	
207.298	190.339	208.193	4.34	1.26	207.298	.53	2.16	
228.543	227.743	220.972	-3.06	1.51	228.543	-3.43	1.60	
238.530	237.442	238.822	.58	1.64	238.530	.12	2.17	
279.684	262.265	279.764	6.26	1.47	279.684	.03	1.91	
299.232	290.583	293.175	.89	2.49	299.232	-2.07	1.58	
303.621	301.309	300.294	-.34	1.62	303.621	-1.11	2.66	
328.523	329.303	324.819	-.15	1.68	.002	100.00	1.60	

.0775603591113

.5693760096262

-.4194138685214

.3240403302842

1.

-.3249436654984

.1551939140795

-.1024288017242

.03645737474271

.3779360199226

1.

-.5596444577106

.464778417743

-.0185464680145

.3441549996034

-.1972412112941

-.147847635276

-.2729614359009

-.5673664094602

-.8309580747926

1.

.787559900419

.1147430736756

-.1441759022772

-.6845007627344

Figure C-2. Edited Output From Program Matrix (Concluded).

```

FRA,T1500,T1500,CH16500,T201314,ATKINSON,54242
FRA,T1500,T1500,CH16500,T201314,ATKINSON,54242
REQUEST,OFFORM,*PF.
ATTACH,NASTRAN,NASTRAN,1D=NASTRAN,SN=AFFDL,MR=1,
LIMIT,7000.
ATTACH,NAS1,NAS1,1D=TRAN,SN=ASDAO.
ATTACH,NAS2,NAS2,1D=TRAN,SN=ASDAD.
LIBRARY,NAS1,NAS2.
RFL,165000.
NASTRAN,,PUNI,ATTACH
RETURN,NASTRAN.
ATTACH,NASTPP,NASTPP,1D=CCSNAST,SN=AFFDL,MR=1.
REWIND,PUN.
RFL,165000.
NASTPP,PUN.
CATALOG,DEFORM,CLEAN,RP=999.
-
1D,ATKINSON,MODEL
APP      DISPLACEMENT
SOL      3
TIME     50
CEND
TITLE = CLEAN
SUBTITLE = SIMPLIFIED PANEL
LABEL = 2 FEB 81
METHOD = 1
SPC = 1
OUTPUT
DISPLACEMENTS(PRINT,PUNCH) = ALL
BEGIN BULK
ASET1  1      2      THRU   52
ASET1  1      54     THRU   64
GRID   1      1      42.5   -18.0   23.5   1
GRID   2      1      42.5   -14.67  23.5   1
GRID   3      1      42.5   -11.33  23.5   1
GRID   4      1      42.5   -8.0    23.5   1
GRID   5      1      42.5   -5.67   23.5   1
GRID   6      1      42.5   -3.33   23.5   1
GRID   7      1      42.5   -1.0    23.5   1
GRID   8      1      42.5   1.33    23.5   1
GRID   9      1      42.5   3.67    23.5   1
GRID  10      1      42.5   6.0    23.5   1
GRID  11      1      42.5   10.0   23.5   1
GRID  12      1      42.5   14.0   23.5   1
GRID  13      1      42.5   18.0   23.5   1
GRID  14      1      42.5   -18.0   17.7   1
GRID  15      1      42.5   -14.67  17.7   1
GRID  16      1      42.5   -11.33  17.7   1
GRID  17      1      42.5   -8.0    17.7   1
GRID  18      1      42.5   -5.67   17.7   1
GRID  19      1      42.5   -3.33   17.7   1
GRID  20      1      42.5   -1.0    17.7   1
GRID  21      1      42.5   1.33    17.7   1
GRID  22      1      42.5   3.67    17.7   1
GRID  23      1      42.5   6.0    17.7   1
GRID  24      1      42.5   10.0   17.7   1
GRID  25      1      42.5   14.0   17.7   1
GRID  26      1      42.5   18.0   17.7   1
GRID  27      1      42.5   -18.0   12.0   1
GRID  28      1      42.5   -14.67  12.0   1
GRID  29      1      42.5   -11.33  12.0   1
GRID  30      1      42.5   -8.0    12.0   1
GRID  31      1      42.5   -5.67   12.0   1
GRID  32      1      42.5   -3.33   12.0   1
GRID  33      1      42.5   -1.0    12.0   1
GRID  34      1      42.5   1.33    12.0   1
GRID  35      1      42.5   3.67    12.0   1
GRID  36      1      42.5   6.0    12.0   1
GRID  37      1      42.5   10.0   12.0   1
GRID  38      1      42.5   14.0   12.0   1
GRID  39      1      42.5   18.0   12.0   1
GRID  40      1      42.5   -18.0   6.25   1
GRID  41      1      42.5   -14.67  6.25   1
GRID  42      1      42.5   -11.33  6.25   1
GRID  43      1      42.5   -8.0    6.25   1
GRID  44      1      42.5   -5.67   6.25   1

```

Figure C-2. Sample NASTRAN Deck.

GRID	45	1	42.5	-3.33	6.25	1	
GRID	46	1	42.5	-1.0	6.25	1	
GRID	47	1	42.5	1.33	6.25	1	
GRID	48	1	42.5	3.67	6.25	1	
GRID	49	1	42.5	6.0	6.25	1	
GRID	50	1	42.5	10.0	6.25	1	
GRID	51	1	42.5	14.0	6.25	1	
GRID	52	1	42.5	18.0	6.25	1	
GRID	53	1	42.5	-18.0	0.5	1	
GRID	54	1	42.5	-14.67	0.5	1	
GRID	55	1	42.5	-11.33	0.5	1	
GRID	56	1	42.5	-8.0	0.5	1	
GRID	57	1	42.5	-5.67	0.5	1	
GRID	58	1	42.5	-3.33	0.5	1	
GRID	59	1	42.5	-1.0	0.5	1	
GRID	60	1	42.5	1.33	0.5	1	
GRID	61	1	42.5	3.67	0.5	1	
GRID	62	1	42.5	6.0	0.5	1	
GRID	63	1	42.5	10.0	0.5	1	
GRID	64	1	42.5	14.0	0.5	1	
GRID	65	1	42.5	18.0	0.5	1	
GRID	66	1	0.0	0.0	22.175	1	123456
GRID	67	1	0.0	0.0	2.3	1	123456
GRID	68	1	0.0	0.0	0.0	1	123456
GRID	69	0	0.0	0.0	0.0		123456
GRID	70	0	0.0	0.0	23.0		123456
GRID	71	0	30.0	0.0	23.0		123456
GRID	72	1	0.0	0.0	23.5	1	123456
GRID	73	1	0.0	0.0	0.5	1	123456
CBAR	1	1	1	2	66	2	+CBAR1
CBAR	2	1	2	3	66	2	+CBAR2
CBAR	3	1	3	4	66	2	+CBAR3
CBAR	4	1	4	5	66	2	+CBAR4
CBAR	5	1	5	6	66	2	+CBAR5
CBAR	6	1	6	7	66	2	+CBAR6
CBAR	7	1	7	8	66	2	+CBAR7
CBAR	8	1	8	9	66	2	+CBAR8
CBAR	9	1	9	10	66	2	+CBAR9
CBAR	10	1	10	11	66	2	+CBAR10
CBAR	11	1	11	12	66	2	+CBAR11
CBAR	12	1	12	13	66	2	+CBAR12
CBAR	13	1	53	54	67	2	+CBAR13
CBAR	14	1	54	55	67	2	+CBAR14
CBAR	15	1	55	56	67	2	+CBAR15
CBAR	16	1	56	57	67	2	+CBAR16
CBAR	17	1	57	58	67	2	+CBAR17
CBAR	18	1	58	59	67	2	+CBAR18
CBAR	19	1	59	60	67	2	+CBAR19
CBAR	20	1	60	61	67	2	+CBAR20
CBAR	21	1	61	62	67	2	+CBAR21
CBAR	22	1	62	63	67	2	+CBAR22
CBAR	23	1	63	64	67	2	+CBAR23
CBAR	24	1	64	65	67	2	+CBAR24
CBAR	25	2	1	14	68	2	+CBAR25
CBAR	26	2	14	27	68	2	+CBAR26
CBAR	27	2	27	40	68	2	+CBAR27
CBAR	28	2	40	53	68	2	+CBAR28
CBAR	29	2	13	26	68	2	+CBAR29
CBAR	30	2	26	39	68	2	+CBAR30
CBAR	31	2	39	52	68	2	+CBAR31
CBAR	32	2	52	65	68	2	+CBAR32
CBAR	33	3	4	17	68	2	+CBAR33
CBAR	34	3	17	30	68	2	+CBAR34
CBAR	35	3	30	43	68	2	+CBAR35
CBAR	36	3	43	56	68	2	+CBAR36
CBAR	37	3	7	20	68	2	+CBAR37
CBAR	38	3	20	31	68	2	+CBAR38
CBAR	39	3	33	46	68	2	+CBAR39
CBAR	40	3	46	59	68	2	+CBAR40
CBAR	41	3	10	23	68	2	+CBAR41
CBAR	42	3	23	36	68	2	+CBAR42
CBAR	43	3	36	49	68	2	+CBAR43
CBAR	44	3	49	62	68	2	+CBAR44
CBAR	45	4	1	2	69	2	+CBAR45
CBAR	46	4	2	3	69	2	+CBAR46
CBAR	47	4	3	4	69	2	+CBAR47

Figure C-2. Sample NASTRAN Deck (Continued).

CBAR	46	4	4	5	69		2	+CBAR44
CBAR	49	4	5	6	69		2	+CBAR47
CBAR	50	4	6	7	72		2	+CBAR49
CBAR	51	4	7	8	72		2	+CBAR51
CBAR	52	4	8	9	72		2	+CBAR52
CBAR	53	4	9	10	72		2	+CBAR53
CBAR	54	4	10	11	72		2	+CBAR54
CBAR	55	4	11	12	72		2	+CBAR55
CBAR	56	4	12	13	72		2	+CBAR56
CBAR	57	5	53	54	73		2	+CBAR57
CBAR	58	5	54	55	73		2	+CBAR58
CBAR	59	5	55	56	73		2	+CBAR59
CBAR	60	5	56	57	73		2	+CBAR60
CBAR	61	5	57	58	73		2	+CBAR61
CBAR	62	5	58	59	73		2	+CBAR62
CBAR	63	5	59	60	73		2	+CBAR63
CBAR	64	5	60	61	73		2	+CBAR64
CBAR	65	5	61	62	73		2	+CBAR65
CBAR	66	5	62	63	73		2	+CBAR66
CBAR	67	5	63	64	73		2	+CBAR67
CBAR	68	6	1	14	68		2	+CBAR68
CBAR	70	6	14	27	68		2	+CBAR70
CBAR	71	6	27	40	68		2	+CBAR71
CBAR	72	6	40	53	68		2	+CBAR72
CBAR	73	6	13	26	68		2	+CBAR73
CBAR	74	6	26	39	68		2	+CBAR74
CBAR	75	6	39	52	68		2	+CBAR75
CBAR	76	6	52	65	68		2	+CBAR76
+CBAR1		-1.25	1.0	-1.325	-1.25	0.0	-1.325	
+CBAR2		-1.25	0.0	-1.325	-1.25	0.0	-1.325	
+CBAR3		-1.25	0.0	-1.325	-1.25	0.0	-1.325	
+CBAR4		-1.25	0.0	-1.325	-1.25	0.0	-1.325	
+CBAR5		-1.25	0.0	-1.325	-1.25	0.0	-1.325	
+CBAR6		-1.25	0.0	-1.325	-1.25	0.0	-1.325	
+CBAR7		-1.25	0.0	-1.325	-1.25	0.0	-1.325	
+CBAR8		-1.25	0.0	-1.325	-1.25	0.0	-1.325	
+CBAR9		-1.25	0.0	-1.325	-1.25	0.0	-1.325	
+CBAR10		-1.25	0.0	-1.325	-1.25	0.0	-1.325	
+CBAR11		-1.25	0.0	-1.325	-1.25	0.0	-1.325	
+CBAR12		-1.25	0.0	-1.325	-1.25	-1.0	-1.325	
+CBAR13		-1.25	1.0	1.8	-1.25	0.0	1.8	
+CBAR14		-1.25	0.0	1.8	-1.25	0.0	1.8	
+CBAR15		-1.25	0.0	1.8	-1.25	0.0	1.8	
+CBAR16		-1.25	0.0	1.8	-1.25	0.0	1.8	
+CBAR17		-1.25	0.0	1.8	-1.25	0.0	1.8	
+CBAR18		-1.25	0.0	1.8	-1.25	0.0	1.8	
+CBAR19		-1.25	0.0	1.8	-1.25	0.0	1.8	
+CBAR20		-1.25	0.0	1.8	-1.25	0.0	1.8	
+CBAR21		-1.25	0.0	1.8	-1.25	0.0	1.8	
+CBAR22		-1.25	0.0	1.8	-1.25	0.0	1.8	
+CBAR23		-1.25	0.0	1.8	-1.25	0.0	1.8	
+CBAR24		-1.25	0.0	1.8	-1.25	-1.0	1.8	
+CBAR25		-0.246	3.0	-0.815	-0.246	3.0	0.0	
+CBAR26		-0.246	3.0	0.0	-0.246	3.0	0.0	
+CBAR27		-0.246	3.0	0.0	-0.246	3.0	0.0	
+CBAR28		-0.246	3.0	0.0	-0.246	3.0	0.5	
+CBAR29		-0.246	-3.0	-0.815	-0.246	-3.0	0.0	
+CBAR30		-0.246	-3.0	0.0	-0.246	-3.0	0.0	
+CBAR31		-0.246	-3.	0.0	-0.246	-3.0	0.0	
+CBAR32		-0.246	-3.	0.0	-0.246	-3.0	0.0	
+CBAR33		-0.25	0.0	-0.815	-0.25	0.0	0.0	
+CBAR34		-0.25	0.0	0.0	-0.25	0.0	0.0	
+CBAR35		-0.25	0.0	0.0	-0.25	0.0	0.0	
+CBAR36		-0.25	0.0	0.0	-0.25	0.0	0.5	
+CBAR37		-0.25	0.0	-0.815	-0.25	0.0	0.0	
+CBAR38		-0.25	0.0	0.0	-0.25	0.0	0.0	
+CBAR39		-0.25	0.0	0.0	-0.25	0.0	0.0	
+CBAR40		-0.25	0.0	0.0	-0.25	0.0	0.5	
+CBAR41		-0.25	0.0	-0.815	-0.25	0.0	0.0	
+CBAR42		-0.25	0.0	0.0	-0.25	0.0	0.0	
+CBAR43		-0.25	0.0	0.0	-0.25	0.0	0.0	
+CBAR44		-0.25	0.0	0.0	-0.25	0.0	0.5	
+CBAR45		-0.02	0.0	0.0	-0.02	0.0	0.0	
+CBAR46		-0.02	0.0	0.0	-0.02	0.0	0.0	
+CBAR47		-0.02	0.0	0.0	-0.02	0.0	0.0	
+CBAR48		-0.02	0.0	0.0	-0.02	0.0	0.0	

Figure C-2. Sample NASTRAN Deck (Continued).

+CRAR49		-0.02	0.0	0.0	-0.02	0.0	0.0
+CBAR50		-0.02	0.0	0.0	-0.02	0.0	0.0
+CBAR51		-0.02	0.0	0.0	-0.02	0.0	0.0
+CBAR52		-0.02	0.0	0.0	-0.02	0.0	0.0
+CBAR53		-0.02	0.0	0.0	-0.02	0.0	0.0
+CBAR54		-0.02	0.0	0.0	-0.02	0.0	0.0
+CBAR55		-0.02	0.0	0.0	-0.02	0.0	0.0
+CBAR56		-0.02	0.0	0.0	-0.02	0.0	0.0
+CBAR57		-0.02	0.0	0.0	-0.02	0.0	0.0
+CBAR58		-0.02	0.0	0.0	-0.02	0.0	0.0
+CBAR59		-0.02	0.0	0.0	-0.02	0.0	0.0
+CBAR60		-0.02	0.0	0.0	-0.02	0.0	0.0
+CBAR61		-0.02	0.0	0.0	-0.02	0.0	0.0
+CBAR62		-0.02	0.0	0.0	-0.02	0.0	0.0
+CBAR63		-0.02	0.0	0.0	-0.02	0.0	0.0
+CBAR64		-0.02	0.0	0.0	-0.02	0.0	0.0
+CBAR65		-0.02	0.0	0.0	-0.02	0.0	0.0
+CRAR66		-0.02	0.0	0.0	-0.02	0.0	0.0
+CBAR67		-0.02	0.0	0.0	-0.02	0.0	0.0
+CBAR68		-0.02	0.0	0.0	-0.02	0.0	0.0
+CBAR69		-0.02	0.0	0.0	-0.02	0.0	0.0
+CBAR70		-0.02	0.0	0.0	-0.02	0.0	0.0
+CBAR71		-0.02	0.0	0.0	-0.02	0.0	0.0
+CBAR72		-0.02	0.0	0.0	-0.02	0.0	0.0
+CBAR73		-0.02	0.0	0.0	-0.02	0.0	0.0
+CBAR74		-0.02	0.0	0.0	-0.02	0.0	0.0
+CBAR75		-0.02	0.0	0.0	-0.02	0.0	0.0
+CBAR76		-0.02	0.0	0.0	-0.02	0.0	0.0
CBAR	68	5	63	64	73		2
CORDIC	1	69	70	71			+CBAR68
CQUAD2	1	1	1	14	15	2	
CQUAD2	2	1	2	15	16	3	
CQUAD2	3	1	3	16	17	4	
CQUAD2	4	1	4	17	18	5	
CQUAD2	5	1	5	18	19	6	
CQUAD2	6	1	6	19	20	7	
CQUAD2	7	1	7	20	21	8	
CQUAD2	8	1	8	21	22	9	
CQUAD2	9	1	9	22	23	10	
CQUAD2	10	1	10	23	24	11	
CQUAD2	11	1	11	24	25	12	
CQUAD2	12	1	12	25	26	13	
CQUAD2	13	1	24	27	28	15	
CQUAD2	14	1	15	28	29	16	
CQUAD2	15	1	16	29	30	17	
CQUAD2	16	1	17	30	31	18	
CQUAD2	17	1	18	31	32	19	
CQUAD2	18	1	19	32	33	20	
CQUAD2	19	1	20	33	34	21	
CQUAD2	20	1	21	34	35	22	
CQUAD2	21	1	22	35	36	23	
CQUAD2	22	1	23	36	37	24	
CQUAD2	23	1	24	37	38	25	
CQUAD2	24	1	25	38	39	26	
CQUAD2	25	1	27	40	41	28	
CQUAD2	26	1	28	41	42	29	
CQUAD2	27	1	29	42	43	30	
CQUAD2	28	1	30	43	44	31	
CQUAD2	29	1	31	44	45	32	
CQUAD2	30	1	32	45	46	33	
CQUAD2	31	1	33	46	47	34	
CQUAD2	32	1	34	47	48	35	
CQUAD2	33	1	35	48	49	36	
CQUAD2	34	1	36	49	50	37	
CQUAD2	35	1	37	50	51	38	
CQUAD2	36	1	38	51	52	39	
CQUAD2	37	1	40	53	54	41	
CQUAD2	38	1	41	54	55	42	
CQUAD2	39	1	42	55	56	43	
CQUAD2	40	1	43	56	57	44	
CQUAD2	41	1	44	57	58	45	
CQUAD2	42	1	45	58	59	46	
CQUAD2	43	1	46	59	60	47	
CQUAD2	44	1	47	60	61	48	
CQUAD2	45	1	48	61	62	49	
CQUAD2	46	1	49	62	63	50	

Figure C-2. Sample NASTRAN Deck (Continued).

COUAD2	47	1	50	63	64	51		
COUAD2	48	1	51	64	65	52		
EIGR	1	GIV	0.0	500.0			1.-10	*EIGR1
*EIGR1 MAX								
MAT1	1	1.+7		0.33	2.588-4			
PARAN	GROPNT	33						
PBAR	1	1	0.375	0.0835	0.0371	0.0019	0.0	
PBAR	2	1	0.121	0.00955	0.01576	0.00157	0.0	
PBAR	3	1	0.14	0.00664	0.0891	0.00074	70.0	
PBAR	4	1	0.1352	0.0007210	0.03218	0.00028	40.0	
PBAR	5	1	0.08	0.0004270	0.06667	0.00170	70.0	
PBAR	6	1	0.08	0.0004270	0.06667	0.00170	70.0	
POUAD2	1	1	0.040	0.0				
SPC1	1	123	1					
SPC1	1	13	53					
SPC1	1	1	65					
ENDDATA								
* END OF RECORD								

Figure C-2. Sample NASTRAN Deck (Concluded).

Figure C-3. Data Acquisition Program for HP5451B Fourier Analyser

1114	X	1	1	1	0	630
1117	Y	88	0	13		
1124	D	0	38	5		
1126	J	0	18	5		
1129	MS	38	6			
1133	MS	20	5821	6		
1137	Y	20				
1141	L	6				
1144	*	1				
1147	X	1				
1150	*	7				
1153	X	1				
1156	D	1				
1158	D	1				
1161	J	2				
1164.						

Figure C-3. (Concluded).

Figure C-4. Sample Y-9 Modal Analysis Set Up with A.) General Information, B.) Post Identification, and C.) Grid Points.

LINE VECTOR	
123	124
125	126
127	128
129	129
130	131
131	132
132	133
133	134
134	135
135	136
136	137
137	138
138	139
139	140
140	141
141	142
142	143
143	144
144	145
145	146
146	147
147	148
148	149
149	150
150	151
151	152
152	153
153	154
154	155
155	156
156	157
157	158
158	159
159	160
160	161
161	162
162	163
163	164
164	165
165	166
166	167
167	168
168	169
169	170
170	171
171	172
172	173
173	174
174	175
175	176
176	177
177	178
178	179
179	180
180	181
181	182
182	183
183	184
184	185
185	186
186	187
187	188
188	189
189	190
190	191
191	192
192	193
193	194
194	195
195	196
196	197
197	198
198	199
199	200
200	201
201	202
202	203
203	204
204	205
205	206
206	207
207	208
208	209
209	210
210	211
211	212
212	213
213	214
214	215
215	216
216	217
217	218
218	219
219	220
220	221
221	222
222	223
223	224
224	225
225	226
226	227
227	228
228	229
229	230
230	231
231	232
232	233
233	234
234	235
235	236
236	237
237	238
238	239
239	240
240	241
241	242
242	243
243	244
244	245
245	246
246	247
247	248
248	249
249	250
250	251
251	252
252	253
253	254
254	255
255	256
256	257
257	258
258	259
259	260
260	261
261	262
262	263
263	264
264	265
265	266
266	267
267	268
268	269
269	270
270	271
271	272
272	273
273	274
274	275
275	276
276	277
277	278
278	279
279	280
280	281
281	282
282	283
283	284
284	285
285	286
286	287
287	288
288	289
289	290
290	291
291	292
292	293
293	294
294	295
295	296
296	297
297	298
298	299
299	300
300	301
301	302
302	303
303	304
304	305
305	306
306	307
307	308
308	309
309	310
310	311
311	312
312	313
313	314

Figure C-5. Sample Y-9 Connectivity Vector.

VITA

Frank Broderick Atkinson was born on 13 November 1947 in Nashville, Tennessee to Robert T. and Ruth B. Atkinson. After graduation from Irving Senior High School in 1965 he attended Arlington State College (now the University of Texas at Arlington). During his studies there he participated in the cooperative education program as a Weight Control Engineer at Bell Helicopter Company in Hurst, Texas. Following graduation in 1970 with a Bachelor of Science degree in Aerospace Engineering, he enlisted in the U. S. Air Force as a Ground Radio Communications Equipment Repairman. He subsequently attained the rank of Sergeant whereupon he was selected to attend Officer's Training School (OTS) at Lackland AFB, Texas. Upon graduation from OTS in January, 1975, he was assigned to the 3246 Test Wing, Guns and Fuze Division, Eglin AFB, Florida as a Wing Munitions Test Engineer. During his tenure at Eglin AFB, he was selected three times as his division's nominee for the Directorate of Test Engineering Test Engineer of the Quarter Award. He also represented the Directorate of Test Engineering as the nominee for the Lt. Robert L. Sullivan Award for the most outstanding junior officer. Capt. Atkinson was assigned to the School of Engineering of the Air Force Institute of Technology in June 1979 in the Graduate Aeronautical Engineering Program.

Permanent address: 90 Mr. and Mrs. R.T. Atkinson

5012 Shannon Drive, Box 84904

Lewisville, Texas 75056

